ABSTRACT

In this thesis the study of the fragmentation process of certain molecule is presented and it has been used to know the nature of fragmentation products. This work is concentrated to the calculation of fragmentation energy of the molecule using *ab initio* quantum chemistry methods and density functional theory (DFT) calculations and with a support by experiment. The influence of the computational method, basis set, and the geometry of molecule on simulation has been presented.

It was compared the fragmentaion of methylphenylsilane (MPS), dimethylphenylsilane (DMPS) and trimethylphenylsilane (TMPS). The fragmentation was initiated by electron impact ionization (EII). The mass spectrometry technique was used to the analysis of the composition of fragmentation products from MPS and TMPS. The fragmentation products measured in this work were interpreted with respect to the ionization energy, appearance energies of fragments and bond dissociation energy of selected bonds. The results for MPS and TMPS were completed with DMPS previously published experimental data in order to have the series of similar compounds, which differ only by number of CH_3 groups. Even the structurally similar molecules have significantly different fragmentation behavior. Comparison with the theoretical bond dissociation energies calculated using the DFT calculations has been presented.

Using the combined experimental and theoretical approaches we have focused our recent studies to the common features as well as basic differences of the fragmentation schemes of all the three molecules. We proposed subtraction of two hydrogen atoms during plasma induced fragmentation process. The subtraction of H_2 molecule, specific for MPS but rarely observed also in the other two compounds was also of high interest in our studies. It can run in two mechanisms: i. subtraction of two hydrogens one-by-one and ii. dissociation of H_2 in one step. We can predict which mechanism is more probable according to the DFT calculated energy profile of reaction. The calculated predictions were in correlation with the composition of fragmentation products from experimental mass spectra.

ABSTRAKT

V této práci je prezentována studie fragmentačního procesu zvolené molekuly a jeho vztah ke složení fragmentačních produktů. Práce je zaměřená na výpočet fragmentační energie molekuly pomocí *ab initio* kvantově chemických metod, metodou „density functional theory (DFT)“ a také srovnáním s experimentem. Je prezentován vliv výpočetní metody, bázového setu, a geometrie molekuly na simulaci.

Byla porovnána fragmentace methylfenylsilanu (MPS), dimethylfenylsilanu (DMPS), a trimetylfenylsilanu (TMPS). Fragmentace byla iniciována monochromatickým elektronovým svazkem (EII). Hmotnostní spektrometrie byla využita ke studiu složení fragmentačních produktů MPS a TMPS. Fragmentační produkty MPS a TMPS měřené v rámci této práce byly doplněny o experimentální studii DMPS, která byla prezentována v literatuře. Takto byla získána řada molekul, které jsou strukturně podobné, ale mají výrazně rozdílné chování během fragmentace. Pomocí měření účinného průřezu byly měřeny disociační energie vazeb a tyto disociační energie byly vypočteny pomocí metody DFT.

Kombinací teoretického výpočtu metodou DFT a experimentálního měření jsme poukázali na společné rysy a na rozdíly ve fragmentačním schématu všech tří molekul. Navrhli jsme odštěpení dvou vodíkových atomů během plazmově indukovaného fragmentačního procesu. Vodíky mohou být odštěpeny pomocí dvou mechanismů: i. odštěpení dvou vodíků jeden po druhém a ii. odštěpení molekuly H_2 v jednom kroku. Z profilů energie dokážeme určit, který mechanismus bude v tom konkrétním případě pravděpodobnější. Předpokládaný mechanismus je v korelaci s experimentálními výsledky fragmentace zjištěnými z hmotnostních spekter.

KEYWORDS

Ab initio, fragmentation energy, Hartree-Fock, density functional theory, geometry optimization, electron impact ionization, mass spectrometry, ionization energy, appearance energy, bond dissociation energy.

KLÍČOVÉ SLOVA

Ab initio, fragmentační energie, Hartree-Fock, density functional theory, optimalizace geometrie, ionizace nárazem elektronu, hmotnostní spektrometrie, ionizační energie, prahová energie vzniku, disociační energie vazby.

Alsheikh Amer A., Modelling of chemical processes, Brno: Vysoké učení technické v Brně, Fakulta chemická, Ústav fyzikální a spotřební chemie, Vedoucí dizertační práce Mgr. Jan Žídek Ph.D.

Declaration

Prohlášení

.....

Signature

CONTENT

1 Introduction

Fragmentation is a process where a large molecule is separated into small molecules. In framework of this thesis, the fragmentation in plasma was investigated using *ab initio* models. The fragmentation is frequently applied for example to the analysis of DNA, where the product of fragmentation can give picture about its structure. DNA fragmentation can be caused by breaking of free radical-induced. Therefore, there is possibility to analyze the fragmentation products of such molecules [1]. Medically, this analysis of DNA fragments can give information about the human fertility [2].

The fragmentation procedures in the gas phase that are driven by electrons are essential to realize the different plasma processes. These processes are widely used in contemporary technologies [3, 4]. By this way, there is possible for example to prepare new polymeric materials that are non-classical. Precursors for these polymers do not contain any double chemical bonds. These properties are strongly dependent on the fragmentation of these precursors.

The calculation of fragmentation energy is very useful, because there is experimentally an ability to change relatively simply the electron energy and thus the creation of different fragment can be optimized. The fragmentation energy can give information about the population of different radicals resulting from the fragmentation. The population analysis can be used as input parameter to investigate the products of subsequent reactions leading to fragmentation. Further, the fragmentation energy can be used as an input property to reflect the chemical reactivity of compound, and it will be possible to study the processes of adsorption and desorption of the resulting radicals or fragments near of some catalyst. This is the reason why our research is focused on the fragmentation energy.

The model enables us to predict the most probable products of fragmentation and supports the interpretation of experimental data. However, the molecules being investigated experimentally are relatively complex like polymers or DNA. The model must be set up and verified on the compound, which is relatively simple. We selected the molecule of propane, as it has a limited number of possible fragmentation products. The properties of propane (fragmentation energy, heat of formation, dissociation energy) are known and thus the model results can be compared with experimental data. That is why the propane molecule was selected. The model can be tested on calculations of fragmentation energy from molecular structure. Then

the model enables us to optimize the condition and estimate the properties again. The experimental analysis of fragmentation energy and reactivity is time and cost consuming. The results from calculation can lead to a more effective experimental work. The modeling of fragmentation energy can help also to calculate the fragmentation energy of compounds which were not yet prepared. The result of model will outline the idea about expected products and their reactivity.

The *ab initio* method should be used for calculating the fragmentation process. The process is driven by dissociation of chemical bonds, which is influenced by electron energy of molecules and their vibrations. Coarse methods such as molecular mechanics and dynamics can describe the molecules on the level of individual atoms but not electrons. *Ab initio* quantum chemistry method will be used because it distinguishes not only individual atoms, but also the wave function of electrons. Next possible method is the DFT calculation. The *ab initio* method calculates the energy of atoms in excited state or ionized state, which is not possible to describe by the DFT method.

2 Goal of the thesis

The main goal of the thesis is an analysis of fragmentation process using quantum mechanical methods. A literature review on fragmentation energy and quantum chemical methods will be carried out.

The propane will be used as an example of simple molecules for testing of fragmentation analysis. The methylphenylsilane, dimethylphenylsilane and trimethyplhenylsilane will be used as an example of complex molecules.

The calculation of simple molecule will be used for optimization methods of calculation: selection of optimal method, basis set.

The fragmentation energy of complex organosilicon molecules will be calculated. The fragmentation energy will be verified by the positive ion mass spectra and relative partial cross sections obtained experimentally. The individual steps of fragmentation mechanism will be analyzed: electron impact ionization and bond dissociation.

3 Literature review

Ab initio quantum chemistry methods have been previously used to predict the fragmentation energy of large molecules. More recently, the EII technique is used to explain ionic chemistry [5] and energies of fragmentation products [6]. The resulting fragmentation energies are completed with chemical kinetics model. This can give more reasonable results of final concentrations of fragments.

3.1 Fragmentation energy

Fragmentation energy is the property of molecular structure and it is defined as the required energy for separation of several chemical bonds of the large molecule and getting smaller particles (fragments). Fragmentation energy was investigated by using the experiment and also some examples of theoretical calculations by quantum chemical methods.

3.1.1 Experimental determination

In all techniques of fragmentation, the principle of fragmentation energy measurement depends on the determination of energies for reactants and products of fragmentation reaction. Then, the fragmentation energy is determined as the difference between the energies of products and reactants. There are several experimental techniques describing the fragmentation process such as:

- Photoionization

Photoionization occurs when the sample (an atom or molecule) absorbs the electromagnetic radiation (a photon of visible or ultraviolet light). Photon must have sufficient energy to ionize the sample. This leads to release an electron from the sample and form a positive ion [7].

- Collision resilience experiment

The molecular ions are generated by ultraviolet laser-induced desorption. Then, these ions are accelerated and directed to the surface. After the collision, ions are measured in a time-of-flight mass spectrometer [8].

- Electron impact ionization

The process of ionization is the result of the collision of the sample in the gas phase with fast moving electrons. An atom or molecule can ionize to form molecular ion. Radical ionizes to form fragment ion [9].

- Plasma

Plasma is created by collisions of electrons (primary free electrons are presented everywhere but at very low concentrations) with neutral atoms or molecules. In principle, these primary electrons are accelerated by electric and/or magnetic field and they obtain high kinetic energy, in contrary of the ions that are heavy and thus they have only low energy. These accelerated electrons are able to ionize other particles (atoms, molecule) and also dissociate molecules. So plasma is created by the collisions of electrons with other particles.

- Mass spectrometry

Mass spectrometry technique uses various ionization methods to describe the fragmentation process of the molecule. The sample is collided with electrons of high energy to form molecular ion. Then, this molecular ion fragments to neutral alkyl and radical [10].

- Collision-induced dissociation

Collision-induced dissociation is used in mass spectrometry at either low or high collision energies. Molecular ions are accelerated by electric field. This leads to activate these ions by their collisions with neutral gas molecule, usually N_2 or Ar, and thus the dissociation of ions into smaller fragments is observed. At low collision energy, fragmentation decreases and thus the number of fragments reduce. But, when high energy is used, additional ions can be observed [11].

- Electron-capture dissociation

This technique is used in mass spectrometry to fragment ions in the gas phase. In this method, electrons with low energy are captured by multiply charged ions [12].

- Electron-transfer dissociation

This method is also used in mass spectrometry to fragment ions in the gas phase. Here, electrons transfer to these ions leading to dissociate them [13].

Experimentally, electron impact ionization and mass spectrometry were selected to describe the fragmentation process.

The EII technique is advantageous because it helps to measure the relative ionization energy of the original neutral molecule and appearance energy of the ionic fragments. Ionization energy is the minimum electron energy required to produce molecular ion. Appearance energy is the minimum electron energy necessary to produce a given ionic fragment. The mass spectrum of the original neutral molecule can be obtained in addition; the fragmentation process gives information about the structure and molecular weight of the molecule. The comparison between the experimental data and *ab initio* calculations can be investigated.

S. Denifl et al. [14] determined experimentally appearance energy for some cations of neutral propane formed by the EII experiment at two different gas temperatures (290 K and 690 K). They observed that the appearance energy values were decreased when the gas temperature was increased. They also verified their calculations using high level quantum chemical methods. They used Gaussian-3 theory (G3 theory) [15], Gaussian-3 theory using density functional theory B3LYP (G3B3) [16], and complete basis set-quadratic Becke 3 (CBS-QB3) method [17]. Firstly, they used these three methods to calculate the appearance energy at the gas temperature 290 K where the results were very close from each other. Secondly, they used CBS-QB3 method to calculate the appearance energy at 290 K and 690 K of gas temperature where their appearance energy was in excellent agreement with experimental data.

J. Kočišek et al. [6] studied the EII technique using crossed electron-molecular beams experiment to investigate the fragmentation of the DMPS molecule. The appearance energies of selected ion fragments were estimated in addition to the ionization energy of the DMPS molecule. They calculated the bond dissociation energy for single bond cleavage as a difference between the appearance energy of the ionic fragment and the ionization energy of the DMPS [18]. They have found that the dissociation energy of methyl group in $DMPS^+$ was in a good agreement with theoretical calculations of the DFT methods performed by Choe [19]. They

found the same results of dissociation energy for other bonds of the $DMPS^+$ except of *m/z* = 78 assigned to $C_6H_6^+$.

Mass spectrometry is a standard analytical method. In this technique, molecule is converted into ions and fragments. Then, the composition of molecule and characteristics of fragmentation products like mass-to-charge ratio can be determined. Many experimental studies have been performed to study the fragmentation of fullerenes in neutral and charged C_{60} [20, 21], C_{70} [22], and metallofullerenes [23-25]. In particular, these studies revealed that fullerenes sequentially lose C_2 fragments from their cages as is shown in the following reaction:

$$C_n \rightarrow C_{n-2} + C_2 \qquad (1)$$

The C_2 fragmentation energy for fullerenes can be determined experimentally using the mass spectrometry technique. Using this technique, it was demonstrated that the C_2 binding energy of C_{60} lies in the range (7-8) eV [21].

3.1.2 Mechanism of fragmentation

Fragmentation mechanism of propane was investigated using mass spectrometry and EII experiments. In mass spectrometry technique, molecule must be ionized. This can be done by collisions of the molecule with high energy electrons to yield molecular ion. This molecular ion can fragment to form neutral alkyl radicals such as methyl radical, ethyl radical, propyl radical and so on. Resulting fragments can be detected based on the ratio of mass to charge of these fragments. According to this mechanism, butane [10] fragments as follows

$$C_4H_{10} \xrightarrow{e-(fast)} C_4H_{10}^{\bullet +} \qquad (m/z = 58) \qquad (2)$$

$$C_4H_{10}^{\bullet +} \xrightarrow{M-15} C_3H_7^{+} + CH_3^{\bullet} \qquad (m/z = 43) \qquad (2a)$$

$$C_4H_{10}^{\bullet +} \xrightarrow{M-29} C_2H_5^{+} + C_2H_5^{\bullet} \qquad (m/z = 29) \qquad (2b)$$

$$C_4H_{10}^{\bullet +} \xrightarrow{M-29} CH_3^{+} + C_3H_7^{\bullet} \qquad (m/z = 15) \qquad (2c)$$

According to the fragmentation mechanism for butane, we proposed the detailed mechanism for propane fragmentation.

$$C_3H_8 \xrightarrow{e-(fast)} C_3H_8^{\bullet +} \qquad (m/z = 44) \qquad (3)$$

$$C_3H_8^{\bullet +} \xrightarrow{M-15} C_2H_5^{+} + CH_3^{\bullet} \qquad (m/z = 29) \qquad (3a)$$

$$C_3H_8^{\bullet +} \xrightarrow{M-29} CH_3^{+} + C_2H_5^{\bullet} \qquad (m/z = 15) \qquad (3b)$$

The EII technique of propane [14] can result the following ionization reactions.

$$C_3H_8 + e^- \rightarrow C_3H_8^{\bullet +} + 2e^- \quad (4)$$

$$C_3H_8 + e^- \rightarrow C_3H_7^+ + H^- + e^- \quad (4a)$$

$$C_3H_8 + e^- \rightarrow C_3H_7^+ + H + 2e^- \quad (4b)$$

$$C_3H_8 + e^- \rightarrow C_3H_5^+ + H_2 + H + 2e^- \quad (4c)$$

$$C_3H_8 + e^- \rightarrow C_3H_3^+ + 2H_2 + H + 2e^- \quad (4d)$$

$$C_3H_8 + e^- \rightarrow C_2H_5^+ + CH_3 + 2e^- \quad (4e)$$

$$C_3H_8 + e^- \rightarrow C_2H_4^+ + CH_4 + 2e^- \quad (4f)$$

$$C_3H_8 + e^- \rightarrow C_2H_3^+ + CH_4 + H + 2e^- \quad (4g)$$

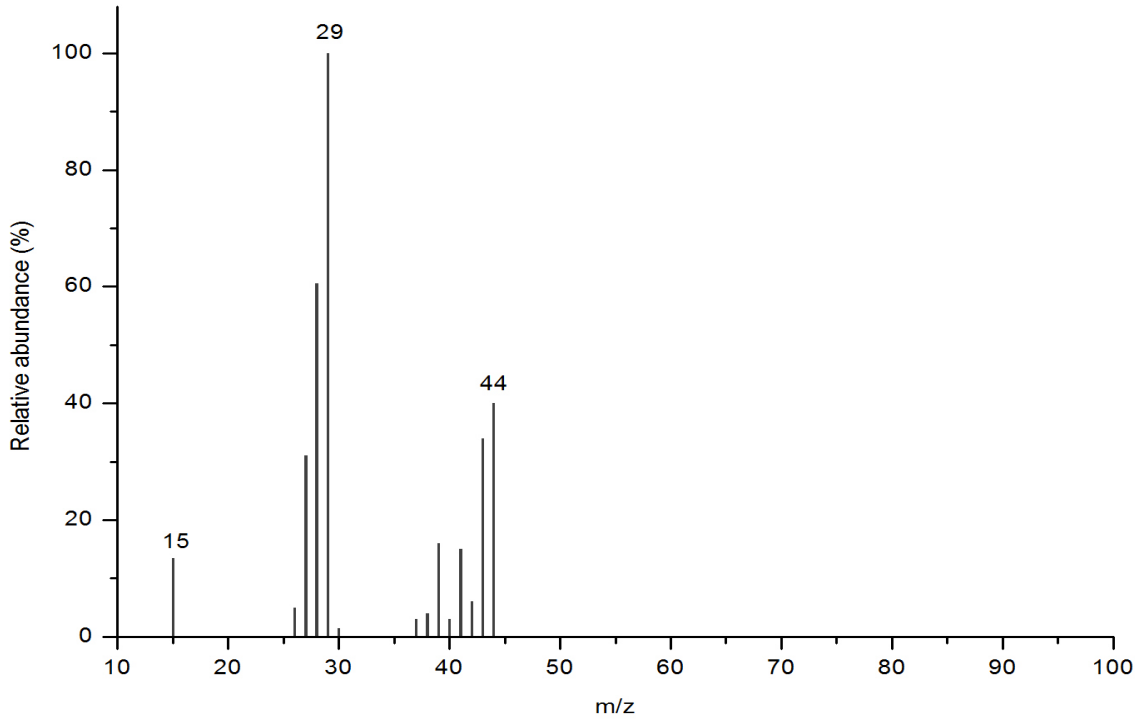

Figure 1. Mass spectrum of propane molecule (C_3H_8; MW = 44) [26]

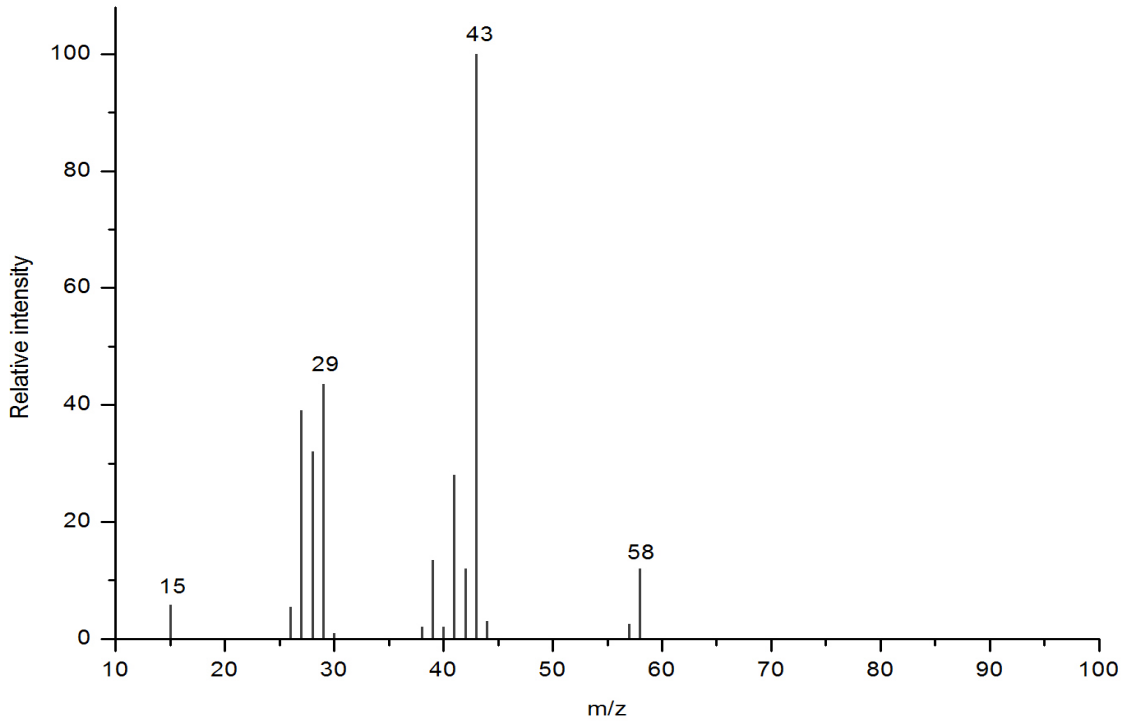

Figure 2. Mass spectrum of butane molecule (C_4H_{10}; MW = 58) [27]

The mass spectra of the propane (Figure 1) and butane (Figure 2) molecules were presented in literature. These mass spectra are in accord with the proposed mechanism.

3.1.3 Theoretical description

Theoretical description of fragmentation process was investigated by *ab initio* quantum chemistry methods and DFT calculations.

E. Vašeková et al. [28] calculated the appearance energy for some cations of neutral ethane using high level *ab initio* quantum chemical methods. They used CBS-QB3 method [15] to calculate the appearance energy of cations of ethane at 293 K and 693 K of gas temperature. The theoretical shift of the appearance energy between these two temperatures was 0.31 eV and was in reasonable agreement with the experimental value.

V. Brites et al. [5] calculated the ionization energy of the $DMPS^+$ dimethylphenylsilane cation that is one of the fragmentation products of tetravinylsilane formed by the EII technique using the second-order Møller-Plesset perturbation theory (MP2/cc-pVDZ) level of theory. The

ionization energy was about 8.91 eV, which was in excellent agreement with the experimental value of (8.92 ± 0.15) eV of Gaidis et al. [29].

S. T. Nakagawa et al. [30] studied the dissociation of small boron clusters. They calculated the ionization potential energy by using the collision of small boron clusters with Xe atoms at low collision energy (<10 eV). The used methods to carry out this calculation were the DFT(B3LYP) calculation and *ab initio* methods such as HF, MP2, MP4, configuration interaction with single excitation (CIS), and configuration interaction with single and double excitations (CISD). In the comparison to experimental data, they found that the results of the DFT calculations were more accurate than *ab initio* methods that they used and the previous *ab initio* methods [31-33]. The dissociation of clusters by using the collision with Xe atoms is advantageous for calculation of fragmentation energy because it gives better results when the method and basis set are properly selected.

G. A. Dolgonos et al. [34] calculated the C_2 fragmentation energy of C_{80} using *ab initio* (HF/STO-3G) and the DFT (B3LYP/3-21G) calculations. The C_2 fragmentation energies were calculated as the difference between the C_{80} isomer energy and the sum of the C_{78} and C_2 product energies. They found that the DFT methods were more reliable than *ab initio* (HF/STO-3G), where the calculated C_2 fragmentation energies were in the range (8.7-9.0) eV and in very good agreement with the experimental value of (9.4 ± 0.7) eV.

W. C. Eckhoff et al. [35] calculated the C_2 fragmentation energy of C_{70} fullerene ($C_{70} \rightarrow C_{68} + C_2$) using *ab initio* Hartree-Fock (SCF/DZ) and the DFT (BLYP/DZ) calculations. Using the Hartree-Fock (HF) method, the energy of C_2 dissociotion from this fullerene was 13.2 eV. The best prediction for the C_2 fragmentation energy of C_{70} was 11.5 eV by using the DFT method. These results were in sharp disagreement with the majority of the experimental studies.

A. D. Boese et al. calculated the dissociation energy of the reaction $C_{60} \rightarrow C_{58} + C_2$ using the DFT and MP2 calculations [36]. They found that the fragmentation energy was around (10-11) eV in agreement with the theoretical values of the dissociation energy (11-12) eV [37-40] and with experimental studies (10.5-10.9) eV [41, 42].

3.2 Quantum Chemical Methods

The electronic structure of materials is described by wavefunction (Ψ), which has a meaning square root of the electron density. The function is determined by Schrödinger's equation [1926]

(SE) [43]. The exact solution of SE is complex for many compounds. Therefore, several approximations are applied. First example is Wentzel–Kramers–Brillouin, which is used for semiclassical calculation in quantum mechanics. It is suitable for solution of one-dimensional problems. Next class of approximation methods is variational principles or perturbation theories [44].

The above stated approximations are used for solution of general problems. The chemical properties of compounds depend primary on electronic structure and Born-Oppenheimer approximation is used [1927]. The approximation separates wavefunction to its nuclear and electronic part: $\Psi_{total} = \Psi_{nuc} . \Psi_{el}$. Only the electronic Schrödinger's equation is solved.

Ab initio or "first principles" method [1950] is directly based on the theoretical principles of quantum mechanics (the Schrödinger's equation) without inclusion of any experimental data. The property of *ab initio* method is that there is no need to perform the experiments for input data, but the structure of the molecule is completely sufficient.

Ab initio method is used to calculate the electronic structure of the chemical system. In *ab initio* method, the Schrödinger's equation is solved using a basis set. The basis set is a set of functions which are combined in linear combinations to create molecular orbitals. Some physical properties can be determined by *ab initio* electronic structure calculations, i.e. from fundamental quantum theory [45]. The main use of the *ab initio* method is limited to the properties, which depend on electron structure:

- Molecular geometries
- Total energy of molecule
- Ionization energy and electron affinity
- Appearance energy of cation fragment
- Bond dissociation energy and dissociation energy
- HOMO (highest occupied molecular orbital) energy, LUMO (lowest unoccupied molecular orbital) energy, and LUMO-HOMO energy gap
- Potential energy surfaces (PES)
- Vibrational frequencies
- Spectra (IR, UV, NMR)
- Dipole moment
- Charge distribution
- Thermodynamic properties of molecule (zero-point vibration energy, heat capacity, entropy, and enthalpy)

The Schrödinger's equation can be written in form:

$$\mathbf{H}_{mol}\,\mathbf{\Psi} = \mathrm{E}\,\mathbf{\Psi} \tag{5}$$

Where E is the total energy of the system, $\mathbf{\Psi}$ is the wavefunction which is a function of the positions of the electrons and the nuclei within the molecule, and $\mathbf{H}_{mol}$ is the molecular Hamiltonian of a system which describes a many body system consisting of nuclei and electrons.

3.2.1 Born-Oppenheimer approximation

The molecular Hamiltonian is a sum of all contributions of potential energies (**V**) and kinetic energies (**T**) of the electrons and the nuclei within the molecule. Both the energy kinds can be calculated for electrons and nuclei. This molecular Hamiltonian is given in the following form:

$$\mathbf{H}_{mol} = \mathbf{T}_{el}\,(\vec{r}) + \mathbf{T}_{nuc}(\vec{\mathbf{R}}) + \mathbf{V}_{el-el}(\vec{r}) + \mathbf{V}_{nuc-nuc}(\vec{\mathbf{R}}) + \mathbf{V}_{el-nuc}(\vec{\mathbf{r}}, \vec{\mathbf{R}}) \tag{6}$$

Where $\vec{r}$ are the position vectors of the electrons, $\vec{\mathbf{R}}$ are the position vectors of the nuclei, $\mathbf{T}_{el}$ is the kinetic energy for the electrons, $\mathbf{T}_{nuc}$ is the kinetic energy for the nuclei, $\mathbf{V}_{el-el}$ is the repulsive electron-electron potential energy, $\mathbf{V}_{nuc-nuc}$ is the repulsive nuclear-nuclear potential energy, and $\mathbf{V}_{el-nuc}$ is the attractive electron-nuclear potential energy.

Ab initio method is based on the Born–Oppenheimer (BO) approximation. It assumes that the electrons in molecules are much lighter and faster than the nuclei, and then the electron motions need to be considered because the nuclei are relatively motionless (stationary). Electrons are treated individually. Therefore, they can be separated the electron motions from the nuclear motions. Since the nuclei have a much larger mass compared to electron's mass, its velocity will be much smaller, and then an electronic Hamiltonian only depends parametrically on the nuclear coordinates and can be written neglecting the kinetic energy for the nuclei.

$$\mathbf{H}_{el}(\vec{\mathbf{R}}) = \mathbf{T}_{el}\,(\vec{\mathbf{r}}) + \mathbf{V}_{el-el}(\vec{\mathbf{r}}) + \mathbf{V}_{el-nuc}(\vec{\mathbf{r}}, \vec{\mathbf{R}}) \tag{7}$$

This Hamiltonian is then used in the Schrödinger's equation describing the motions of electrons in the field of fixed nuclei [46].

3.2.2 Single particle approximation (Hartree-Fock)

For more complicated systems, the HF approach is applied [47]. This method does not include the full treatment of the effects of electron correlation where the coulombic repulsion between two electrons is not explicitly considered but its average effect is included in the calculation. This means that each electron in a molecule moves in an average electric field generated by all of the other electrons.

For the system containing only one electron, the Schrödinger's equation can be exactly solved. In the HF method, the total wavefunction of a many-electron system (molecule containing n electrons) is divided into the contributions of single-electron wavefunctions. The Schrödinger's equation for many-electron system can be converted into a set of simple one-electron equations. Each one-electron equation is solved to result a single-electron wavefunction called a molecular spatial orbital ψ. Then, these orbitals ψ are multiplied by one of the spin function α or β to yield occupied spin orbitals. The total molecular wavefunction Ψ is written as their linear combination and practically it can be obtained by a Slater determinant. The HF method is variational method, meaning that the energies predicted by this method are always equal to or greater than the real energy resulting from the exact solution of the Schrödinger's equation [48]. The HF method is suitable to compute the structures, vibrational frequencies of stable molecules, the ground states and some transition states of molecule. However, it is insufficient to study the bond dissociation because it does not completely treat the electron correlation problem [46]. In addition, excited states are difficult to calculate using the HF theory [49].

3.2.3 Linear combination of atomic orbitals (LCAO)

This approximation involves expressing the molecular orbitals as linear combinations of basis functions. These basis functions are usually identified with atomic orbitals. An individual molecular orbital is defined as

$$\psi_i(\mathrm{r}) = \sum_{s=1}^{\mathrm{m}} c_{si}\ \Phi_s(\mathrm{r}) \qquad i = 1, 2, 3, \ldots, \mathrm{m}\ \text{(component MOs)} \tag{8}$$

Where ψ_i is the molecular orbital i, c_{si} is the expansion coefficient of the atomic orbital s in the molecular orbital i, Φ_s is the atomic orbital s, and m is the number of atomic orbitals. This approximation is usually called the linear combination of atomic orbitals (LCAO) approach that

leads to linear equation for the coefficients of the molecular orbitals [50]. The coefficients of the expansion c_{si} are output data that can be determined by the HF procedure. The atomic orbital Φ_s(r) has exponential function that differs with the type of atomic orbital (s, p, d, and f). This exponential function contains orbital exponent that can be obtained from basis set.

3.2.4 Post-Hartree-Fock methods

As mentioned in the previous section, the HF method neglects the correlated motion of electrons resulting from Coulombic interactions. The difference between the HF and exact (nonrelativistic) energies is the correlation energy,

$$E \text{ (exact)} = E \text{ (Hartree-Fock)} - E \text{ (correlation)} \quad (9)$$

The neglection of correlation between opposite spins electrons leads to deficiencies in the description of electronic structure and some clearly anomalous results [51, 52]. Therefore, other theoretical methods, which take into account effects of spin electron correlation, have been developed. The electron correlation describes the energy contributions resulting from the interaction between the motions of different electrons in the electronic structure. Such methods are referred to as post-Hartree-Fock methods because they add correlation corrections to the HF mothod. There are various post-Hartree-Fock methods such as Møller-Plesset perturbation theory MPn, configuration interaction (CI), coupled cluster (CC) methods. Post-Hartree-Fock methods provide accurate treatment of the structures and energies of molecules, but they differ in computational costs [53]. For instance, Table 1 lists the predicted bond energy of hydrogen fluoride using the 6-311++G(3df,3pd) basis set, the predicted isomerization energy between acetaldehyde and ethylene oxide with 6-31G(d) basis set, and the geometry optimizations of ozone using the 6-31G(d) basis set. These predicted values have been computed with various methods (HF and post-Hartree-Fock) [46].

Table 1. Influence of the HF and post-Hartree-Fock methods on the bond energy (kJ/mol), isomerization energy (kJ/mol), and the structure (bond length (ang) and bond angle (deg)) for hydrogen fluoride [46].

Property	HF	MP2	MP3	MP4(SDTQ)	QCISD	QCISD(T)	Experiment
H-F	409.90	606.70	577.40	593.70	581.10	588.70	591.10
Isomerization energy	131.47	116.39	-	122.67	121.42	121.00	115.43
O-O	-	1.307	-	-	1.311	1.30	1.27
O-O-O	-	113.20	-	-	114.60	116.70	116.80

The HF value has uncertainty by over 175 kJ/mol. The computed MP2 bond energy is too large, with higher levels of correlation lowering it. However, both values calculated using the fourth-order Møller-Plesset perturbation theory (MP4) and quadratic configuration interaction with single, double, and triple excitations QCISD(T) methods are in excellent agreement with experiment. The methods including electron correlation all produce good estimates of the isomerization energy. It turns out that the MP2 value is fortuitously good; increasing the basis set size would produce a poorer result at the MP2 level. For the MP4, quadratic configuration interaction with single and double excitations (QCISD), and QCISD(T) methods, the predicted isomerization energy would continue to converge toward the experimental value as the basis set size increases. For the geometry of ozone, only the QCISD(T) geometry can be termed accurate (however its bond length is still too long) [46].

Table 2 shows the predicted structures of dioxygen difluoride F_2O_2 with different *ab initio* methods and basis sets. The coupled cluster with single, double, and triple excitations CCSD(T) method with a small basis set predicts more accurate structure compared to the HF or MP2 method with very large basis set. The CCSD(T) method with the larger basis set produces a structure in excellent agreement with experiment. Results can be summarized as follows:

1. The predicted values depend on the selected method.
2. Post-Hartree-Fock methods are more accurate than HF theory.
3. According to the literature, the CC and QCI methods are very similar to one another.
4. The best results are obtained by the QCISD(T) and the CCSD(T) methods.

Table 2. Influence of the variety of levels of theory on the structure of F_2O_2 (bond length (ang), bond and dihedral angle (deg)) [46].

Structure	HF 6-311+G(3df)	MP2 6-311+G(3df)	CCSD(T) 6-31G(d)	CCSD(T) 6-311G(2d)	Experiment
O-O	1.30	1.14	1.28	1.22	1.22
O-F	1.35	1.67	1.54	1.61	1.58
F-O-O	106.30	111.40	107.50	108.90	109.50
F-O-O-F	85.10	89.30	86.80	87.80	87.50

Møller-Plesset perturbation theory (MPn), where n is the order of the perturbation, is a method to compute the correlation energy using the many-body perturbation theory [54, 55]. The principle of perturbation theory is that the system is subjected to external potential (perturbation) such as a magnetic field or electromagnetic radiation relative to the internal HF potential in

which the electrons are moving. Then the system of interest is perturbed or changed slightly from a system whereby the mathematical solution is known (is solved exactly or approximately). This is described mathematically by defining a Hamiltonian operator for the system on interest (perturbed system) where can be divided into the part representing system with a known solution, and then into a number of additional parts that correspond to perturbations from the known system to the system of interest.

$$\mathbf{H} = \lambda^0 \mathbf{H}^{(0)} + \lambda^1 \mathbf{H}^{(1)} + \lambda^2 \mathbf{H}^{(2)} + \ldots \quad (10)$$

Where $\mathbf{H}^{(0)}$ is the normal electronic Hamiltonian operator that is the sum of the one-electron Fock operators of the HF(SCF) method, $\mathbf{H}^{(1)}$ is a first-order operator of perturbation, $\mathbf{H}^{(2)}$ is a second-order operator of perturbation, and λ is a (variable) parameter determining the strength of the perturbation where it varies from 0 to 1 [56-58].

There are several levels of MP energy such as MP0, MP1, MP2, etc. The zero-order perturbation energy MP0 is the sum of the orbitals energies for the occupied molecular orbitals. The first-order perturbation energy MP1 is just the HF energy. The MP2 method is the HF energy plus correction energy [50]. The advantage of many-body perturbation theory is that it is size-consistent in the sense that for two widely-separated fragments, the energy obtained using this method equals to the sum of the energies of these two fragments computed separately, however, it is not variational [59].

In the CI calculation, the electron correlation is treated [60]. On the other hand, the HF calculation is performed to result the occupied MOs (corresponding to the HF determinant), then the excited Slater determinants are generated by replacing one or more occupied orbitals with unoccupied (virtual) orbitals of higher energy. The total wavefunction is written as a linear combination of determinants (HF determinant and excited Slater determinants) with the molecular orbital expansion coefficients that can be determined when the energy is minimal (or at least stationary). According to the number of occupied HF MOs that can be exchanged by unoccupied MOs, The excited states are single (S), double (D), triple (T), and quadruple (Q). Therefore, there are several variants of the CI method such as CIS, CID, CISD, and CISDT [56, 57]. All variants of CI method are not size-consistent, but, they are variational. The quadratic configuration interaction [61] method (QCI) that is an extension of the CI calculation [62] was developed to correct the defect of size-consistency in the all single and double excitations of the

CI methods (CISD) [63]. The QCI calculation is very similar to the CC method (see below). The QCI calculation with single, double, and triple excitations QCISD(T) method adds triple excitations to the QCISD method and gives similar results to the CCSD(T) method [64].

When the total wavefunction of system contains all possible excited configurations, the calculation is called as full configuration interaction (FCI) [50]. Full CI method is size-consistent and variational. However, it is very expensive and the number of configurations (determinants) increases with the size of the system. For many-electron systems with large basis sets, FCI results are not practical. In practice, full CI calculations can only be performed with a small number of electrons (small systems) and small basis sets [65].

The CC method is similar to the CI calculation, where the total wavefunction is as a sum of the HF ground state determinant and determinants representing the transmission of electrons from HF determinant to virtual MOs. In the CC calculation, the selection of determinants is more difficult than selection them in a CI method [66]. The CC theory [67-69] takes into account electron correlation. In the CC method, excitations are also included in calculation, for example double excitations (D) in CCD [70], single (S) and (D) excitations in CCSD [71], and S, D, and T excitations in CCSD(T) [72]. All CC methods are size-consistent [73]. However, CC methods are not variational [74].

3.2.5 Multi-configuration self-consistent field methods

In previous section, the wavefunction of system was represented starting from a single HF determinant with occupied bonding orbitals (HOMO orbitals). Multi-configuration self-consistent field (MCSCF) method uses more than one configuration (HF determinant) to describe the total wavefunction. In MCSCF method, bonding and antibonding orbitals are treated to yield configurations. The consideration of antibonding orbitals is very important to study the dissociation of the molecule with stretched bond lengths where the energy gap is very small. Both the coefficients of the configurations that are in front of the determinants and the MOs used for constructing the determinants are optimized by the variational principle [75].

There is developed type of MCSCF calculation called complete active space self-consistent field approach (CASSCF) [76] used to study chemical reactions and to calculate electronic spectra. In this approach, very large numbers of configurations are included in the calculation [77] by dividing the molecular orbitals into three sets:

- A set of inactive orbitals composed of the lowest energy molecular orbitals which are doubly occupied in all configurations (determinants).
- A set of virtual orbitals of very high energy molecular orbitals which are unoccupied in all configurations.
- A set of active orbitals which are energetically intermediate between the inactive and virtual orbitals.

3.2.6 Density functional theory

The DFT calculation [78, 79] was developed by Hohenberg and Kohn (1964) and by Kohn and Sham (1965). The DFT method is an alternative to *ab initio* methods. The difference between this method and *ab initio* method is that the energy of the molecule can be determined in the DFT method from the electron density while from the wavefunction in *ab initio* method. In the DFT methods [80], electron correlation effects are taken into account and the exchange-correlation energy is computed using functional of the electron density. Functional is a function defined by another function. There are a variety of functionals used in the DFT methods such as Becke style three parameters [81] density functional method with the Lee-Yang-Parr correlation functional (B3LYP) and Becke style three parameters density functional method with the Perdew-Wang (B3PW91) [82]. Correlation functional (B3LYP) is very popular. In our case, each single function represents electron density of one atom. Using the functional, the electronic energy can be divided via the Kohn-Sham equations [83] into several terms which are computed separately:

1. The kinetic energy resulting from the motion of the electrons.
2. The potential energy of nuclear-electron interaction and nuclear-nuclear repulsion.
3. The electron-electron repulsion.
4. The exchange-correlation that represents the quantum mechanical exchange energy and the dynamic correlation energy.

For comparison, the total atomization energy and bond length of carbon dioxide were calculated using different methods with the 6-31G(d) basis set. The results are summarized in Table 3. Table 3 shows that two functionals, B3LYP and B3PW91, give the best geometries and these structures are in good agreement with the experimental data. The HF theory is not good to

predict the atomization energy of carbon dioxide because there is a large difference between theory and experiment. The MP2 and DFT (B3LYP and B3PW91) methods are suitable.

Table 3. Total atomization energy (kJ/mol) and bond length (ang) of carbon dioxide [46].

Property	HF	B3LYP	B3PW91	MP2	Experiment
C-O	1.14	1.17	1.17	1.18	1.16
Atomization energy	982.64	1581.77	1595.17	1585.96	1598.94
Δ(Exp)	616.30	17.17	3.77	12.98	-

3.2.7 Current state of the art

For many-body system, *ab initio* method requires to find a solution of the Schrödinger's equation. So far, there is no exact solution of the Schrödinger's equation, but by using some approximations, the physical properties, electronic structure, and total energy of molecule can be calculated. The PES and the HOMO and LUMO energies and their energy gap were selected. The PES is a concept used in computational chemistry to represent the relation between the energy of the system and its geometry. On this PES, minima and saddle points can be characterized.

Minima are observed at equilibrium structures and correspond to optimized geometries, and saddle points correspond to a transition structure of the system. The HOMO and LUMO energies and their energy gap reflect the chemical reactivity and kinetic stability of the system. When the energy gap is large, the system is less reactive and not kinetically stable, and when the energy gap is small, the system is more reactive and kinetically stable. These are the reasons why the calculations of the PES, HOMO energy, and LUMO energy were selected.

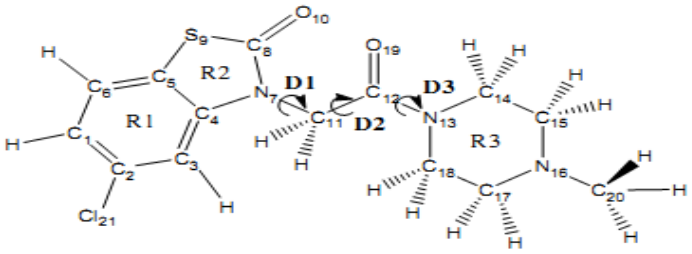

Figure 3. 5-chloro-3-(2-(4-methylpiperrazin-1-yl)-2-oxo-ethyl)benzo[d]thiazol-2(3H)-one (5CMOT) [84].

As example of the PES is a work of E. Tasar et al. [84]. The studied molecule was 5-chloro-3-(2-(4-methylpiperrazin-1-yl)-2-oxo-ethyl) benzo[d] thiazol-2(3H)-one molecule (abbreviated

as 5CMOT). The schematic depiction of 5CMOT is shown in Figure 3. They used the DFT(B3LYP) method with 6-31G(d) to calculate the PES. They found that the 5CMOT molecule has three different conformers. There was one conformer that has stable structure corresponding to the lowest energy value (local minimum) on the PES graphs.

The PES is advantageous for calculation of fragmentation energy because the determination of the most stable structure of molecules produces more reliable results of the fragmentation energy and other physical properties. They also calculated vibrational spectra of the most stable structure using the DFT(B3LYP) and *ab initio* HF methods. The results of the DFT methods were in an agreement with the experimental data.

As example of the HOMO energy, LUMO energy, and LUMO-HOMO energy gap is a work of R. J. Xavier et al. [85]. For this calculation, they used the HF and DFT(B3LYP) methods with 6-311++G(d, p) basis set. It was found that the DFT(B3LYP) method gives a lower energy gap in comparison with the HF method. The calculation of energy gap between HOMO and LUMO orbitals is good to get information about the chemical reactivity of the molecule where the lower value of this energy implies that the system is more reactive and kinetically stable and its electrons can more easily be excited. Recently this energy gap is used to prove the bioactivity from intermolecular charge transfer [86, 87].

3.3 Setting of the model

Here, basis set is used. Basis set is the set of mathematical functions used to describe the molecular orbitals within a molecule. Using this assumption, the total electronic wavefunction of the system can be approximated as the combination of resulting molecular orbitals [50]. There are several types of basis sets such as minimal basis set, split valence basis set, polarized basis set, and diffuse basis set. Minimal basis sets contain the minimum number of basis functions and they are used for very large molecules. The most popular minimal basis set is the STO-3G basis set where each atomic orbital represents one basis function composed of three Gaussian primitives GTOs combined to approximate the Slater type orbitals (STO) [46].

Split valence basis sets allow orbitals to change size by increasing the number of basis functions of the same angular type (secondary quantum number) per atom. Split valence basis set can be double or triple according to the number of sizes of basis functions for each valence orbital. For example, double zeta basis set 3-21G uses two sizes of basis functions for each

valence orbital, while triple split valence basis set 6-311G uses three sizes of basis functions. The notation 3-21G means that each core atomic orbital is represented by three GTO primitives and each valence atomic orbital is divided into two parts, an inner shell is represented by two GTO primitives, and the outer shell is represented by one GTO primitive [50].

Polarized basis sets are the modified form of split valence basis sets. These Polarized basis sets allow orbitals to change shape by adding basis functions (orbitals) with higher angular momentum. In polarized basis set, d functions are added to heavy atoms (all atoms, except hydrogen atoms), p functions are added to hydrogen atoms, and f functions are added to transition metals. Polarized basis sets can be characterized by adding one or two asterisks. The 6-31G* and 6-31G** are examples of this type of basis sets. In the notation 6-31G*, this basis set is also known as 6-31G(d), a single asterisk indicates that a set of d functions are added to polarize the p functions in 6-31G, meaning that the 6-31G basis set with d functions added to heavy atoms. In the basis set 6-31G**, also known as 6-31G(d,p), two asterisks mean that the 6-31G basis set with p functions added to hydrogen atoms and d functions to heavy atoms. Polarized basis sets are appropriate to compute geometries and vibrational frequencies [66].

Diffusion basis sets are more developed form of polarized basis sets. These basis sets allow orbitals to occupy a larger region of space by adding highly diffuse functions to atoms. Here, one or two plus signs are added. The 6-31+G* and 6-31++G* are examples of diffusion basis sets. The notation 6-31+G* is the 6-31G* basis set with diffuse functions added to heavy atoms. Diffusion basis set 6-31++G* is the 6-31G* basis set with diffuse functions added to all atoms (heavy atoms and hydrogen atoms). Diffusion basis sets are important to study systems with low ionization potentials, anions, and systems in excited states [46].

Table 4. Bond dissociation energy for different systems using MP2 and different basis sets [57].

HX	MP2/6-31G*	MP2/6-311+G(2d,p)	experimental
CH_4	109.39	101.75	101.75
NH_3	106.05	98.40	96.97
H_2O	102.46	94.58	95.06
C_2H_2	96.25	91.24	91.00
SiH_4	92.19	91.24	90.28
HF	98.17	89.33	89.81
PH_3	91.48	89.57	89.81
H_2S	86.70	85.03	85.51
HCN	89.33	84.79	85.75
HCl	80.97	80.01	80.49

The bond dissociation energies of the reaction $HX \rightarrow H^+ + X^-$ were calculated using the MP2 method with different basis sets. All values are expressed in KJ/mol. Table 4 shows the results. Evidently, 6-311+G(2d,p) basis set gives bond dissociation energy more accurate than 6-31G* basis set [54].

3.4 Fragmentation in plasma

Chemical vapor deposition technique has been used for thin film production for more than 50 years. Main applications of organosilicon precursors are in microelectronics [88], automotive and food industry [89]. During 1980's, this deposition technique has been improved by adding plasma to the process. Plasma enhanced chemical vapor deposition (PECVD) or plasma assisted chemical vapor deposition (PACVD) allow using many new types of precursors, especially organosilicones. For example, the MPS molecule can be used as a compatibilization agent. The plasma deposition is accompanied by fragmentation of molecule. The composition of fragments is important parameter for reactivity of inorganic surface. These precursors offer several advantages. Organic groups have nearly infinite options for proper control of deposited layers. Additionally, they are compatible with other organic compounds and provide elasticity, preventing the layer to crack. Silicon atoms support binding of organic, polymers and biomaterials to inorganic substrates including glass, or ceramics. In that case the bio- or organic phase must be attached to inorganic surface in controlled way [90]. Hexamethyldisiloxane (HMDSO) and tetraethyl orthosilicate (TEOS) are used as PECVD precursors very often [91].

3.5 Fragmentation of organosilicon compounds

The organosilicone molecules play a key role in plasma physical chemistry [92, 93]. However, they can be applied also for the understanding of fragmentation process. The understanding of structure–properties relations can be highlighted by the cases, which are structurally similar and have different response. Fragmentation of organosilicones by electron impact is the critical point with respect to plasma based CVD techniques. The presented study deals for the investigation of the role of organic content in organosilicones that differ by number of CH_3 functional groups in their structure. Particularly, we would like to find relation between primary chemical structure and fragmentation properties of the MPS, DMPS, and TMPS compounds. These three molecules have similar structure, however, their electron fragmentation products according to the mass spectra proved to be significantly different. The reason is

probably that the detailed individual mechanisms may be specific for such three molecules. We found, that some reactions show common features. For example subtraction of two hydrogens from molecule runs sometimes step-by-step and in other cases it runs irregularly. The mechanism in two variants is present for all molecules. We believe that some reactions can be observed in general in the mechanism independently on molecule. We combine the quantum chemical simulations and experimental technique (mass spectra of fragments obtained by monochromatic electron impact) in order to find the most important reactions causing specific for the fragmented molecule.

In general, the molecular ions are not too stable under electron impact and they rapidly form various fragments. The process after the ionization depends on the energy profile of bond dissociation. The phenylsilane dissociation by the EII technique was described in the literature as typical example of similar compounds [94, 95]. The organosilicon molecules are also interesting from theoretical point of view. The silicone as a central atom has more complex electron orbitals than carbon atom in analogous molecules, and the C-Si bond is covalent. Some aspects of their fragmentation process are presented in literature. The fragmentation mechanism of the DMPS molecule shown by Scheme 1 was proposed [6].

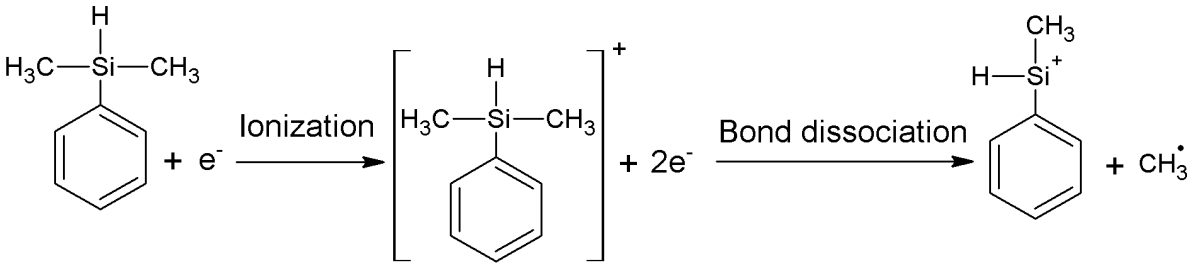

Scheme 1. Scheme of dimethylphenylsilane fragmentation process: Phase 1: electron induced ionization; Phase 2: bond dissociation; in Scheme is only example; in reality, the fragmentations can run in several ways according to the bond being cleaved [6].

The mechanism presented in Scheme 1 is as an example of one dissociation reaction for the DMPS molecule. However, the second phase, bond dissociation, can vary for different molecules. There can be large combination of the bonds being dissociated. We have investigated the fragmentation process initialized by the EII technique experimentally by mass spectra and theoretically by quantum chemistry calculations (DFT method). The fragmentation energy in the first approximation is calculated from the energies of fragmentation products and of original

molecule [36]. Later the mechanism from Scheme 1 was included also into theoretical models. T. Veszpremi et al. [96] calculated the ionization energy of the TMPS molecule and measured it based on the mass spectrum produced by ultraviolet photoelectron spectroscopy. Choe [19] calculated the dissociation energies required to lose benzene from the phenylsilane derivatives (except for TMPS molecule). The DFT calculations showed that the increase of methyl substituents at the silicon atom made the dissociation process easier.

4 Methods and models

Firstly, energies of molecule and its fragments are calculated using MOLPRO software. Secondly, these energies are applied to kinetic description of molecule fragmentation process.

4.1 *Ab initio* simulation

First of all, we need to set up MOLPRO program [97] that is an *ab initio* software package, which serves for calculating the molecular electronic structure by quantum chemical methods. Then, it is necessary to write and prepare input file that contains some information about the molecule (geometry of molecule), computational method, and basis set.

Concerning the molecule, we have to be acquainted with the geometry of the molecule that describes the shape of a molecule and the relative position of the atomic nuclei of a molecule. The geometry of molecule must be firstly described as input property, and then the computational chemistry program computes the gradients of the energy to find the molecular geometry corresponding to the lowest energy (minimum energy). The geometry of molecule may be given either in Cartesian coordinates for each atom or by using Z-matrix that defines connectivity between atoms in a molecule. This connectivity is described with three parameters, bond distances, bond angles, and dihedral or torsion angles [66]. The most important problem is the selection of the best method for calculation that may be the HF method or post-Hartree-Fock or DFT methods. The selection of method depends on the time required for calculation and the accuracy of calculation. Basis set is an important parameter. The best basis set is that gives an excellent agreement between the calculated results and experimental data. The output file contains information about an electronic structure of molecule and information regarding energies that can be used for geometry optimization, reaction energetics, and activation energies for kinetics.

4.2 Chemical kinetics

The calculated energies resulting from simulation using MOLPRPO software are the input data for kinetic description of fragmentation of molecule. The numerical model of kinetics can be described using software “Chemical Kinetics Simulator” (CKS) [98, 99]. This software is used to simulate the chemical reactions. For the calculation, the mechanism of fragmentation must be known. The fragmentation of propane molecule is shown in Figure 4.

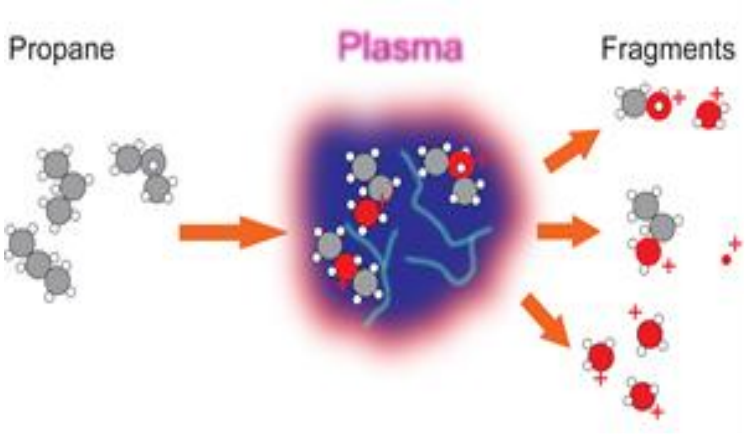

Figure 4. The fragmentation of propane molecule.

The activation energy for each partial reaction can be calculated as a difference in energy between products and reactants.

$$\Delta E = \sum E\ (prod.) - \sum E\ (react.) \tag{11}$$

Where *prod.* and *react.* are all products and reactants for the partial reaction. According to Arrhenius's equation, the kinetic constants are based on the values of activation energy and temperature as illustrated in the following equation.

$$k = A \exp\left(-\frac{\Delta E}{RT}\right) \tag{12}$$

Where k is the rate constant of chemical reaction, T is the absolute temperature in Kelvin, R is the gas constant, and A is the pre-exponential factor that depends on the vibrations of atomic bonds. The vibrations of bonds are calculated from infrared (IR) spectrum of molecule.

$$\upsilon = \frac{1}{2\pi}\sqrt{\frac{K}{\mu}} \tag{13}$$

Where K is the molecular force constant, υ is the vibrational frequency of bond, and μ is the reduced mass given by the following equation

$$\mu = \frac{m_1 . m_2}{m_1 + m_2} \tag{14}$$

The molecular force constant can be calculated from vibration energy according to the following equation.

$$E = h\,c\,\vartheta_{IR} = \frac{1}{2}\,K\,X^2 \tag{15}$$

Where ϑ_{IR} is wavenumber from infrared spectra. The result of the simulation of process kinetics using chemical kinetics simulator will be the concentrations of fragments versus time, pressure, and volume. Results can be displayed as graphs and tables.

4.3 Kinetic stability and chemical reactivity

The LUMO-HOMO energy gap, dipole moment, and total energy have influence on the kinetic stability and chemical reactivity of a molecule. The HOMO and LUMO molecular orbitals are the most important orbitals in the molecule. These orbitals are named as the frontier molecular orbitals. The HOMO orbital acts as an electron donor and the LUMO orbital acts as the electron acceptor. The LUMO-HOMO energy gap plays an important role in determining the way the molecule interacts with other species and in characterizing the kinetic stability and chemical reactivity of the molecule. When the LUMO-HOMO energy gap is large, this indicates that the molecule is generally associated with a low chemical reactivity and high kinetic stability. On the contrary, the small LUMO-HOMO energy gap implies that the molecule has high chemical reactivity and low kinetic stability [100].

Dipole moment is an important property to probe the chemical reactivity of the molecule. This property is the measure of the molecular charge distribution and is given as a vector in three dimensions. Dipole moment has relation to the electronegativity, which is the power of an atom in a molecule to attract electrons to it. The increase of an electronegativity of atom leads to the increase of dipole moment [101]. Chemical reactivity usually increases with increase in dipole moment property (molecule is more polarizable) [102].

The total potential energy of the system affects its stability, where a system with low potential energy has high kinetic stability [103, 104].

4.4 Electron impact ionization

The fragmentation process can also be described experimentally. It was investigated the EII experiment for the MPS, DMPS and TMPS compounds using the mass spectrometry technique. The composition of fragmentation products from MPS and TMPS measured by this EII experiment is interpreted with respect to the ionization energy, appearance energies of fragments and bond dissociation energy of selected bonds. The results are compared to the previously published experimental data for DMPS molecule. Comparison with the theoretical bond dissociation energies calculated using the DFT calculations is presented.

We describe the mechanism, where the bond dissociation is preceded by the EII experiment while radical-ion appears. The radical ion can be subject of three types of fragmentation reactions: cleavage of σ bond, cleavage of two σ bonds, and cleavage with complex rearrangements [105]. The cleavage of single bonds can run serially. In some cases, the cleavage of bonds in the original molecule can be followed by destruction into fragments.

The complete description of the process needs many parameters such as ionization energies, appearance energy, and heats of formation. All the parameters must be known for the many radicals and ions. Some of the parameters (i.e. appearance energy, ionization energy) and mass spectra were presented in literature (Gaidis et al. [29], Dube et al. [106], Kuritka et al. [107], Kočišek et al. [6]).

The EII technique is the classical ionization method used in mass spectroscopy. By the EII reaction of molecule, the nature of fragmentation products formed can be assigned. The EII reaction can be expressed by the following equation:

$$M + e^- \rightarrow M^+ + 2e^- \qquad (16)$$

Where M^+ is the molecular ion that can have a stable form or may be subject of fragmentation or isomerization. The fragmentation products may be either fragment ions or radicals. We have measured the electron ionization of methylphenylsilane (molecular weight 122.24 g/mol) and trimethylphenylsilane (molecular weight 150.29 g/mol) molecules. Both samples are liquids and were obtained from Sigma-Aldrichs with high purity (≥98% for MPS and ≥99% for TMPS). The electron impact experiments were done using the crossed electron-molecule beam apparatus. The apparatus was described in detail in the work of Stano et al [108]. A schematic view of the main parts is shown in Figure 5.

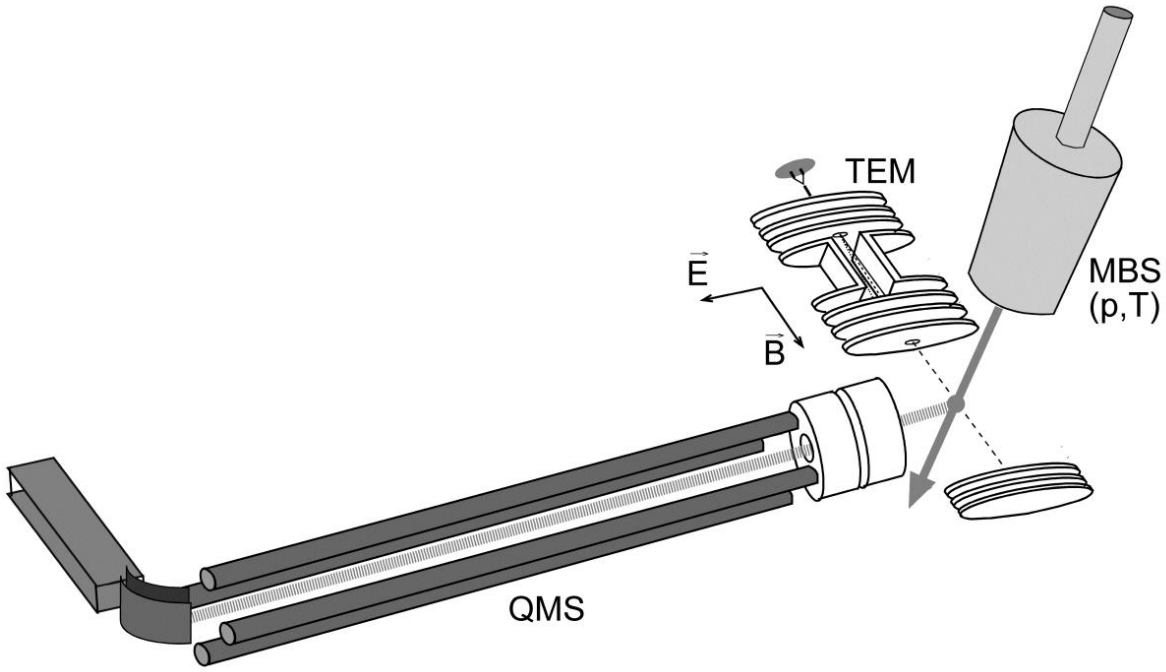

Figure 5. Schematic view of the apparatus. TEM- trochoidal electron monochromator, (QMS)-quadrupole mass spectrometer, MBS- molecular beam source, E- homogenous electric field, B-homogenous magnetic field [108].

The electron beam is formed by a trochoidal electron monochromator (TEM), where the electron energy resolution of the electron beam in present experimental study was 300 meV. The molecular beam is formed in the molecular beam source (MBS) by effusion of gas phase MPS/TMPS samples through a capillary (0.5 mm diameter and 4 mm long) into the reaction chamber. The temperature of the molecular beam source was ~300 K, and the pressure can be varied in the range (1-10) Pa. The molecular beam crosses perpendicularly the electron beam. Due to a weak electric field, the ions formed in the intersection volume are extracted into quadrupole mass spectrometer (QMS), where these ions can be analyzed. The calibration of the electron energy scale for the measured ion efficiency curves was carried out using the ionization energy for the reaction $Ar + e^- \rightarrow Ar^+ + 2e^-$ with an ionization energy of (15.759 ± 0.001) eV [109]. In our experimental study, we used two basic modes of operation. The first one is mass spectra, and the second mode is relative cross sections.

4.5 Mass spectra experiments

In this experiment, the standard mass spectra (relative abundances of the *m/z* products) for the MPS and TMPS compounds were recorded at constant electron energy of 70 eV. The mass spectrum of DMPS was taken from literature [6]. These mass spectra reflect the composition of molecule and give us the overview of fragmentation products.

4.6 Relative cross sections experiments

In our experiment, the ion efficiency as function of the incident electron energy (the relative cross section of ion) was measured for fixed *m/z* mass values. The appearance energies of the molecular ion and the corresponding ionic fragments were evaluated by fitting an expected dependence of ionization cross section on electron energy to a model function based on a Wannier threshold law [110].

$$\sigma(E) = b + a(E - AE)^d \tag{17}$$

Here *AE, b, a, d* are the variable fitting parameters, σ is an ionization cross section close to the ionization threshold, *E* represents electron energy, *b* is the background signal from the detector, *a* is a scaling factor, and *d* is an adjustable exponential factor. The fitting procedure is a convolution of the expected cross section and monochromatized electron energy distribution function, which is assumed to be Gaussian function. If there are two ionic states close to the threshold region (the case for the calibration gas Ar^+), other parameters can be added to previous Wannier threshold law.

$$\sigma(E) = b + a_1(E - AE_1)^{d_1} + a_2(E - AE_2)^{d_2} \tag{18}$$

In this case, the fitting procedure contains seven independent variables. Bond dissociation energy (AB^+-C) can be derived from the ionization (ABC^+) and appearance energy (AB^+) or from two corresponding appearance energies (for (A^+-B) from (AB^+) and (A^+)).

In the literature, the fragmentation of simple systems was mostly focused to the study of electron impact phase [111, 112]. The process was studied experimentally and theoretically in order to analyze detailed aspects of the process such as ionization cross section of molecules that is the probability of an ionization process during an electron impact. The experimental description of the process was focused to electron impact cross section of molecule [113, 114].

The electron impact cross-section is efficient part of atom cross-section, where electron can induce ionization and thus it determines the ability of ionization of given molecule or atom. Most of authors describe the cross-section to the charge +1, however, the cross-sections for ionization to the charge +2 and +3 can be measured, too [115]. The cross-section can be calculated theoretically using different theoretical models such as binary encounter dipole (BED) models [116, 117].

5 Results and discussion

Our calculations were performed using quantum chemistry computations, where *ab initio* and DFT calculations were used to compute some chemical properties for selected compounds. MOLPRO program was used to make simulations [97]. The calculations can be divided into three main groups:

- Quantum chemistry computations of simple molecule (propane)
- Anlysis of complex compounds (organisilicones)
- New approach to the fragmentation process

5.1 Quantum chemistry computations of simple molecule (propane)

Some selected properties for propane were investigated through:

- The influence of computational method on simulation
- The influence of basis set on simulation
- Calculation of the PES in ground and excited state.
- Calculation of kinetics

5.1.1 The choice of computational method

Geometry optimization or energy minimization is used in computational chemistry to find the lower energy shape that corresponds to equilibrium structure of molecule (minima on the PES graph). The influence of method was investigated on propane molecule. Geometry optimization was calculated using the same basis set 6-311G(d,p) and different methods such as HF, MP2, MP3 (third-order Møller-Plesset perturbation theory), MP4, CI, QCISD, QCISD(T), CCSD, CCSD(T), multireference configuration interaction (MRCI), and the DFT(B3LYP) method. Predicted results of energy minimization are shown in Figure 6.

Evidently, the DFT(B3LYP) calculation gives the lowest value of energy minimization. On the contrary, the HF calculation results the highest energy minimization. Concerning Møller-Plesset perturbation theory (MPn) methods, the energy minimization decreases with the increase of the order of the perturbation (n), where MP2>MP3>MP4. Energy minimization using the CI methods decreases with the increase of excitations CI> QCISD>QCISD(T). The CC methods have the same result like in the CI methods, where the energy minimization CCSD>CCSD(T).

The CI and MRCI methods have the same exact results. Results of CCSD(T) and QCISD(T) methods are relatively similar.

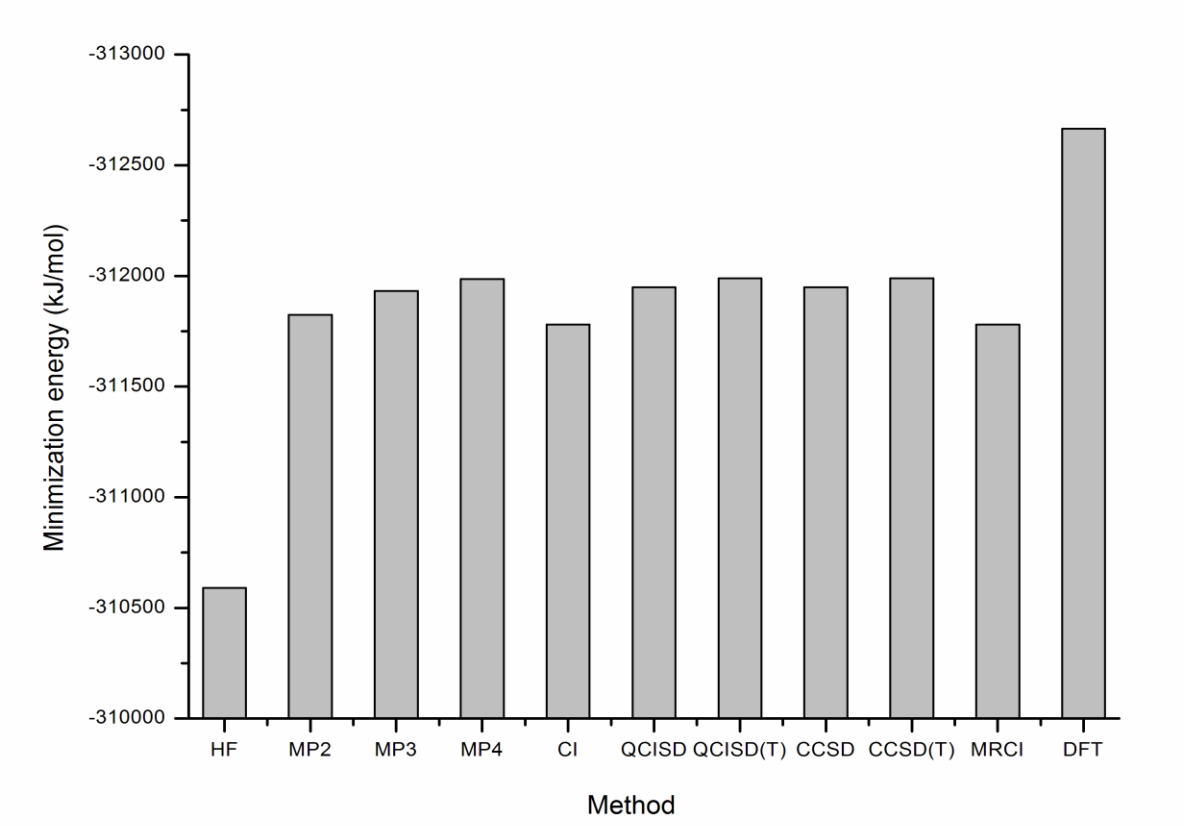

Figure 6. Energy minimization of C_3H_8 using different methods with the same basis set 6-311G(d,p).

Molecular orbitals can be used to explain the distribution of charge and dipole moment for the molecule. The calculations of molecular orbital energies specifically, the HOMO and LUMO energies were performed to determine the energy gap between HOMO and LUMO orbitals. Firstly, molecular orbitals MOs of C_3H_8 molecule were calculated using MOLPRO software [97]. Secondly, molecular orbitals were visualized using visual molecular dynamics (VMD) program [118]. According to this calculation, it has been found that propane molecule has 23 molecular orbitals. The HOMO and LUMO energies were calculated using different methods with the same basis set 6-311G(d,p). From the energy gap between HOMO and LUMO orbitals, wavelengths at which the compound can absorb the light were calculated and compared with maximum absorption of ultraviolet and visible spectra (λ_{max} is approximately equal to 135 nm

[119]). The calculated values of HOMO energy, LUMO energy, LUMO-HOMO energy gap, and wavelength of propane are shown in Table 5.

Table 5. HOMO energy, LUMO energy, LUMO-HOMO energy, and wavelength of C_3H_8 molecule calculated using different methods and the same basis set 6-311G(d,p).

Method	HOMO energy (kJ/mol)	LUMO energy (kJ/mol)	LUMO-HOMO energy (kJ/mol)	λ_{max} (nm)
HF	-1231.73	412.53	1644.26	72.88
MP2	-1228.58	411.39	1639.97	73.07
MP3	-1229.41	411.08	1640.49	73.05
MP4	-1228.33	410.40	1638.73	73.13
CI	-1229.89	412.04	1641.93	72.99
QCISD	-1228.15	410.61	1638.76	73.13
QCISD(T)	-1228.24	410.27	1638.51	73.14
CCSD	-1228.21	410.65	1638.86	73.12
CCSD(T)	-1228.25	410.29	1638.54	73.14
MRCI	-1229.89	412.04	1641.93	72.99
DFT(B,LYP)	-741.64	67.59	809.23	148.09

As can be seen from Table 5, the HF and post-Hartree-Fock methods give relatively similar values of LUMO-HOMO energy gap. The LUMO-HOMO energy gap calculated using the DFT(B,LYP) method is smaller than that of the HF and post-HF methods. The small value of energy gap indicates that the molecule can be easily excited and there is easier decomposition of bond. Wavelengths calculated and measured show that the DFT method achieves more agreement with experiment compared with HF and post-HF methods. The 3D plots of the HOMO orbital, LUMO orbital, and electron density for propane molecule calculated using the DFT(B,LYP)/6-311G(d,p) method are shown in Figure 7.

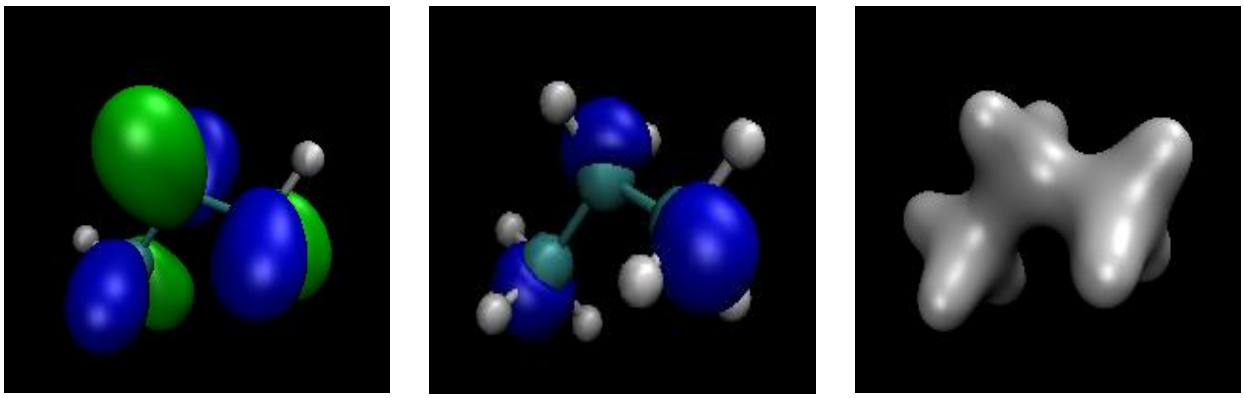

HOMO orbital LUMO orbital Electron density

Figure 7. Plots of HOMO orbital, LUMO orbital, and electron density of propane calculated using the DFT(B,LYP)/6-311G(d,p) method.

Calculations of geometry optimization of propane molecule were performed using the DFT calculations with the same basis set 6-311G(d,p) to test the DFT methods. Density functional methods used are standard Kohn-Sham density functional theory calculation using the spin-restricted (KS) form, Kohn-Sham density functional theory calculation using spin-unrestricted (UKS) form, Kohn-Sham calculation using Becke's exchange functional and the Lee-Yang-Parr correlation functional (KS,B,LYP), and the hybrid (B3LYP) functional consisting of weighted combinations of various density functionals together with a fraction of exact HF exchange (KS,B3LYP). Predicted results of energy minimization are shown in Figure 8. From figure 8, the DFT methods (RKS and UKS) give the same exact values of energy minimization. The DFT methods (B3LYP and B,LYP) yield relatively same energy minimization, but the energy calculated by the DFT(B,LYP) method is slightly smaller than of the DFT(B3LYP) method.

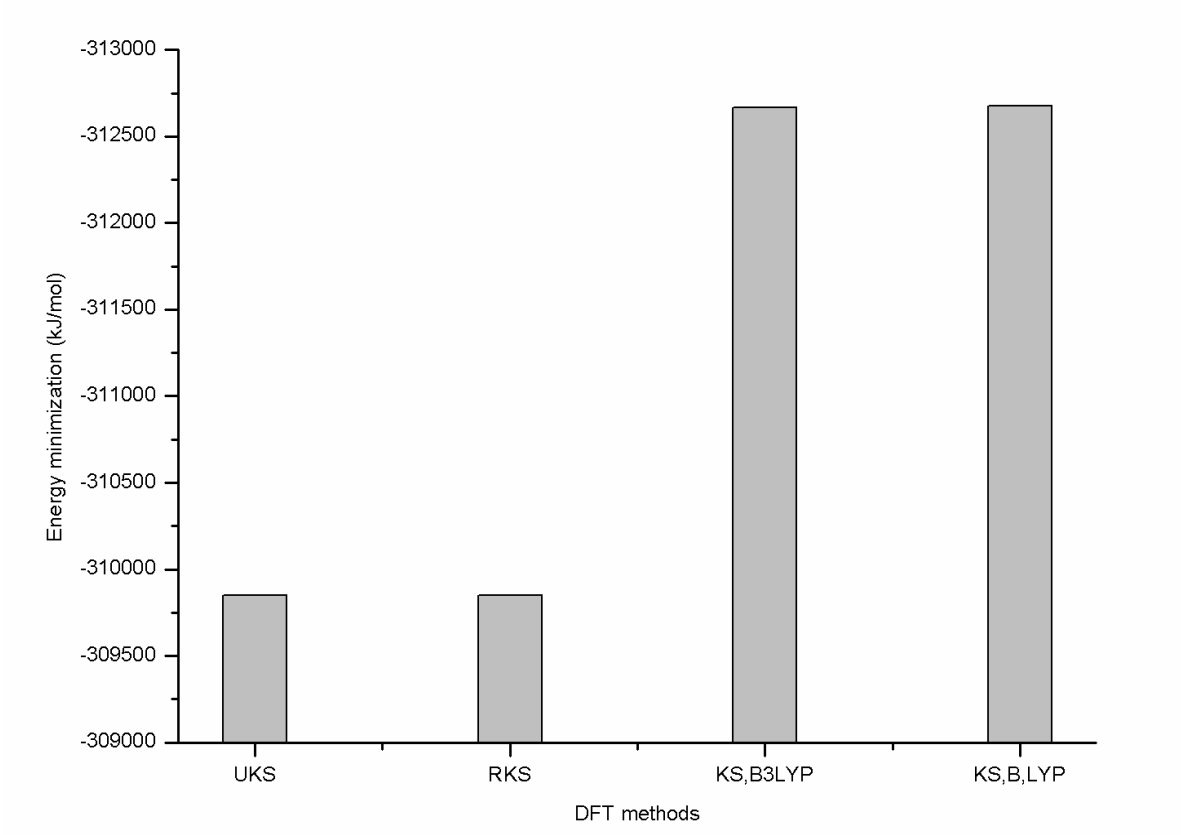

Figure 8. Geometry optimization of propane using the DFT methods and 6-311G(d,p).

The HOMO energy, LUMO energy, LUMO-HOMO energy gap, and wavelength were also calculated using the DFT [RKS, UKS, B3LYP, and (B,LYP)] methods and the same basis set 6-

311G(d,p) to test DFT calculations. Theoretical results of wavelengths were compared with the previous experimental value. Results of the DFT calculations for propane with 6-311G(d,p) basis set are shown in Table 6.

Table 6. HOMO energy, LUMO energy, LUMO-HOMO energy, and wavelength of C_3H_8 molecule calculated using DFT methods and 6-311G(d,p) basis set.

Method	HOMO energy (kJ/mol)	LUMO energy (kJ/mol)	LUMO-HOMO energy (kJ/mol)	λ_{max} (nm)
RKS	-735.19	52.60	787.79	152.12
UKS	-735.19	52.60	787.79	152.12
KS,B3LYP	-856.72	124.74	981.46	122.10
KS,B,LYP	-741.64	67.59	809.23	148.09

The DFT methods (RKS and UKS) give the same results of λ_{max}. Results of the DFT (B3LYP and B,LYP) methods are in better correlation with experiment in comparison with the DFT(RKS and UKS) methods.

The ionization energy of propane molecule was calculated using the DFT [RKS, UKS, B3LYP, and (B,LYP)] methods and the same basis set 6-311G(d,p) to test the DFT calculations. Theoretical results of ionization energies were compared with the experimental value (experimental ionization energy of propane is (11.01 ± 0.07) eV [120] and (10.9 ± 0.1) eV [121]. Results of the DFT calculations for propane with 6-311G(d,p) basis set are shown in Table 7.

Table 7. Ionization energy of of C_3H_8 molecule calculated using the DFT methods and 6-311G(d,p) basis set.

Method	C_3H_8 energy (eV)	$C_3H_8^+$ energy (eV)	Ionization energy (eV)
RKS	-3211.33	-3200.87	10.46
UKS	-3211.33	-3200.88	10.45
B3LYP	-3240.53	-3229.69	10.84
B,LYP	-3240.62	-3230.10	10.52

As shown in Table 7, the ionization energy calculated using the DFT(B3LYP)/6-311G(d,p) method has the best agreement with experiment compared with the other DFT methods.

5.1.2 The choice of basis set

The DFT(B3LYP) calculations with the variety of different basis sets were used to test the influence of basis set size on properties such as geometry optimization, HOMO energy, LUMO energy, LUMO-HOMO energy gap, and wavelength of propane molecule. Theoretical results of wavelength were compared with experimental value (λ_{max} ~ 135 nm). Predicted results of these properties are reported in Table 8.

It is clear from Table 8 that, the small basis set (STO-3G) gives the highest energy minimization, but the large basis set (V5Z) yields the lowest energy minimization. The comparison of calculated values of wavelengths with the experimental value shows that the large basis sets give better agreement with experiment in comparison to the small basis sets.

Table 8. Energy minimization, HOMO energy, LUMO energy, LUMO-HOMO energy, and wavelength of C_3H_8 molecule calculated using the DFT(B3LYP) method and different basis sets.

Basis set	Optimization energy (kJ/mol)	HOMO energy (kJ/mol)	LUMO energy (kJ/mol)	LUMO-HOMO Energy (kJ/mol)	Wavelength (nm)
STO-3G	-308866.97	-761.08	999.38	1760.46	68.07
3-21G	-310883.92	-843.48	323.26	1166.74	102.71
6-21G	-312255.55	-841.12	320.84	1161.96	103.13
6-31G	-312497.91	-842.28	257.97	1100.25	108.92
6-311G	-312566.82	-859.41	123.18	982.59	121.96
6-31G*	-312564.30	-843.02	260.72	1103.74	108.57
6-311G*	-312637.89	-859.16	124.20	983.36	121.87
6-31G**	-312592.98	-840.24	261.10	1101.34	108.81
6-311G**	-312665.46	-856.72	124.74	981.46	122.10
6-31+G*	-312575.66	-857.86	43.12	900.98	133.01
6-31+G**	-312603.24	-854.80	41.34	896.14	133.73
6-31++G**	-312603.47	-854.93	-22.49	832.44	143.96
6-311+G*	-312638.89	-860.11	23.10	883.21	135.68
6-311+G**	-312666.57	-858.30	22.17	880.47	136.11
6-311++G**	-312666.71	-858.33	-24.30	834.03	143.69
6-31G(3df,3pd)	-312612.16	-847.74	198.59	1046.33	114.53
6-311G(2df,2pd)	-312688.99	-856.42	110.32	966.74	123.96
6-311G(3df,3pd)	-312689.90	-857.10	100.92	958.02	125.09
6-311+G(2d,p)	-312673.73	-858.26	21.77	880.03	136.17
6-311+G(2d,2p)	-312682.65	-858.71	20.95	879.66	136.23
6-311++G(2d,2p)	-312682.71	-858.75	-23.67	835.08	143.50
6-311++G(3df,2p)	-312685.97	-858.29	-25.62	832.67	143.92
6-311++G(3df,3pd)	-312690.59	-858.24	-12.56	845.68	141.71
VDZ	-312569.31	-842.77	167.28	1010.05	118.65
VTZ	-312696.27	-856.78	103.37	960.15	124.81
VQZ	-312720.44	-858.22	66.25	924.47	129.63
V5Z	-312728.63	-858.61	41.93	900.54	133.07
aug-cc-pVDZ	-312594.45	-853.79	-29.95	823.84	145.46
aug-cc-pVTZ	-312697.91	-857.64	-19.17	838.47	142.92
aug-cc-pVQZ	-312721.48	-858.50	-20.41	838.09	142.99

The DFT(B3LYP) calculations with different basis sets were also studied to test the influence of basis set size on ionization energy of propane molecule. Theoretical results of ionization energy were compared with previous experimental data. Predicted results of ionization energy are given in Table 9.

The comparison of calculated values of ionization energies with the experimental data shows that the large basis sets give better correlation between theory and experiment in comparison to the small basis sets.

Table 9. Ionization energy of C_3H_8 calculated using the DFT(B3LYP) method and different basis sets.

Basis set	C_3H_8 energy (eV)	$C_3H_8^+$ energy (eV)	Ionization energy (eV)
STO-3G	-3201.16	-3190.80	10.36
3-21G	-3222.06	-3211.20	10.86
6-21G	-3236.28	-3225.44	10.84
6-31G	-3238.79	-3227.97	10.82
6-311G	-3239.51	-3228.57	10.94
6-31G*	-3239.48	-3228.67	10.81
6-311G*	-3240.24	-3229.35	10.89
6-31G**	-3239.78	-3229.03	10.75
6-311G**	-3240.53	-3229.69	10.84
6-31+G*	-3239.60	-3228.70	10.90
6-31+G**	-3239.88	-3229.05	10.83
6-31++G**	-3239.88	-3229.06	10.82
6-311+G*	-3240.25	-3229.36	10.89
6-311+G**	-3240.54	-3229.70	10.84
6-311++G**	-3240.54	-3229.70	10.84
6-31G(3df,3pd)	-3239.97	-3229.22	10.75
6-311G(2df,2pd)	-3240.77	-3229.95	10.82
6-311G(3df,3pd)	-3240.78	-3229.96	10.82
6-311+G(2d,p)	-3240.61	-3229.78	10.83
6-311+G(2d,2p)	-3240.71	-3229.87	10.84
6-311++G(2d,2p)	-3240.71	-3229.87	10.84
6-311++G(3df,2p)	-3240.74	-3229.91	10.83
6-311++G(3df,3pd)	-3240.79	-3229.96	10.83
VDZ	-3239.53	-3228.83	10.70
VTZ	-3240.85	-3230.03	10.82
VQZ	-3241.10	-3230.27	10.83
V5Z	-3241.18	-3230.35	10.83
aug-cc-pVDZ	-3239.79	-3229.02	10.77
aug-cc-pVTZ	-3240.86	-3230.04	10.82
aug-cc-pVQZ	-3241.11	-3230.28	10.83

5.1.3 Potential energy surface for propane molecule

The PES calculations of propane molecule in an electronic ground and excited states were investigated for understanding the relationship between the energy of propane molecule and its structure. This calculation was performed in two steps with considering of two parameters C-H and C-C bond lengths. The first step was the calculation of energies at different geometries by *ab initio* calculations. The second step was the use of calculated energies as input data in MATLAB software to get the PES graphs. The calculation of the PES in the ground and excited states was performed using the CCSD(T)/6-311G level of theory. Figures of PES of propane in ground and excited states are shown in Figures 9 and 10, respectively. Figure 9 explains the minimum energy for C-H and C-C bond lengths that corresponds to the equilibrium structure of molecule. Figure 10 shows that the potential energy of excited state increases when two atoms are approaching from each other, meaning that when the vibration stretching decreases.

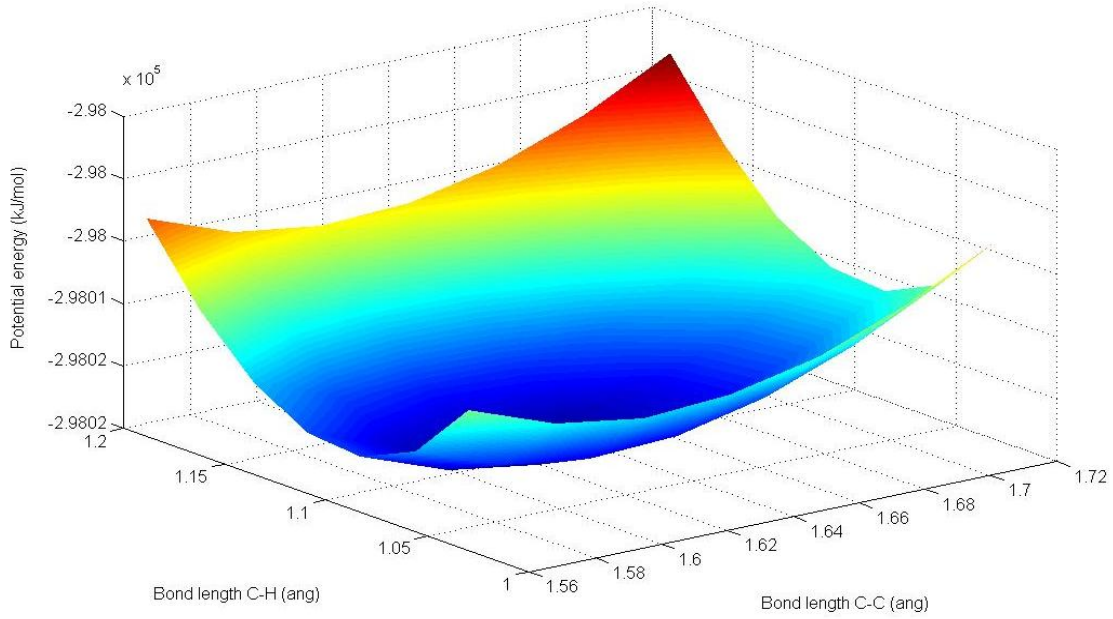

Figure 9. Potential energy surface of electronic ground state of propane using CCSD(T)/6-311G level.

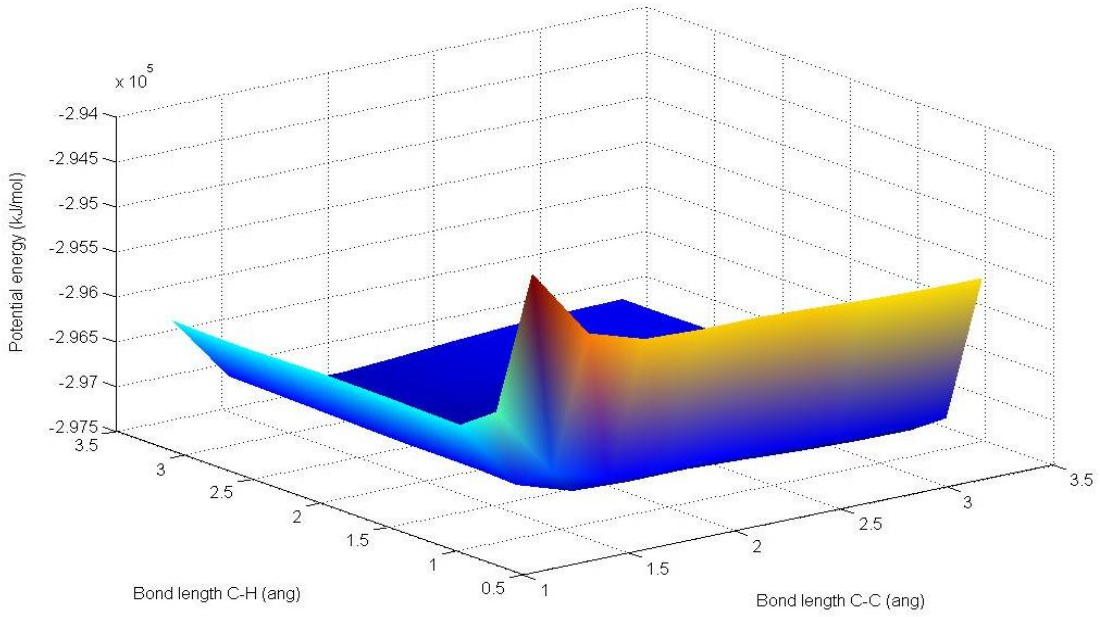

Figure 10. Potential energy surface of electronic excited state of propane using CCSD(T)/6-311G level.

5.1.4 Kinetics

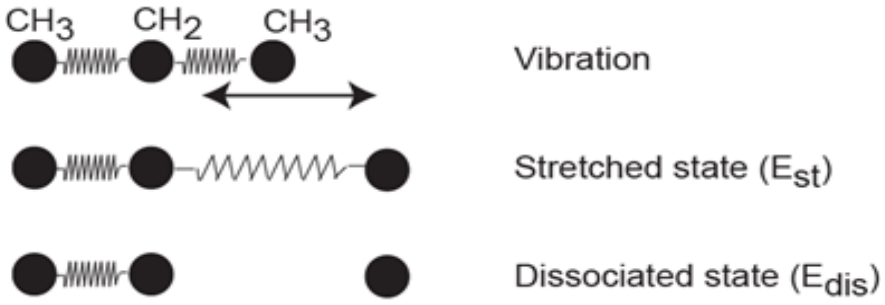

Figure 11. Mechanism of dissociation.

The fragmentation of propane molecule was calculated with considering of vibration (see Figure 11). The vibration of molecule is observed. It was assumed, that in the stretched state, the molecule can be dissociated. The probability of dissociation is driven by dissociation energy, which is the difference of energy in stretched state and energy in dissociated state.

Amplitude of vibration and equilibrium distances of C-H and C-C bond lengths are input data to calculate the energy of propane in vibrated state (Eq. 13-15). Vibration amplitude of bond was calculated by equation $E = \frac{1}{2} K X^2$ where K is force constant of bond and E is vibration energy of bond. Vibration energy was calculated by equation $E = h\vartheta$ where h is the Planck's constant and ϑ is the vibration frequency of bond. Vibration frequency was calculated from equation (13).

As it was mentioned, the activation energy (difference between the energy of products and the energy in vibrated state) was calculated for the PES in ground state (Figure 9). The Figure 9 describes the energy of two vibrations C-C at x-axis and C-H at y-axis.

1. Vibration of C-C bond, which leads to the dissociation of CH_3 group from propane.
2. Vibration of C-H bond, which leads to the dissociation of H atom from propane.

There are four states

1. Both C-C and C-H bonds are compressed (no dissociation of bond is expected).
2. C-C compressed and C-H stretched (only dissociation of H from molecule is expected).
3. C-H compressed and C-C stretched (only dissociation of CH_3 from molecule is expected).
4. Both bonds stretched (dissociation of both -CH_3 and H- bonds is expected).

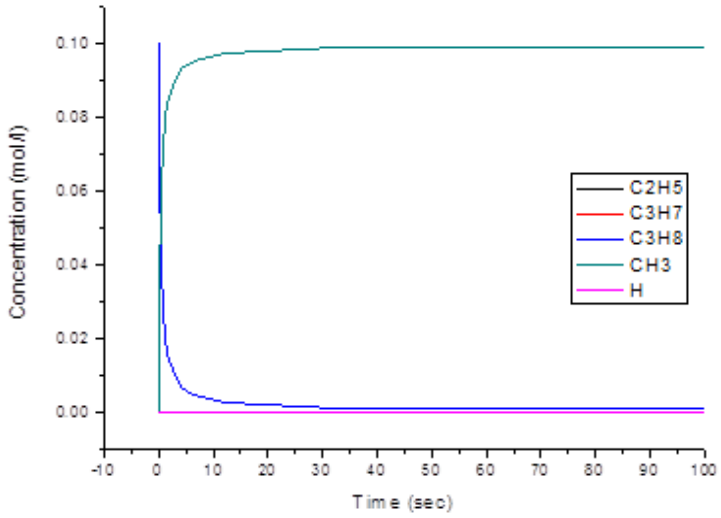

Figure 12. Kinetics of propane at 5000K.

The difference of C-C and C-H energies were calculated, when the bond was stretched (i.e. bond length was above the minimum in Figure 9). Activation energy and vibration frequency were introduced to chemical kinetics simulator to calculate the kinetics. Propane has two C-C bonds and eight C-H bonds. Therefore, there are the following partial reactions

$$8C_3H_8 \rightarrow 8C_3H_7 + 8H \qquad Ea_1 = 3988.49 \text{ kJ/mol} \qquad (19)$$

$$2C_3H_8 \rightarrow 2C_2H_5 + 2CH_3 \qquad Ea_2 = 1537.63 \text{ kJ/mol} \qquad (20)$$

For the calculation of kinetics, we considered a simulation with initial concentration of propane 0.1 mole/l. The change of concentration of products in time was calculated. Kinetics was calculated at normal temperature (300K). It was observed very long time of dissociation ($2\ 10^{194}$ sec). The influence of temperature was increased up to 5000K. Results of kinetic model at 5000K are shown in Figure 12. The model indicates that the decomposition of C-C bond will be more probable than the decomposition of C-H. It is in qualitative agreement with the observation from mass spectra of propane [26]. However, the dissociation of C-H is almost not observed in a model, whereas in real systems it is.

The behavior of model differs from behavior of real systems in many aspects. T. Kolke et al. [122] studied thermal decomposition of propane in the range of temperature (1300-1700K). The thermal decomposition of our model is observed at 5000K. One possible interpretation was, that the calculated activation energy is too high. We found several articles, where the dissociation

energy was experimentally measured and calculated. The comparison between the kinetic model, theory, and experiment of dissociation of C-C bond is shown in Table 10. Our model was different from theory and experiment. The reason is probably that the calculation was carried out using high activation energy. Our activation energy is significantly higher than those presented in literature.

Table 10. Comparison between model, theory, experiment of reaction $C_3H_8 \rightarrow C_2H_5 + CH_3$.

	Temperature (K)	Activation energy (kJ/mol)	Reference
Present work	5000	1537.63	
Theory	300-3000	382.77	[123]
	200-2500	369.10	[124]
	760-766	355.03	[125]
	1130-1250	300.15	[126]
Experiment	300-2500	357.52	[127]
	773-2500	370.83	[128]
	600-1653	407.49	[129]
	1000-1100	338.00	[130]
	743-803	364.17	[131]

The activation energy is usually a difference of two large numbers: energy of products-energy of propane.

$E_{propane}$= -297203.00 kJ/mol.

$E_{products}$= (-99668.10 for CH_3 and -195997.30 for C_2H_5) kJ/mol.

Such energies were similar to the energies obtained in the literature. However, the difference of energies ($E_{products}$-$E_{propane}$) is much smaller than absolute values of energies (1537.63 kJ/mol). So the small error of total energy (<1%) can lead to large error in activation energy. The total energy must be calculated very exactly in order to obtain realistic activation energy. The value of activation energy in ground state was calculated using HF/6-311G method. It was investigated influence of the method of calculation to the exactness of estimation. Another method CCSD(T)/6-311G was used instead of the HF method. The activation energy was not improved.

The results are probably sensitive to efficient geometry optimization of both products and propane. There can be also found influence of the basis set. In the present conditions, both the model and real system do not dissociate and the dissociation is observed at high temperature. However, there exist conditions, where the dissociation is accelerated. One of them is a molecule of propane in excited state. It is corresponding to the molecules after irradiation with UV light. The dissociation is then easier. Also the PES for excited state (Figure 10) has less deep energy

well than the PES of ground state (Figure 9). Next possibility is giving this model to plasma where it is supposed that the kinetics will be much quicker because in plasma, there is ionization step which will be relatively quick.

5.2 Analysis of complex compounds (organisilicones)

The MPS, DMPS, and TMPS are used as an example of complex compounds.

5.2.1 Characterization of materials

In this section, we present theoretical results of (IR) infrared spectra, harmonic vibrational frequencies, and the thermodynamic properties for the MPS, DMPS, and TMPS compounds. The DFT(B3LYP) calculations with 6-311++G(d,p) basis set were used to perform the computations. Infrared spectra of MPS, DMPS, and TMPS compounds are shown in Figures 13, 14, and 15, respectively.

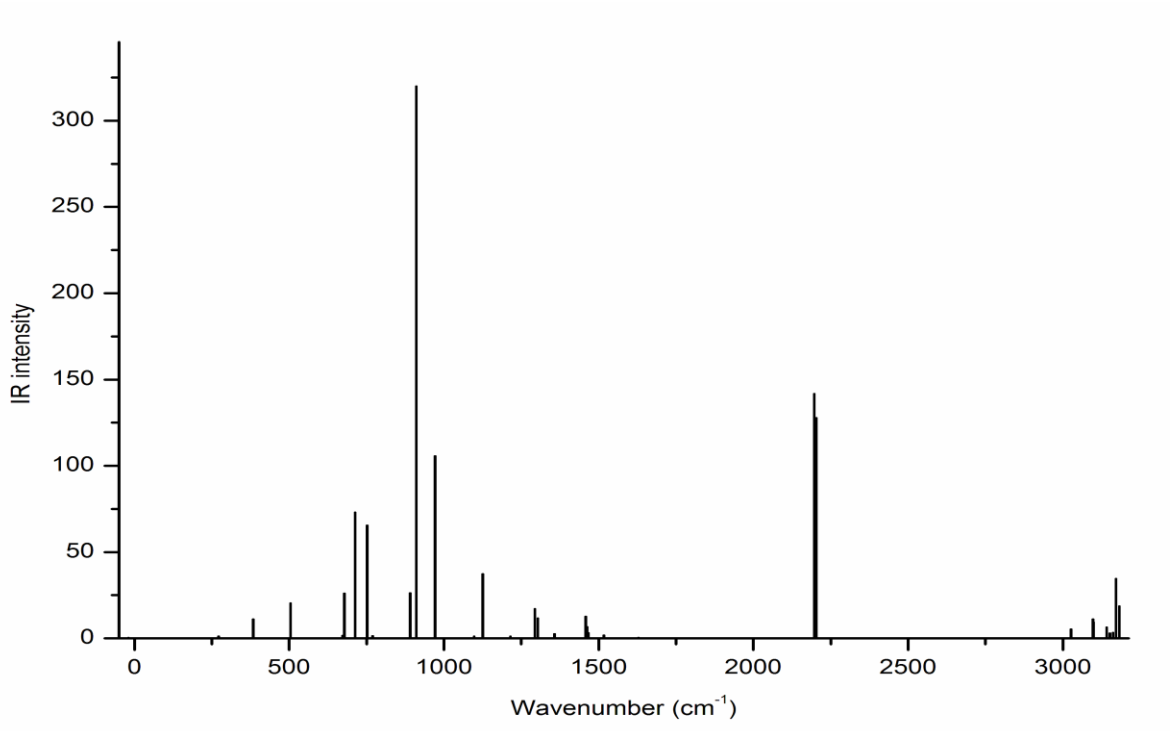

Figure 13. Infrared spectrum of methylphenylsilane calculated using the DFT(B3LYP)/6-311++G(d,p) method.

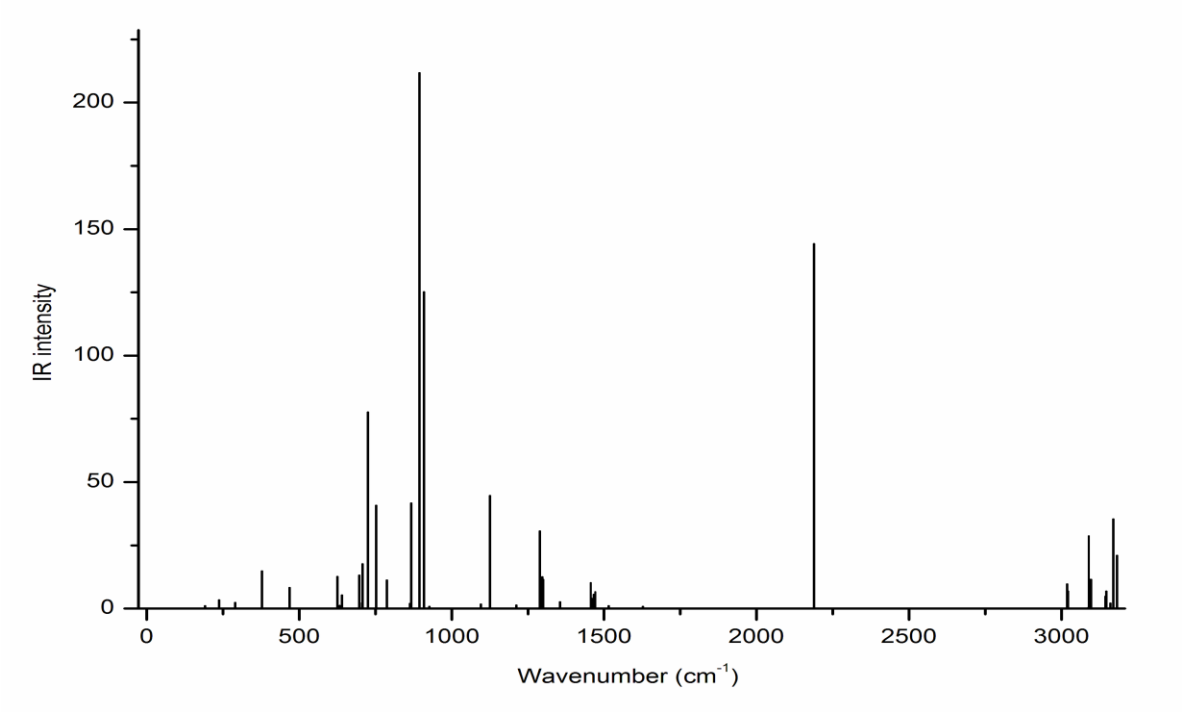

Figure 14. Infrared spectrum of dimethylphenylsilane calculated using the DFT(B3LYP)/6-311++G(d,p) method.

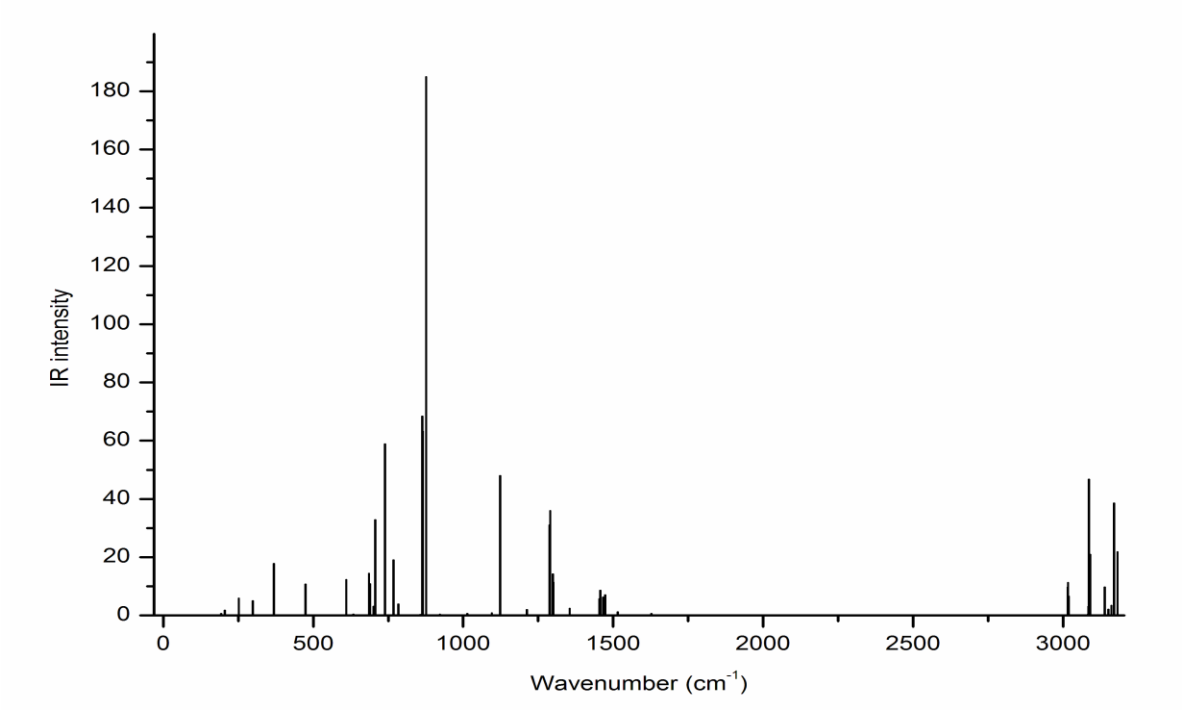

Figure 15. Infrared spectrum of trimethylphenylsilane calculated using the DFT(B3LYP)/6-311++G(d,p) method.

IR spectra are approximately similar, as these three molecules have similar structures. The main difference is the vibration of the Si-H bond, where it can be observed in MPS and DMPS, but there is not in TMPS. In IR spectra of MPS and DMPS, the Si-H bond is expected to be found at 2196.65 cm^{-1} and 2188.31 cm^{-1} wavenumbers, respectively.

Concerning the harmonic vibrational frequencies, it has been found that the fundamental number of vibrations in MPS, DMPS, and TMPS is 47, 56, and 65 vibrations, respectively. Therefore, the predicted bands in IR spectra are 47, 56, and 65 for MPS, DMPS, and TMPS, respectively.

The thermodynamic properties such as the zero-point vibrational energy (ZPVE), enthalpy H(T)-H(0), heat capacity C_v, and entropy S, then, thermal energies including ZPVE [H(T)-E(0) and U(T)-E(0)] have been calculated for standard temperature and pressure (T=298.150 K, P=1 atm). The thermodynamic properties of MPS, DMPS, and TMPS compounds are shown in Table 11. It is evident from Table 11 that, the zero-point vibrational energy (ZPVE) and thermal energies including ZPVE [H(T)-E(0) and U(T)-E(0)] have relations TMPS>DMPS>MPS.

Table 11. Thermodynamic properties of MPS, DMPS, and TMPS compounds calculated using the DFT(B3LYP)/6-311++G(d,p) method.

Parameter	MPS			DMPS			TMPS		
	H(T)-H(0) (kJ/mol)	C_v (J/mol.K)	S (J/mol.K)	H(T)-H(0) (kJ/mol)	C_v (J/mol.K)	S (J/mol.K)	H(T)-H(0) (kJ/mol)	C_v (J/mol.K)	S (J/mol.K)
Electronic	0.00	0.00	0.00	0.00	0.00	0.00	0.00	0.00	0.00
Translation	3.72	12.47	168.69	3.72	12.47	170.04	3.72	12.47	171.26
Rotation	3.72	12.47	120.79	3.72	12.47	124.07	3.72	12.47	126.51
Vibration	12.80	102.49	70.36	17.50	129.22	100.70	22.70	157.74	133.95
Volume RT	2.48	0.00	0.00	2.48	0.00	0.00	2.48	0.00	0.00
Total	22.72	127.43	359.84	27.42	154.16	394.81	32.62	182.68	431.72
ZPVE		377.75			452.77			526.70	
H(T)-E(0)		400.47			480.19			559.32	
U(T)-E(0)		397.99			477.71			556.84	

5.2.2 Kinetic stability and chemical reactivity analysis

The more complicated compounds such as MPS, DMPS, and TMPS were analyzed by the DFT calculations. The energy gap between the HOMO energy, LUMO energy, dipole moment, electronegativity, and total energy have been calculated to reflect the chemical reactivity and kinetic stability of the compounds. The DFT method at the B3LYP/6-311++G(d,p) level of theory was used to calculate the optimized geometric structures and perform simulations. The HOMO energies, LUMO energies, LUMO-HOMO energy gaps, dipole moments,

electronegativities, and total energies for the MPS, DMPS, and TMPS compounds calculated using the DFT(B3LYP)/6-311++G(d,p) level of theory are reported in the Table 12.

Table 12. Some molecular properties of MPS, DMPS, and TMPS compounds calculated using the DFT(B3LYP)/6-311++G(d,p) level of theory.

Compound	HOMO energy (eV)	LUMO energy (eV)	LUMO-HOMO Energy gap (eV)	Dipole moment (Debye)	Electronegativity (eV)	Total energy (eV)
MPS	-6.89	-0.56	6.33	0.77	3.72	-15296.25
DMPS	-6.82	-0.48	6.34	0.56	3.65	-16365.95
TMPS	-6.75	-0.40	6.35	0.04	3.57	-17435.64

From the calculations made using the DFT(B3LYP)/6-311++G(d,p) method (Table 12), the E_{HOMO}-E_{LUMO} energy gap of TMPS (6.35 eV) is greater than that of DMPS (6.34 eV) and MPS (6.33 eV). This suggests that TMPS compound would be of higher kinetic stability than DMPS and MPS compounds. The higher kinetic stability of TMPS compound would indicate a lower chemical reactivity relative to DMPS and MPS compounds.

According to our theoretical calculations, the dipole moment of MPS (0.77 D) is greater than that of DMPS (0.56 D) and TMPS (0.04 D). This indicates that MPS compound would have a higher chemical reactivity than DMPS and TMPS compounds, which would implies that MPS would be less stable than DMPS and TMPS compounds. From the calculated HOMO and LUMO molecular orbital energies, given in Table 12, the electronegativity of compounds are derived. It is clear that, the MPS compound is the most reactive compound due to the highest electronegativity.

The results obtained by B3LYP/6-311++G(d,p) method concerning total energies also support LUMO-HOMO energy gap, dipole moment, and electronegativity results, where they show that TMPS compound has the lowest total energy with comparison to DMPS and MPS compounds. This indicates that TMPS is the most stable compound among these organosilicones.

The optimized geometric structures, 3D plots of HOMO and LUMO molecular orbitals, and 3D plots of electron densities for MPS, DMPS, and TMPS compounds calculated using the DFT(B3LYP)/6-311++G(d,p) method are presented in Table 13. According to results of properties: frontier orbital LUMO-HOMO energy gap, dipole moment, electronegativity, and total potential energy (Table 12) calculated using the DFT(B3LYP)/6-311++G(d,p) method, the MPS compound has the highest chemical reactivity and the lowest kinetic stability in comparison with DMPS and TMPS compounds, and vice versa.

Table 13. Optimized structures and 3D plots of molecular orbitals (HOMO and LUMO) and electron density of MPS, DMPS, and TMPS compounds calculated using the DFT(B3LYP)/6-311++G(d,p) method.

Compound	HOMO orbital	LUMO orbital	Electron density
MPS	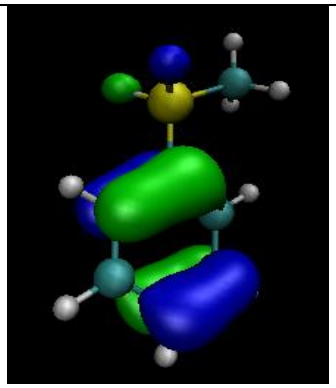	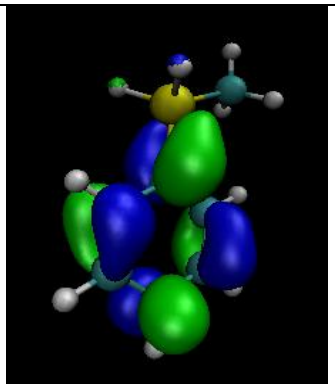	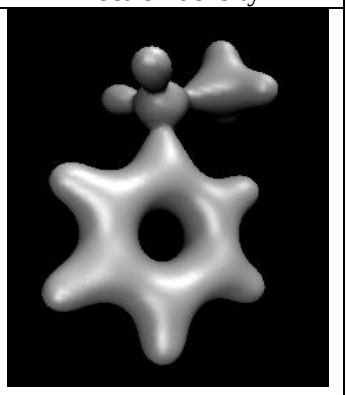
DMPS	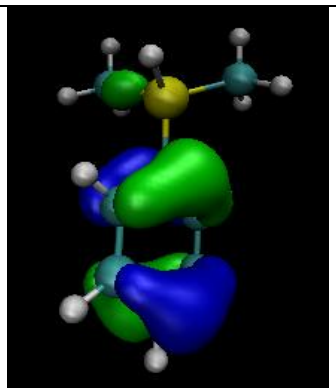	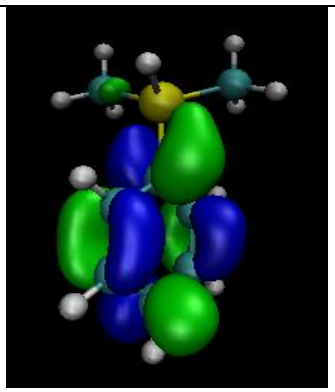	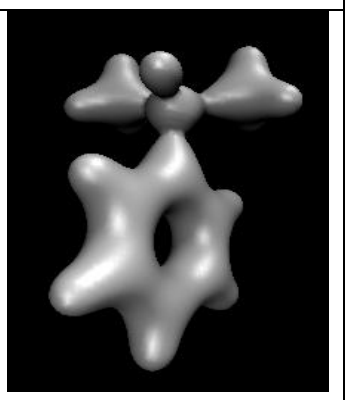
TMPS	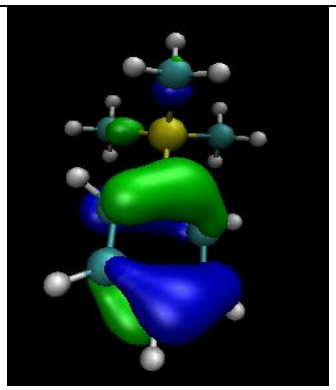	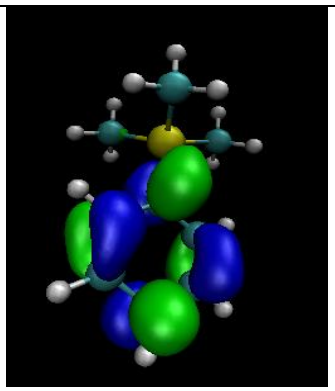	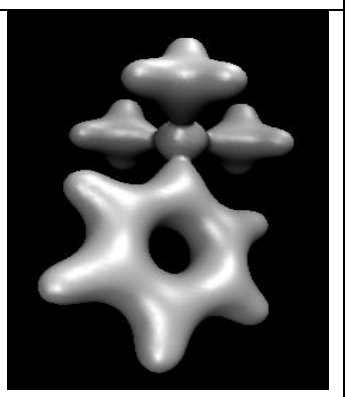

5.2.3 Mass spetcra

Organosilicon compounds such as MPS, DMPS, and TMPS were analyzed by the DFT calculations. The analysis was also supported by electron impact experiment. Electon impact ionization technique was applied to MPS and TMPS compounds to carry out two types of experiments

- Mass spectrum experiment
- Relative cross section experiment

The first type of electron impact experiments is the determination of mass spectrum of the sample.

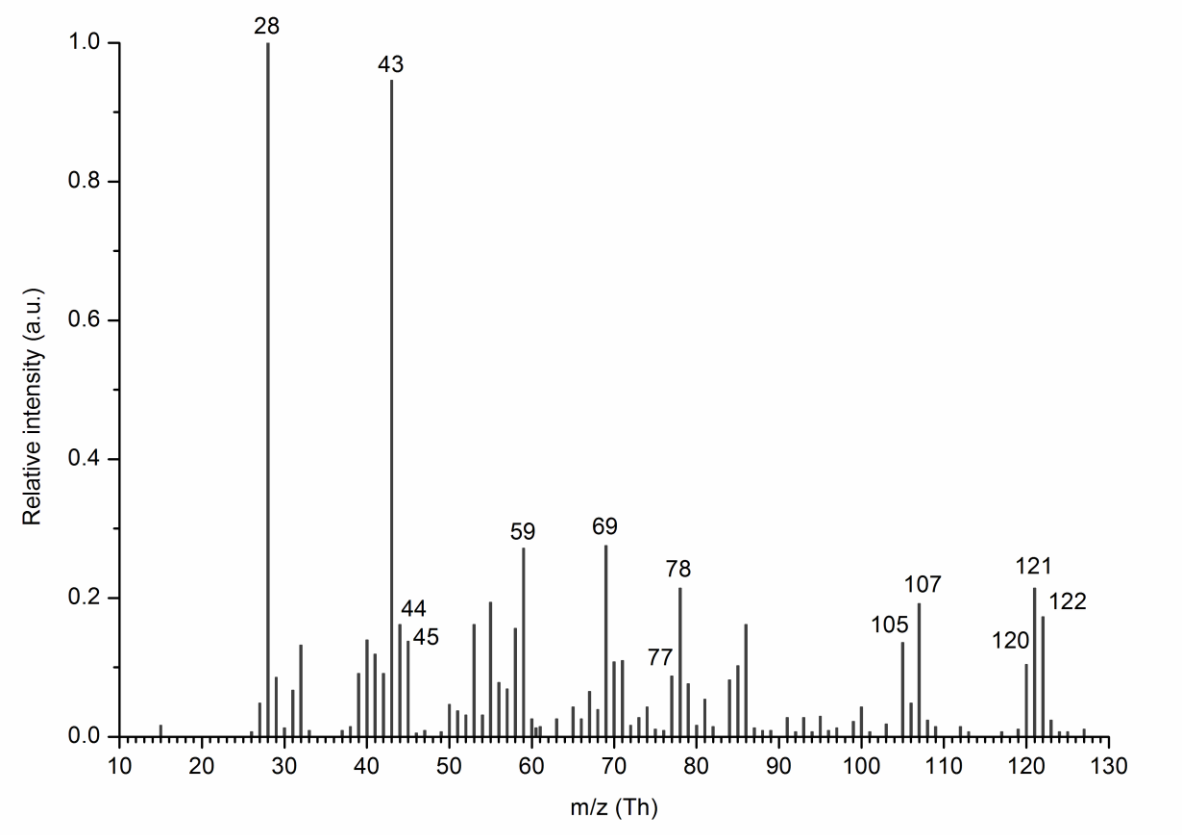

Figure 16. Electron impact mass spectrum of methylphenylsilane at electron energy of 70 eV.

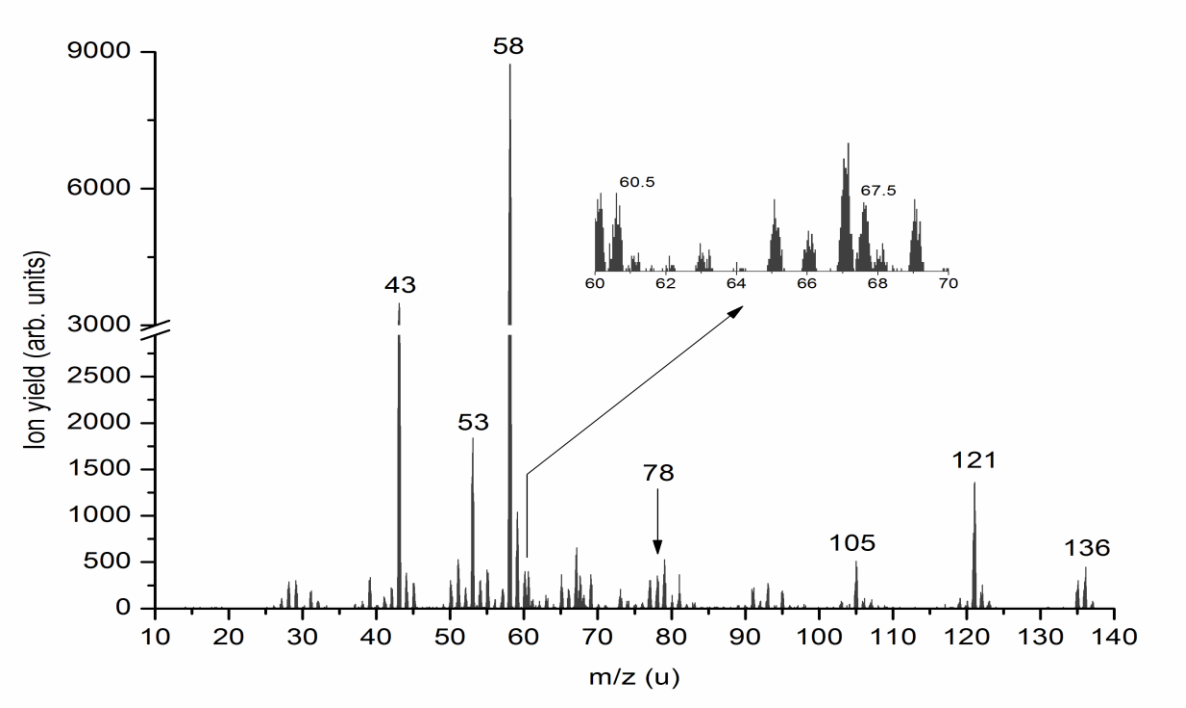

Figure 17. Electron impact mass spectrum of dimethylphenylsilane at electron energy of 70 eV [6].

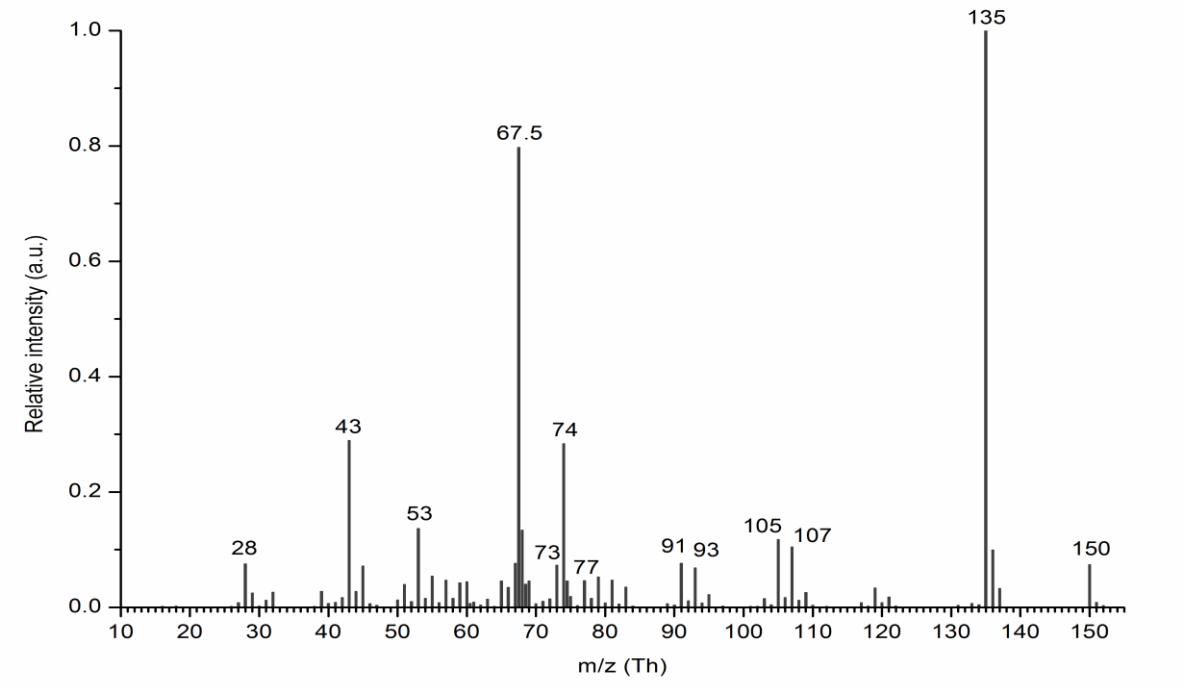

Figure 18. Electron impact mass spectrum of trimethylphenylsilane at electron energy of 70 eV.

The mass spectra of MPS (Figure 16), and TMPS (Figure 18) were measured. They reflect the composition of molecule and give us the overview of fragmentation products. The remaining mass spectrum of DMPS (Figure 17) was taken from the work of Kočišek et al. [6], which was measured with similar methodology. We found that the MPS, DMPS, and TMPS compounds have significantly different mass spectra and fragmentation products. The mass spectrum contains general information about all fragmentation products. We cannot assign the products to individual steps in Scheme 1. The mechanism enables the molecule number of combinations of different partial reactions. Each step of fragmentation process was analyzed for each compound (MPS, DMPS and TMPS). In all steps we analyzed, whether the fragmentation of compounds is similar or it is different. The initial hypothesis is, that the spectra are different as the molecules have different number of hydrogens and methyl groups attached to the Si atom. The peaks from mass spectra are summarized in Table 14.

Table 14. The expected ions and their corresponding masses for MPS, DMPS, and TMPS compounds. *m/z* – x axis of mass spectra; Reaction – origin of fragment: ***I*** – ionization reaction; ***P*** – primary bond cleavage; ***C*** – consecutive reaction; ***N*** – not known; ***DI*** – double ionization; ***DP*** – double ionization with primary bond cleavage.

MPS			DMPS			TMPS		
m/z	Fragment	Reaction	*m/z*	Fragment	Reaction	*m/z*	Fragment	Reaction
122	$C_6H_5SiH_2CH_3^+$	I	136	$C_6H_5SiH(CH_3)_2^+$	I	150	$C_6H_5Si(CH_3)_3^+$	I
121	$C_6H_5SiHCH_3^+$	P	135	$C_6H_5Si(CH_3)_2^+$	P	135	$C_6H_5Si(CH_3)_2^+$	P
120	$C_6H_5SiCH_3^+$	C	121	$C_6H_5SiHCH_3^+$	P	107	$C_6H_7Si^+$	C
107	$C_6H_5SiH_2^+$	P	106	$C_6H_5SiH^+$	C	105	$C_6H_5Si^+$	C
105	$C_6H_5Si^+$	C	105	$C_6H_5Si^+$	C	77	$C_6H_5^+$	P
78	$C_6H_6^+$	C	79	$C_6H_7^+$	N	74	$C_3H_{10}Si^+$	N
77	$C_6H_5^+$	P	78	$C_6H_6^+$	C	73	$(CH_3)_3Si^+$	P
69	$C_3H_5Si^+$	N	77	$C_6H_5^+$	P	67.5	$C_6H_5Si(CH_3)_2^{++}$	DP
59	$C_2H_7Si^+$	N	68	$C_6H_5SiH(CH_3)_2^{++}$	DI	53	C_2HSi^+	N
45	CH_5Si^+	P	67.5	$C_6H_5Si(CH_3)_2^{++}$	DP	43	CH_3Si^+	C
44	CH_4Si^+	C	60.5	$C_6H_5SiHCH_3^{++}$	DP			
43	CH_3Si^+	C	59	$(CH_3)_2SiH^+$	P			
28	$C_2H_4^+$, N_2, $C_2H_4^+$	N	58	$(CH_3)_2Si^+$	C			
			43	CH_3Si^+	C			

The Table 14 shows also information about origin of the fragments. The fragments from mass spectra, which appeared during ionization (I) can be detected unambiguously. Then, there can be predicted, which fragments can appear during the primary bond cleavage (P). Then there are compounds, which appear during consecutive reactions (C). We did not detect the origin of some fragments (N), but they show small peak in mass spectra. As mentioned above, the consecutive reactions are described more in detail.

5.2.4 Cross sections

The second type of electron impact experiments is the determination of the relative cross section of ionic fragments resulting from the fragmentation process. The primary results of experiment were the functions of signal intensity depending on initial energy (Figures 19 for MPS and 20 for TMPS). Initial energy is considered as energy of electron before impact. The data were fitted according to the Wannier law (equation 17). The results of fitting are the ionization threshold values. We measured them for selected ionic fragments of MPS and TMPS compounds. The ionization threshold for DMPS was taken from literature (Table 16).

The measurement of cross section is time consuming experiment. Therefore, it is advantageous to have possibility to calculate it theoretically. Moreover, the measurement of cross section is pre-requisite to the bond dissociation energy. Mapping the fragmentation of some complex molecule could be consuming to experimental time. The calculated energy must be corresponding to the experimental one. This is the reason why ionization energy will be calculated in the next section.

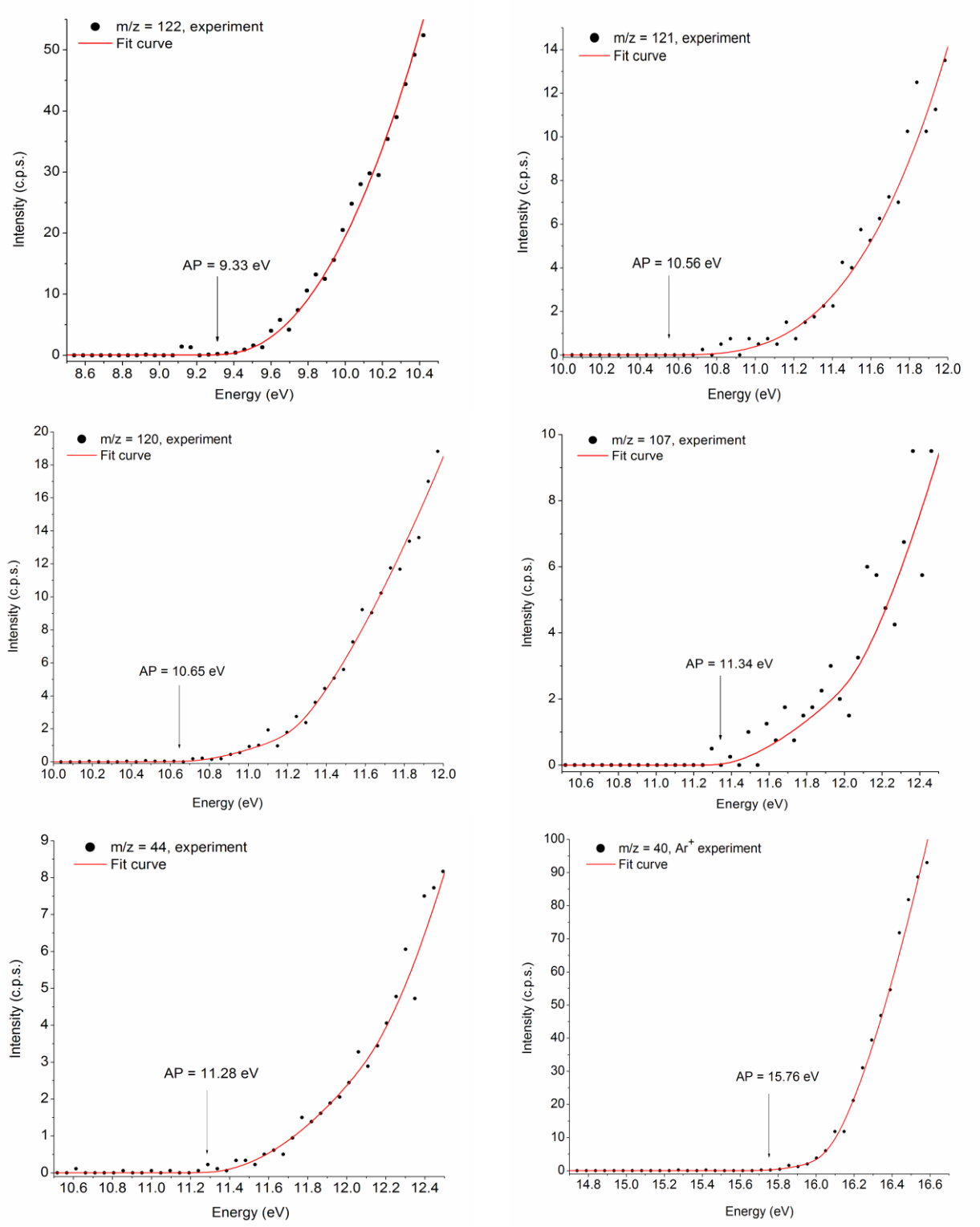

Figure 19. Ion efficiency curves near the threshold region for selected ionic fragments methylphenylsilane. The measured data are shown as dark circles; the fit curves are shown as solid lines. Arrows indicate the ionization energies derived by the fitting procedure described in text.

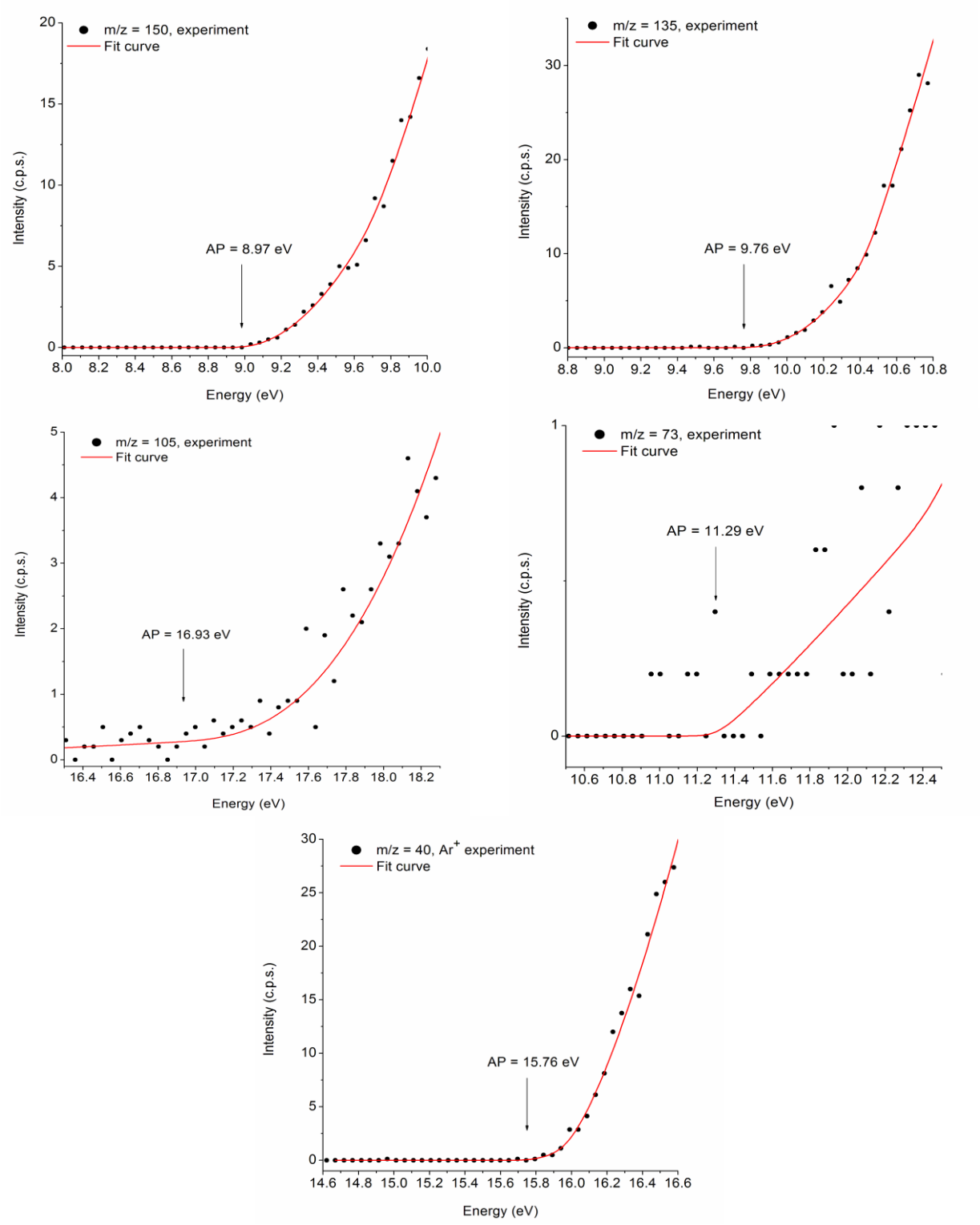

Figure 20. Ion efficiency curves near the threshold region for selected ionic fragments trimethylphenylsilane. The measured data are shown as dark circles; the fit curves are shown as solid lines. Arrows indicate the ionization energies derived by the fitting procedure described in text.

5.2.5 Density functional theory (DFT) calculations

The computations were performed with MOLPRO program package [97]. The DFT calculations were performed to support experimental study. The Z-matrices of MPS, DMPS, and TMPS compounds and their fragments were edited by MOLDEN package [118]. Structures were optimized using the DFT calculations at the B3LYP level of theory using different basis sets. The influence of the size of basis set on some calculations will be presented later. In our main calculations, we present only the results with optimal 6-311++G(d,p) basis set. The optimized geometrical structures were calculated and their energies were taken into account to compute ionization energies as well as bond dissociation energies. Appearance energies for cationic fragments were calculated from ionization energies and bond dissociation energies.

5.3 Fragmentation mechanism of organosilicones

We describe some details of the fragmentation mechanism, which consists of ionization, primary cleavage of bond, and consecutive cleavage of bonds followed by subtraction of primary fragmentation products. All the steps were described both experimentally, and by the DFT calculations. We will focus to the consecutive reactions, so the ionization and primary cleavage will be described more briefly.

5.3.1 Ionization

The ionization is the first phase of fragmentation. It can be assumed, that the reactivity of compounds is influenced by stability of cations which appear during fragmentation. The Scheme 2 shows the ionization process of the MPS, DMPS, and TMPS compounds. It is a formation of the $MPS^{+\bullet}$, $DMPS^{+\bullet}$, and $TMPS^{+\bullet}$ metastable molecular ions.

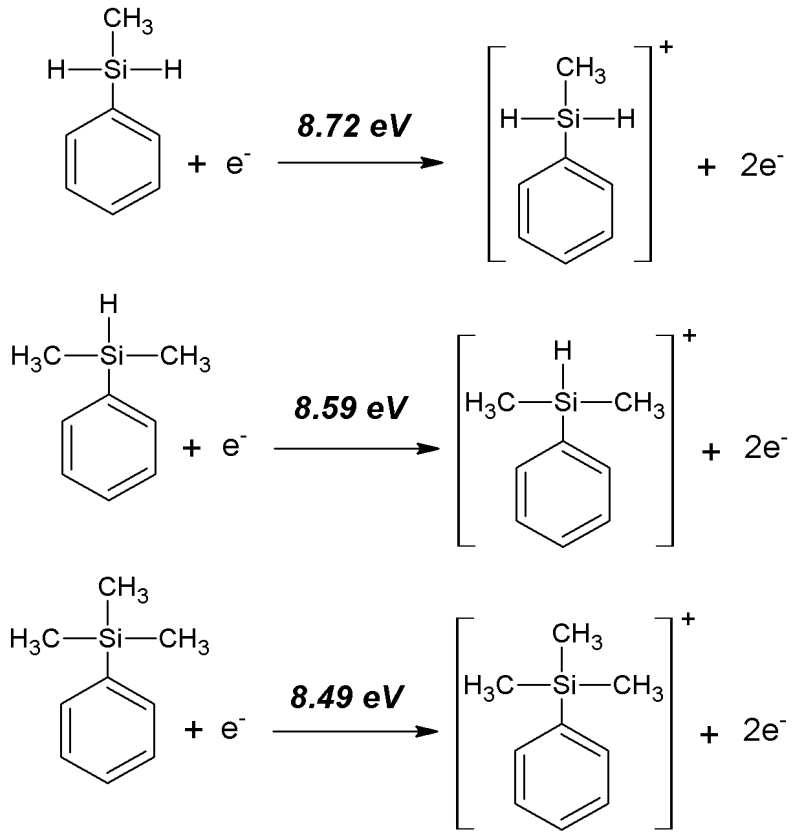

Scheme 2. Scheme of ionization process of the MPS, DMPS, and TMPS compounds.

The optimized geometric structures of MPS, DMPS, and TMPS compounds and their corresponding cations (MPS^+, $DMPS^+$, and $TMPS^+$) are presented in Table 15 including some main bond lengths calculated using the DFT(B3LYP)/6-311++G(d,p) method. It is evident from Table 15 that, the optimized geometry of neutral molecule is different from the optimized geometry of its cation.

The ionization energies for MPS and TMPS neutrals were experimentally measured using previously described fitting procedure from the near threshold part of relative cross sections. The ionization energies of MPS, DMPS, and TMPS compounds were also calculated as the energy difference between the neutral molecule and its cation. The individual energies were calculated from the DFT simulation using B3LYP/6-311++G(d,p) method (Table 16).

Table 15. Optimized geometric structures of MPS, DMPS, and TMPS compounds and their corresponding cations (MPS^+, $DMPS^+$, and $TMPS^+$) calculated using the DFT(B3LYP)/6-311++G(d,p) method; numbers at bonds are bond lengths in Angstrom.

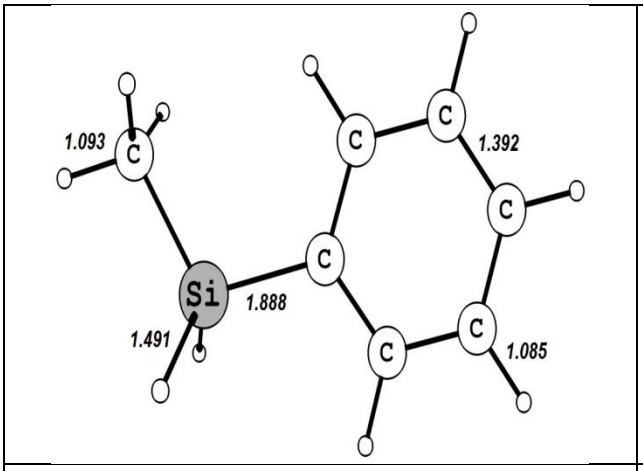	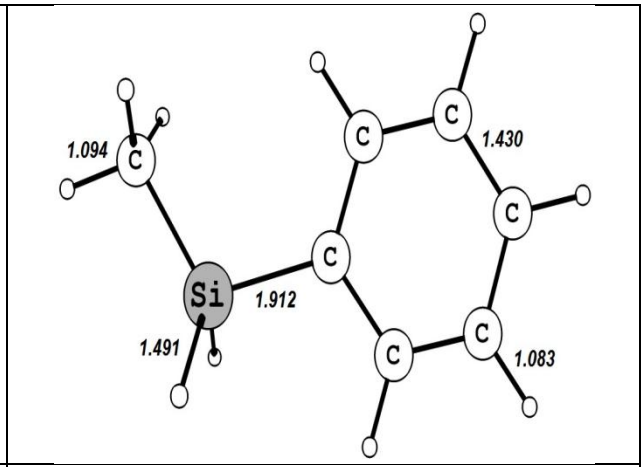
MPS	MPS^+
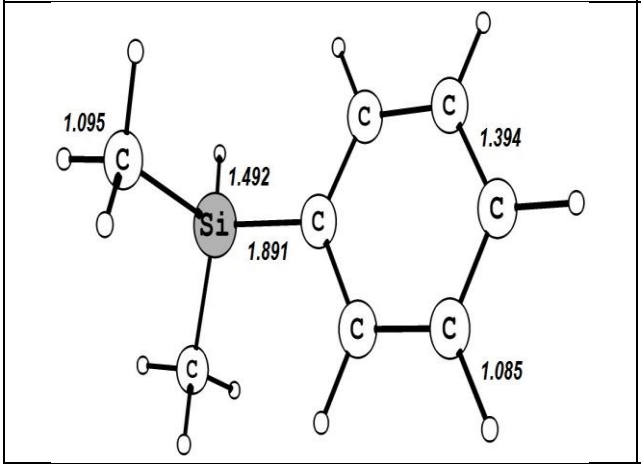	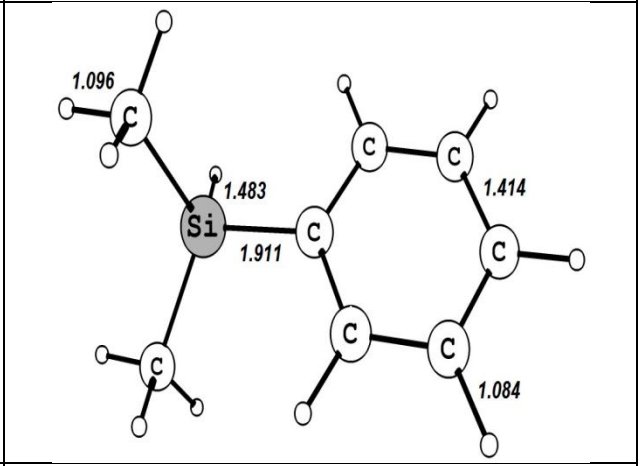
DMPS	$DMPS^+$
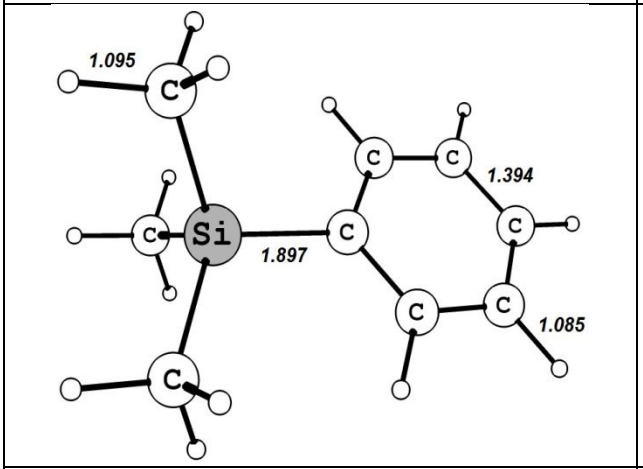	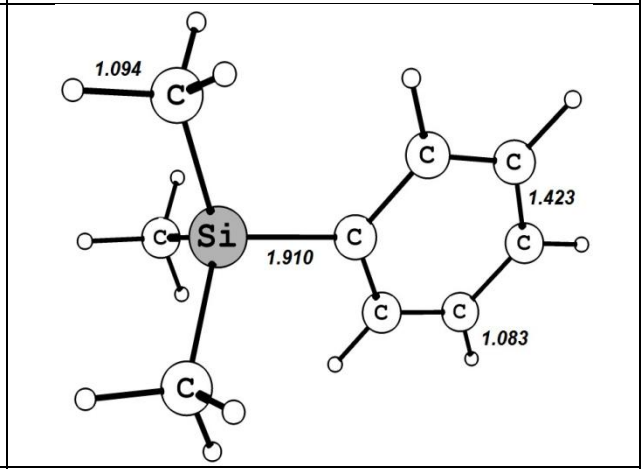
TMPS	$TMPS^+$

Table 16. The ionization energies for MPS, DMPS, and TMPS determined from experiment compared with the theoretical values from B3LYP/6-311++G(d,p) level.

Compound	Ionization energy (eV)	
	Experiment	Theory
MPS	**9.33 ± 0.25**	**8.72**
DMPS	9.04 ± 0.06 [17]	**8.59**
	8.92 ± 0.15 [18]	
	8.72 ± 0.20 [19]	
TMPS	**8.97 ± 0.25**	**8.49**
	8.81 ± 0.15 [18]	8.91 [22]
	9.05 ± 0.03 [22]	

Both the experimental and theoretical data are more or less corresponding each to other. The theoretical values are always slightly lower than the experimental ones. Also the trends are the same. The ionization energies have relations MPS>DMPS>TMPS.

5.3.2 Primary bond cleavage

We have found that the differences between ionization energies are insignificant. There is no reason for different fragmentation products due to the ionization, so the differences should be in primary bond cleavage, where the $MPS^{+\bullet}$, $DMPS^{+\bullet}$ and $TMPS^{+\bullet}$ parent metastable ionization products dissociate into more stable fragment ions. The products of such steps can be investigated systematically as there are only few bonds, which can be broken: Si-H, Si-CH_3, Si-Ph bonds and a less pronounced cleavage of different C-H bonds for these molecules. Each molecule has dissociation in order to produce one cation and one radical. The bond Si-X can be distributed both Si^+ and X* or vice versa. Thus each primary bond cleavage can produce 4 or 6 possible fragmentation products with positive charge, which can be detected in mass spectra. We do not consider any dissociation of hydrogen from CH_3 group or dissociation within the benzene ring. The comparison of the mass spectra indicates that there are some differences although such three compounds are relatively similar. For example, the position of the major peaks were recorded at *m/z* = 43, 58, and 135, for MPS, DMPS and TMPS respectively. We can sketch the basic outline of differences between the compounds. Primary fragmentation reaction of MPS and DMPS starts with dissociation of phenyl group and on the other hand, the TMPS starts with dissociation of CH_3 group. The MPS molecule is presented as an example (Scheme 3). The reactions from Scheme 3 are associated with a single bond cleavage of H atom, CH_3 group and C_6H_5 phenyl group. There are two possibilities of fragmentation according to the distribution of the positive charge. The mechanism for DMPS and TMPS compounds is presented later. We

investigated influence of charge distribution on the fragmentation properties of n-methylphenylsilanes. The charge distribution is presented in Table 17. The influence of the ionization can be observed on the example of the MPS molecule. We define four charge groups: central silicon atom (Si), hydrogen (H), methyl (CH_3), and phenyl (Ph). The partial charge of the group is a sum of all atom charges in the group. In the neutral molecule, the Si group has a large positive partial charge. The positive charge is compensated by negative charge of all groups attached to Si. Different charge distribution is in ionized molecule, where the phenyl group switched to partial positive charge. The electron was probably detached from phenyl group during the ionization phase. Usually, the cations are stabilized with electron rich group in the neighborhood. It is the case of phenyl group in the neutral molecule, while the Ph group in charged molecule does not stabilize the cation. The partial charge on the silicon is stabilized only by negative CH_3 group.

The distribution of charge groups has a consequence to the dissociation of individual bonds. As it was mentioned, the dissociation of bond $(A\text{-}B)^+$ has two variants: $A^\bullet + B^+$ and $A^+ + B^\bullet$. The groups in bond Si-Ph have both positive charges. They will have tendency to repulse due to electrostatic force. The bond Si-Ph is almost nonpolar and both the variants the $Ph^+ + SiH_2CH_3^\bullet$ and $Ph^\bullet + SiH_2CH_3^+$ can appear. Both cations (*m/z* = 45, and 77) are observed in the mass spectrum of MPS (Figure 16). Next, the CH_3 group has strongly negative charge. Therefore, the dissociation will prefer combination $CH_3^\bullet$ and $(MPS\text{-}CH_3)^+$ (*m/z* = 107). On the other hand, the CH_3^+ group (*m/z* = 15) is almost not observed. The hydrogens, nevertheless they have formally zero charge, they are more negative than silicon. The Si-H bond will be dissociated probably also $H^\bullet$, $(Si\text{-}H)^+$ (*m/z* = 121). In the case of DMPS, the electron is again subtracted from phenyl cycle. The partial charge on silicon is lower, and the stabilization effect of each single CH_3 group is lower than in the case of MPS. However, the stabilization effect of both CH_3 groups together is higher than the effect of one CH_3 group in the MPS. That leads to high positive charge on the phenyl group. Again it leads to dissociation of Ph-Si bonds. The situation changes in the case of TMPS. The partial charge on the silicon is significantly lower than in two previous cases. The polarity of Si-Ph bond is now higher than polarity of $Si\text{-}CH_3$ bond. That can cause the dissociation of CH_3 rather than Ph group.

Table 17. Charge distribution for (MPS, DMPS, and TMPS) neutrals and (MPS^+, $DMPS^+$, and $TMPS^+$) cations calculated using B3LYP/6-311++G(d,p). The partial atomic charges at each atom are given in brackets.

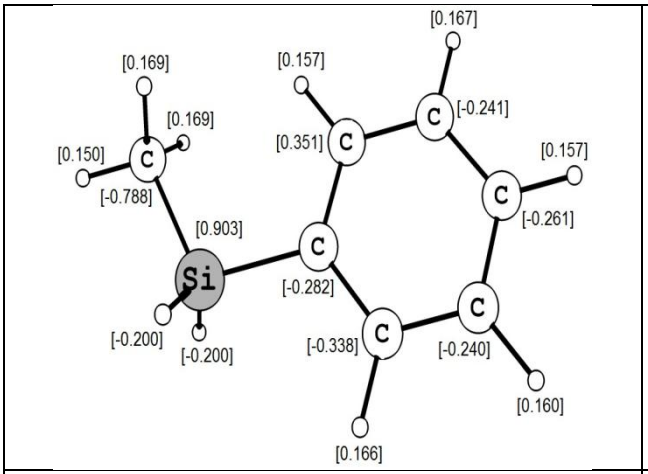

MPS

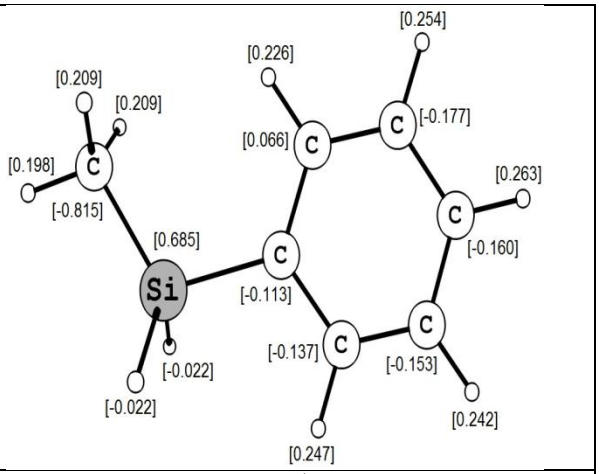

MPS^+

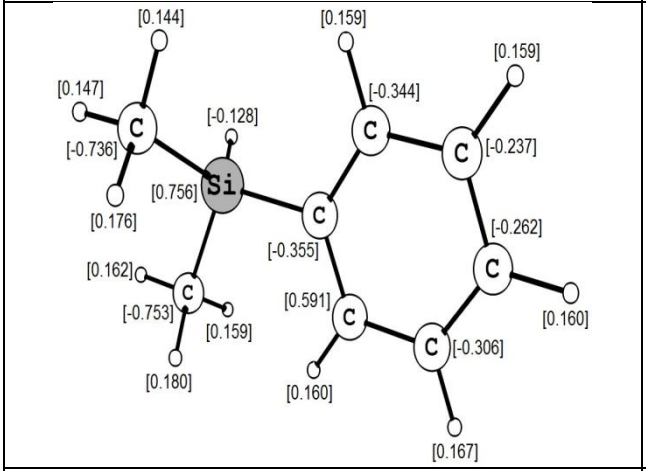

DMPS

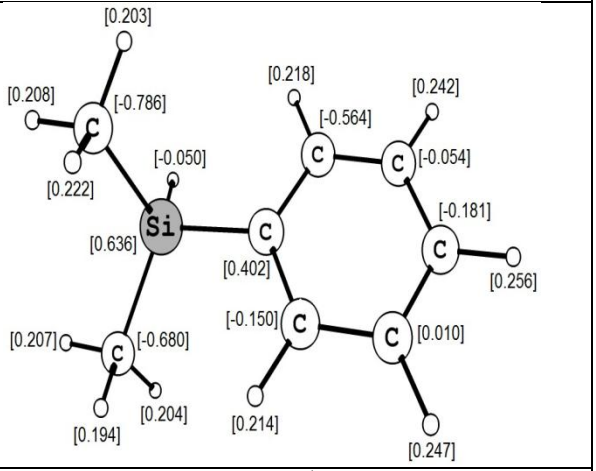

$DMPS^+$

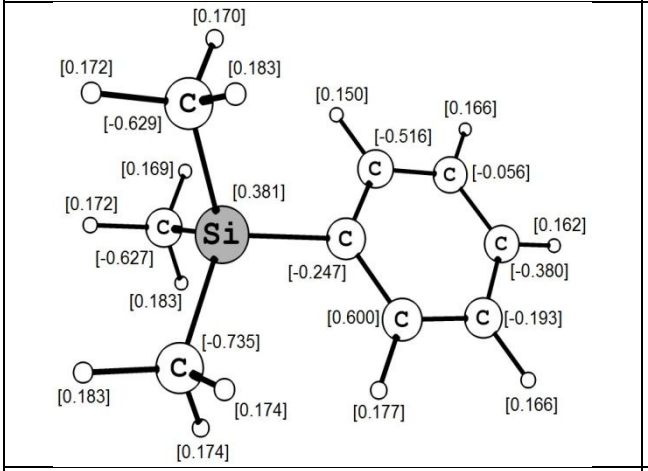

TMPS

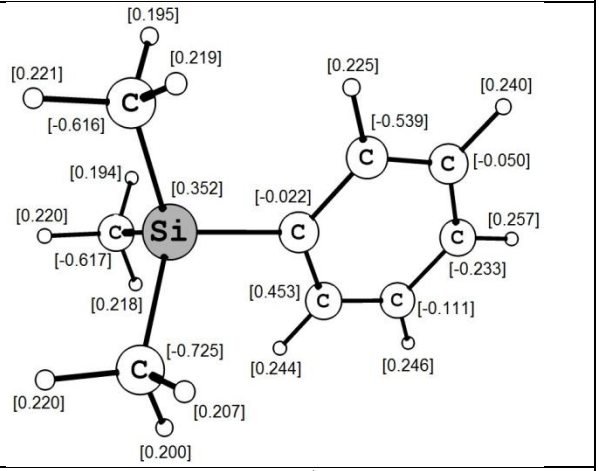

$TMPS^+$

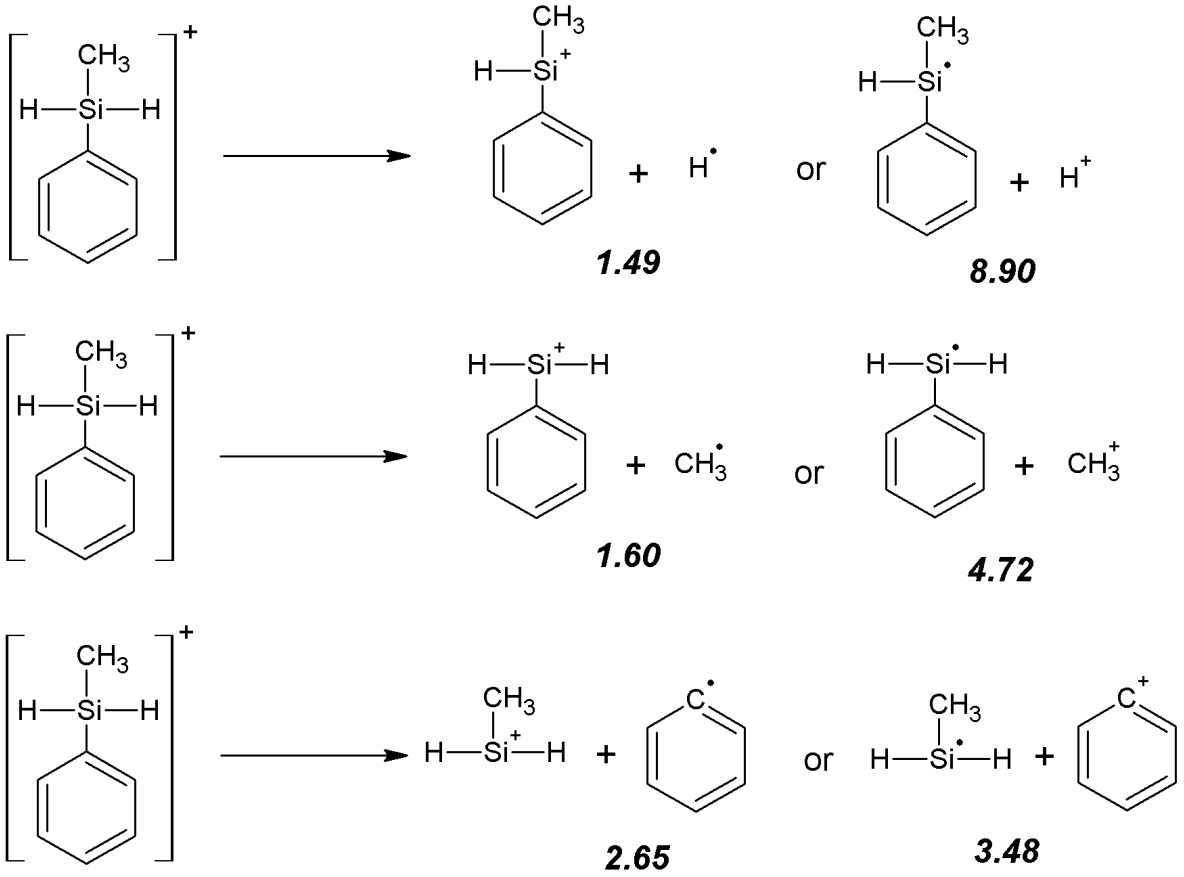

Scheme 3. Scheme of the H, CH_3 and C_6H_5 losses from $MPS^{+\bullet}$ molecular ion. The italic numbers are the bond dissociation energies (in eV) calculated using B3LYP/6-311++G(d,p) method.

The numbers in Scheme 3 are bond dissociation energies. For their evaluation, we need appearance energies (AE) of corresponding ions, which were calculated as the difference between the sum of energies of products containing the fragment ion and the energy of MPS neutral, and experimentally obtained from the fitting procedure (equation 17). We present the appearance energies from calculations and experiment in Tables 18, 19 and 20 for MPS, DMPS and TMPS, respectively.

The calculation of bond dissociation energies for theoretical and experimental data is evaluated from a difference between the appearance energy of the ionic fragment and the present value of the ionization energy (IE), or of appearance energies between two corresponding ionic fragments (equation 22).

$$BDE = AE - IE \quad (21)$$

$$BDE = AE1 - AE2 \quad (22)$$

This method (equation 21) is widely used for calculating dissociation energy of ions [18]. The bond dissociation energies and appearance energies of selected particular ions for MPS determined from experiment and calculated with theory from B3LYP/6-311++G(d,p) level are summarized in Table 18. We also compare our data which were previously calculated by Choe [19].

Table 18. The appearance energies and bond dissociation energies of selected positive ions for methylphenylsilane determined from experiment and calculated with theory from B3LYP/6-311++G(d,p) level.

m/z	Expected ion	Appearance energy (eV)		Bond dissociation energy (eV)			
		Experiment	Theory	Bond	Experiment	Theory	Theory [23]
122	MPS^+	9.33 ± 0.25	8.72		0	0	
121	$(MPS\text{-}H)^+$	10.56 ± 0.25	10.21	$(C_6H_5)(CH_3)HSi^+ - H$	1.23	1.49	1.37
120	$(MPS\text{-}2H)^+$	10.65 ± 0.25	14.27	$(C_6H_5)CH_3Si^+ - H$	0.09	4.06	
120	$(MPS\text{-}H_2)^+$		9.50			-0.71	
107	$(MPS\text{-}CH_3)^+$	11.34 ± 0.25	10.32	$(C_6H_5)H_2Si^+ - CH_3$	2.01	1.60	2.01
106	$(MPS\text{-}CH_3\text{-}H)^+$		14.41	$(C_6H_5)HSi^+ - H$		4.09	
105	$C_6H_5Si^+$ $(MPS\text{-}CH_3\text{-}2H)^+$	12.27 ± 0.50	16.63	$C_6H_5Si^+ - CH_3$	1.62	2.22	
105	$C_6H_5Si^+$ $(MPS\text{-}CH_3\text{-}H_2)^+$		11.86			2.36	
78	$C_6H_6^+$	9.46 ± 0.25	11.13				
77	$C_6H_5^+$		12.20	$C_6H_5^+ - Si(CH_3)H_2$		3.48	
69	$C_3H_5Si^+$	18 ± 0.50	13.33				
59	$C_2H_7Si^+$	11.31 ± 0.50	12.50				
45	$(MPS\text{-}C_6H_5)^+$	11.76 ± 0.50	11.37	$(CH_3)H_2Si^+ - C_6H_5$	2.43	2.65	
44	$(MPS\text{-}C_6H_6)^+$	11.28 ± 0.25	10.29	$(CH_3)HSi^+ - H$	0.72		
43	CH_3Si^+ $(-C_6H_6\text{-}H)$	11.7 ± 0.50	12.44	$CH_3Si^+ - H$	1.05	2.23	
43	CH_3Si^+ $(-C_6H_5\text{-}H_2)$		12.79			3.29	
28	Si^+, N_2, $C_2H_4^+$	15.53 ± 0.50	16.37	$Si^+ - C_6H_5$	3.26		

The single bond cleavage of the H atom, CH_3 methyl group, and C_6H_5 phenyl group leads to form ions with *m/z* = 121, 107, 45, respectively. According to the bond dissociation energies (Scheme 3), the loss of H, corresponding to the production of the *m/z* = 121 ion, is energetically more favorable than the production of the *m/z* = 107 and 45 ions. The experimental and theoretical results for the DMPS and TMPS compounds are reported in the Tables 19 and 20, respectively. The TMPS compound is different from DMPS and MPS compounds in the aspect that it does not contain the Si-H bond, where $(TMPS\text{-}H)^+$ ion was not detected in mass spectrum.

Table 19. The appearance energies and bond dissociation energies of selected positive ions for dimethylphenylsilane determined from experiment and calculated with theory from B3LYP/6-311++G(d,p) level.

m/z	Expected ion	Appearance energy (eV)		Bond dissociation energy (eV)			
		Experiment [17]	Theory	Bond	Experiment [17]	Theory	Theory [23]
136	$DMPS^+$	9.04 ± 0.06	8.59		0	0	
135	$(DMPS\text{-}H)^+$	10.42 ± 0.09	9.89	$(C_6H_5)(CH_3)_2Si^+ - H$	1.38	1.30	1.17
121	$(DMPS\text{-}CH_3)^+$	10.51 ± 0.15	9.92	$(C_6H_5)(CH_3)HSi^+ - CH_3$	1.47 1.34 [19]	1.33	1.16
106	$C_6H_5SiH^+$ $(-2CH_3)$	9.6 ± 0.20		$(C_6H_5)HSi^+ - CH_3$	-0.91		
106	$C_6H_5SiH^+$ $(-C_2H_6)$		10.01			0.09	
105	$C_6H_5Si^+$ $(-2CH_3\text{-}H)$	13.47 ± 0.10		$C_6H_5Si^+ - H$	3.87		
105	$C_6H_5Si^+$ $(-C_2H_6\text{-}H)$		12.23			2.22	
78	$C_6H_6^+$	10.2 ± 0.30	11.11				
68	$DMPS^{+2}$	26.3± 1.00	20.16				
67.5	$(DMPS\text{-}H)^{+2}$	27.3± 1.00	22.95	$(C_6H_5)(CH_3)_2Si^{+2} - H$	1.00	2.79	
60.5	$(DMPS\text{-}CH_3)^{+2}$	29.3± 1.00	23.26	$(C_6H_5)(CH_3)HSi^{+2} - CH_3$	2.00	3.10	
59	$(DMPS\text{-}C_6H_5)^+$	12.4± 1.00	10.8	$(CH_3)_2HSi^+ - C_6H_5$	3.36	2.21	
58	$(DMPS\text{-}C_6H_6)^+$	10.26 ± 0.14	9.69	$(CH_3)_2Si^+ - H$	-0.16	-0.20	
43	CH_3Si^+	13.9 ± 0.20	12.16	$CH_3Si^+ - CH_3$	3.64	2.47	

Table 20. The appearance energies and bond dissociation energies of selected positive ions for trimethylphenylsilane determined from experiment and calculated with theory from B3LYP/6-311++G(d,p) level. For fragment with *m/z* = 105 we report the average bond energy* of $PhSi^+\text{-}CH_3$ bond.

m/z	Expected ion	Appearance energy (eV)		Bond dissociation energy (eV)		
		Experiment	Theory	Bond	Experiment	Theory
150	$TMPS^+$	8.97 ± 0.25	8.49		0	0
135	$(TMPS\text{-}CH_3)^+$	9.76 ± 0.25	9.57	$(C_6H_5)(CH_3)_2Si^+ - CH_3$	0.79	1.08
107	$C_6H_7Si^+$	14.54 ± 0.25	15.88			
105	$(TMPS\text{-}3CH_3)^+$	16.93 ± 0.50	16.02	$*C_6H_5Si^+ - CH_3$	2.65*	2.51*
77	$C_6H_5^+$	12.5 ± 0.50	12.25	$C_6H_5^+ - Si(CH_3)_3$	3.53	3.76
74	$C_3H_{10}Si^+$	10.69 ± 0.50	13.63			
73	$(TMPS\text{-}C_6H_5)^+$	11.29 ± 0.50	10.32	$(CH_3)_2Si^+ - C_6H_5$	2.32	1.83
67.5	$(TMPS\text{-}CH_3)^{+2}$	23.79 ± 0.50	22.63			
53	$C_6H_5SiH^{+2}$	20.09 ± 1.00	24.07			
43	CH_3Si^+	11.5 ± 0.50	12.41			

As mentioned above, the Tables 18-20 are important for calculation of energy profile of reactions. They can be used in general for any fragmentation reaction including the consecutive reactions discussed later. The energy profile of any reaction is a difference of B3LYP energies on the left and right side of equation. In the next text, the conclusions from theoretically calculated data for supporting of the mechanisms are presented. However, the experimental data qualitatively follow the theoretical ones. One can calculate the bond dissociation energies from experimental data.

The description of asymmetric bond cleavage can be one indication, that the results from models can be used for interpretation of real mass spectra. The primary cleavage of some selected bond can have two variants. For example, the bond cleavage presented in the Scheme 3 leads to the production of CH_3^+ cation with *m/z* = 15 and complementary radical. The second variant is the production of ion $(MPS\text{-}CH_3)^+$ with *m/z* = 107 and CH_3 radical. Only the ions are detectable in mass spectra.

We compare the energies from Scheme 3 and the *m/z* = 107 ion, is energetically more preferred than the production of CH_3 cation. This result has correlation with mass spectrum, where the intensity of the ion with *m/z* = 107 is higher than the ion with opposite distribution of charge. Next example is the bond cleavage of Si-Ph bond. The loss of C_6H_5 group, corresponding to the production of the *m/z* = 45 ion, is energetically more favorable than the production of C_6H_5 positive ion due to its low bond dissociation energy.

TMPS has lower value of CH_3 dissociation energy in comparison to MPS and DMPS (Table 18). This result is reflected in mass spectra of all components, where the loss of CH_3 methyl group from $TMPS^{+\bullet}$ molecular ion becomes more pronounced than the other two $MPS^{+\bullet}$ and $DMPS^{+\bullet}$ molecular ions.

In the case of MPS, the dissociation of H and CH_3 will be preferred and the $(MPS\text{-}H)^+$ and $(MPS\text{-}CH_3)^+$ can be found in the mass spectrum. Also the dissociation of phenyl group leading to $(MPS\text{-}C_6H_5)^+$ can be identified in the mass spectra and the bond dissociation energies derived from experimental value of appearance energies (Tables 18 and 20) are in reasonable agreement with our theoretical prediction.

In the case of simple mechanism of single bond cleavage, there are expectable fragmentation products, which can be highlighted in mass spectra according to their value *m/z* (Tables 18-20). If the single bond cleavage mechanism is valid, its products should be detected in mass spectra in

significantly higher intensities than the other fragments. It is not the case of any of the presented compounds. The complete mechanism must be even more complex. The mass spectra in reality contain significantly more fragmentation products, than would be expected from reactions from this and previous section. The second reason is the intensity of the peaks from primary products. The intensity of phenyl (*m/z* = 77) as an example of product of primary bond cleavage is relatively low. In contrast, the intensity of benzene peak (*m/z* = 78), which appears by consecutive reaction, is higher. The next example is a complementary molecule after decomposition of phenyl group. It has *m/z* = 45, but in mass spectra, there is major intensity peak is at *m/z* = 43. The fragments must be subject to additional consequent reactions.

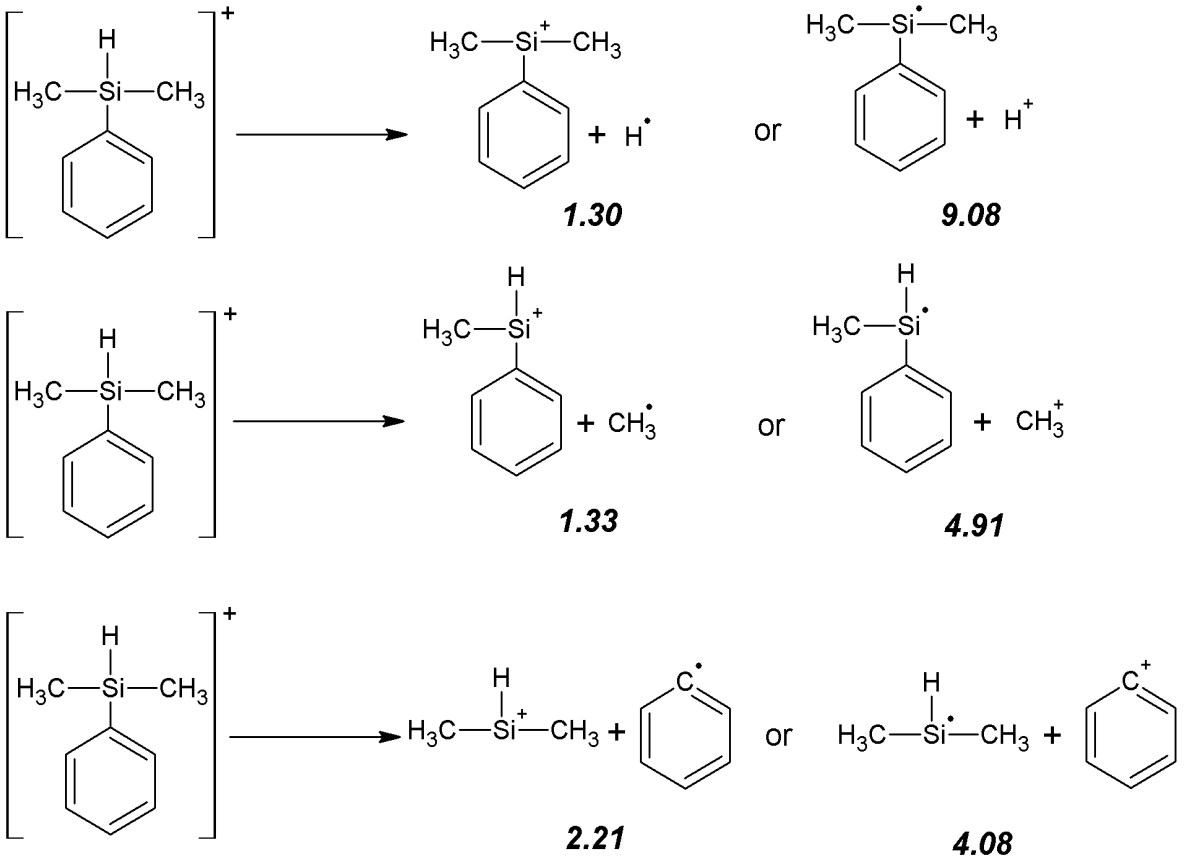

Scheme 4. Losses of the H, CH_3, and C_6H_5 from $DMPS^{+\bullet}$ molecular ion using the DFT(B3LYP)/6-311++G(d,p) level. The italic numbers are the bond dissociation energies (in eV).

As we have mentioned above, the DMPS and TMPS compounds are relatively similar to MPS compound. The main difference is the number of CH_3 functional groups connected to the Si atom. For the DMPS and TMPS compounds, we have found other consecutive fragmentation

reactions, which we suspect that they have the same fragmentation mechanism as we proposed for MPS compound. The primary bond cleavage of the $DMPS^{+\bullet}$ and $TMPS^{+\bullet}$ molecular ions is shown in the Schemes 4 and 5, respectively.

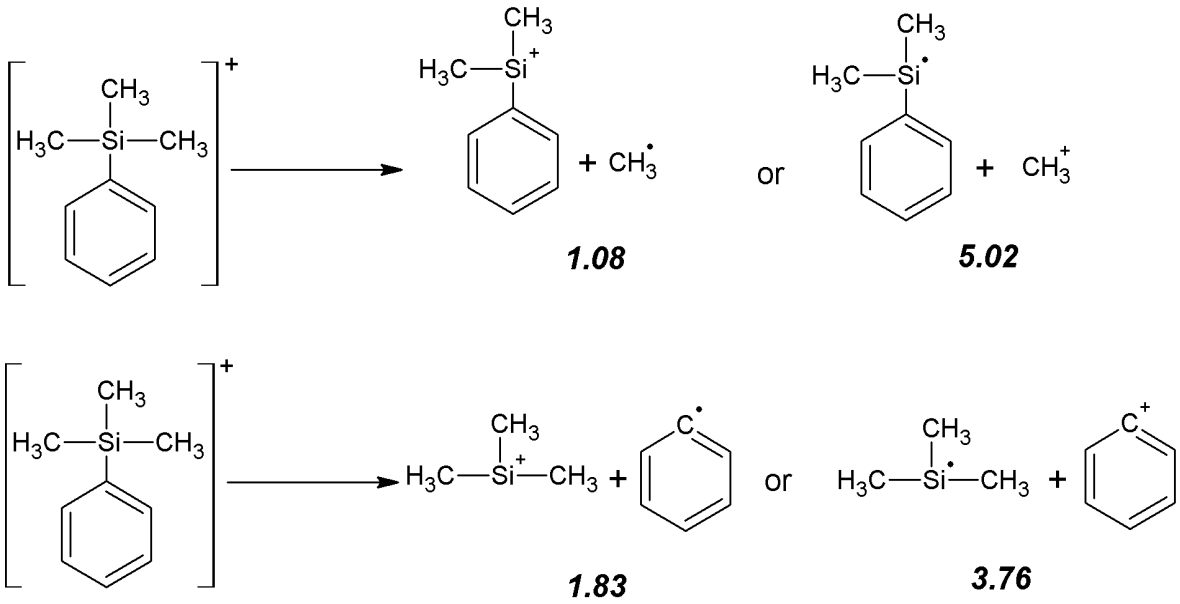

Scheme 5. Losses of the CH_3 and C_6H_5 from $TMPS^{+\bullet}$ molecular ion using the DFT(B3LYP)/6-311++G(d,p) level. The italic numbers are the bond dissociation energies (in eV).

It is evident from Schemes 4 and 5, the primary bond cleavage of the Si-H, Si-CH_3, and Si-C_6H_5 bonds can be observed in the $DMPS^{+\bullet}$ molecular ion, but the cleavage of the Si-CH_3 and Si-C_6H_5 can only be seen in the $TMPS^{+\bullet}$ molecular ion because the dissociation of the H atom from the $TMPS^{+\bullet}$ molecular ion is not possible due to the absence of the Si-H bond.

As mentioned above, the fragmentation process of organosilicones was investigated by the DFT(B3LYP)/6-311++G(d,p) level of theory. The influence of the size of basis set on appearance energies was investigated. Therefore, we have also recalculated the appearance energies of cationic fragments for MPS, DMPS, and TMPS using the same method DFT(B3LYP) but, with variety of basis sets such as 6-31G and 6-311G as well as 6-311++G(d,p) previously used. The appearance energies of selected cationic fragments measured by experiment and calculated from the DFT(B3LYP) method and different basis sets are reported in the Tables 21, 22, and 23.

Table 21. The appearance energies of selected positive ions for methylphenylsilane determined from experiment and calculated with theory from B3LYP and different basis sets.

m/z	Expected ion	Appearance energy (eV)			
		Experiment EI	Theory B3LYP/6-31G	Theory B3LYP/ 6-311G	Theory B3LYP/6-311++G(d,p)
122	MPS^+	9.33 ± 0.25	8.56	8.74	8.72
121	$(MPS-H)^+$	10.56 ± 0.25	9.97	10.06	10.21
120	$(MPS-2H)^+$	10.65 ± 0.25	13.84	13.90	14.27
120	$(MPS-H_2)^+$		9.08	9.21	9.50
107	$(MPS-CH_3)^+$	11.34 ± 0.25	10.09	10.16	10.32
106	$(MPS-CH_3-H)^+$		14.00	14.04	14.41
105	$C_6H_5Si^+$ $(MPS-CH_3-2H)^+$	12.27 ± 0.50	16.10	16.07	16.63
105	$C_6H_5Si^+$ $(MPS-CH_3-H_2)^+$		11.34	11.38	11.86
78	$C_6H_6^+$	9.46 ± 0.25	10.63	10.82	11.13
77	$C_6H_5^+$		12.02	12.17	12.20
69	$C_3H_5Si^+$	18 ± 0.50	12.97	12.87	13.33
59	$C_2H_7Si^+$	11.31 ± 0.50	12.52	12.37	12.50
45	$MPS-C_6H_5^+$	11.76 ± 0.50	11.26	11.29	11.37
44	$MPS-C_6H_6^+$	11.28 ± 0.25	9.93	9.99	10.29
43	CH_3Si^+ $(-C_6H_6-H)^+$	11.7 ± 0.50	13.90	11.93	12.44
43	CH_3Si^+ $(-C_6H_5-H_2)^+$		14.30	12.34	12.79
28	Si^+, N_2, $C_2H_4^+$	15.53 ± 0.50	16.37	16.42	16.37

Table 22. The appearance energies of selected positive ions for dimethylphenylsilane determined from experiment and calculated with theory from B3LYP and different basis sets.

m/z	Expected ion	Appearance energy (eV)			
		Experiment EI [17]	Theory B3LYP/ 6-31G	Theory B3LYP/ 6-311G	Theory B3LYP/6-311++G(d,p)
136	$DMPS^+$	9.04 ± 0.06	8.42	8.62	8.59
135	$(DMPS-H)^+$	10.42 ± 0.09	9.65	9.79	9.89
121	$(DMPS-CH_3)^+$	10.51 ± 0.15	9.71	9.81	9.92
106	$C_6H_5SiH^+$ $(-2CH_3)$	9.6 ± 0.20			
106	$C_6H_5SiH^+$ $(-C_2H_6)$		9.62	9.74	10.01
105	$C_6H_5Si^+$ $(-2CH_3-H)$	13.47 ± 0.10			
105	$C_6H_5Si^+$ $(-C_2H_6-H)$		11.72	11.78	12.23
78	$C_6H_6^+$	10.2 ± 0.30	10.59	10.77	11.11
68	$DMPS^{+2}$	26.3± 1.00	20.06	20.32	20.16
67.5	$(DMPS-H)^{+2}$	27.3± 1.00	22.60	22.86	22.95
60.5	$(DMPS-CH_3)^{+2}$	29.3± 1.00	22.94	23.17	23.26
59	$(DMPS-C_6H_5)^+$	12.4± 1.00	10.70	10.76	10.8
58	$(DMPS-C_6H_6)^+$	10.26 ± 0.14	9.32	9.41	9.69
43	CH_3Si^+	13.9 ± 0.20	11.67	11.67	12.16

Table 23. The appearance energies of selected positive ions for trimethylphenylsilane determined from experiment and calculated with theory from B3LYP and different basis sets.

m/z	Expected ion	Appearance energy (eV)			
		Experiment EI	Theory B3LYP/ 6-31G	Theory B3LYP/6-311G	Theory B3LYP/6-311++G(d,p)
150	$TMPS^+$	8.97 ± 0.25	8.31	8.52	8.49
135	$(TMPS\text{-}CH_3)^+$	9.76 ± 0.25	9.38	9.49	9.57
107	$C_6H_7Si^+$	14.54 ± 0.25	16.00	15.96	15.88
105	$TMPS\text{-}3CH_3^+$	16.93 ± 0.50	15.57	15.54	16.02
77	$C_6H_5^+$	12.5 ± 0.50	12.12	12.25	12.25
74	$C_3H_{10}Si^+$	10.69 ± 0.50	13.75	13.81	13.63
73	$(TMPS\text{-}C_6H_5)^+$	11.29 ± 0.50	10.22	10.29	10.32
67.5	$(TMPS\text{-}CH_3)^{+2}$	23.79 ± 0.50	22.33	22.58	22.63
53	$C_6H_5SiH^{+2}$	20.09 ± 1.00	23.57	23.80	24.07
43	CH_3Si^+	11.5 ± 0.50	11.96	11.96	12.41

From Tables 21, 22, and 23, the comparison of experimental data with theoretical results of appearance energies shows that, for the most cationic fragments, the large 6-311++G(d,p) basis set gives the best agreement with experiment compared to the small 6-31G, 6-311G basis sets. This also supports our previous results about the principle of the choice of basis set. This is the reason why we have selected the 6-311++G(d,p) basis set to perform our main calculations.

5.3.3 Consequent fragmentation-subtraction of hydrogen

We would like to propose some reactions, which are generally observed in all the fragmentation mechanisms of MPS, DMPS, and TMPS. As they are applied to different original molecules, they lead to different products of fragmentation. Individual steps of mechanisms will be also analyzed by a model. The models enable us to describe the energy of individual steps in mechanism, which cannot be measured experimentally. However, the parameters needed to be calculated in order to have detailed picture of mechanism. In the second step, we demonstrate an ability of theoretical models to predict another mechanism, where the experimental work was still not performed. In our case, the new anionic mechanism is small modification of previously calculated one (electron impact), which we analyzed theoretically and experimentally. The prediction of fragmentation products can be useful during the designing the processes as it can replace significant part of experimental work.

In this section, we would like to present a mechanism and its relation to the mass spectra and some general mechanism, which can be found in three compounds fragmentation. The results of the prediction are qualitative comparison, which peaks will be present in mass spectra and which peaks will have higher intensity. The quantitative comparison, which would enable us also

compare the peak heights, needs the optimization of the model. We have focused on the consecutive reactions that follow the primary bond cleavage. We would like to investigate three approaches of fragmentation process:

- Cationic fragmentation mechanism
- Anionic fragmentation mechanism
- New approach to the fragmentation

5.3.3.1 Cationic fragmentation mechanism

The next steps of the fragmentation process are various consecutive reactions, where these fragmentation reactions follow the primary bond cleavage. Here, we consider the fragmentation mechanism resulting from the electron detachment process from MPS compound leading to the formation of positively charged fragments or cations. The consecutive reactions for the fragmentation of the MPS compound can be summarized in the Scheme 6.

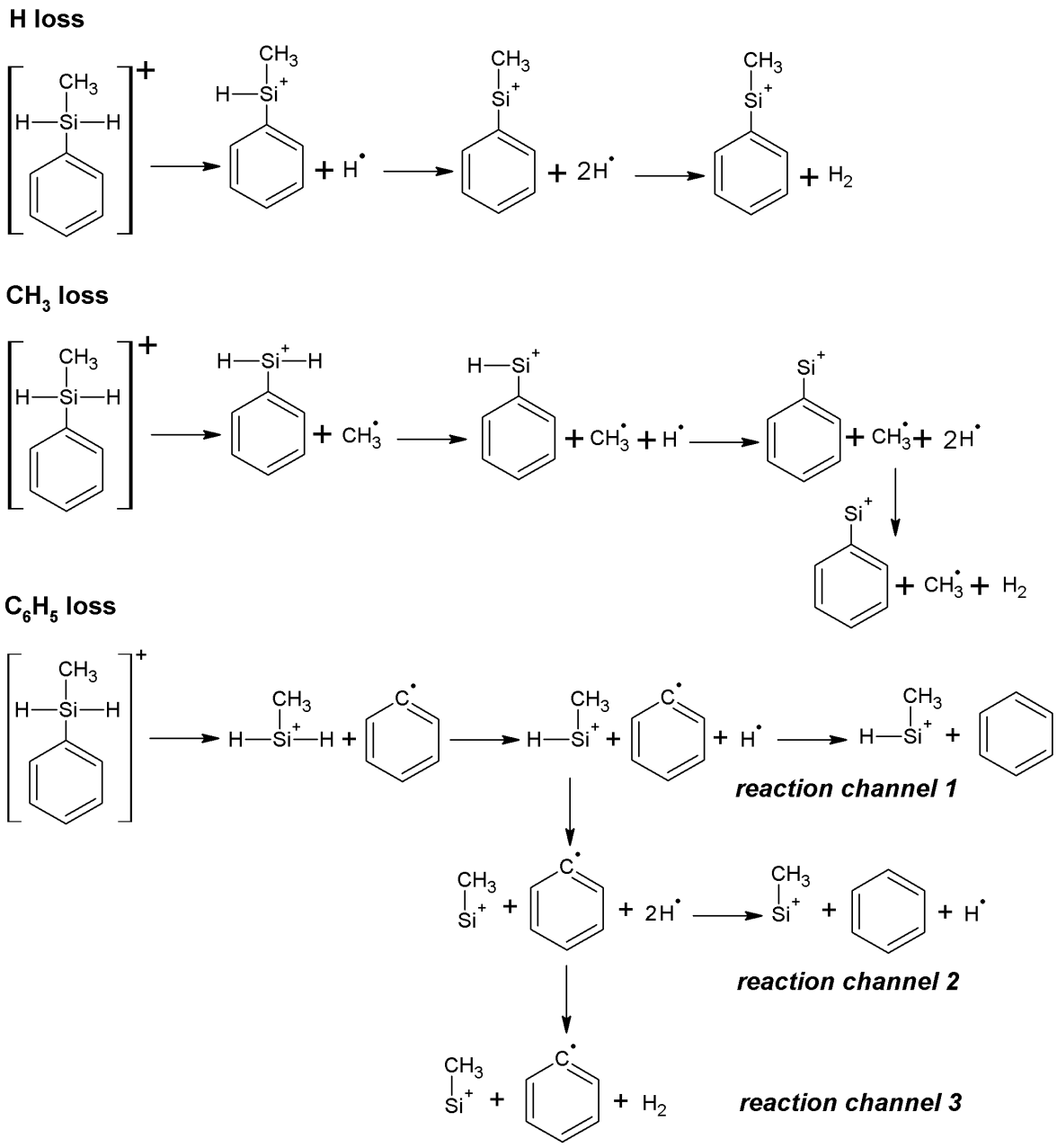

Scheme 6. Consecutive reactions of the H, CH_3, and C_6H_5 losses from the $MPS^{+\bullet}$ molecular ion.

Mass spectra indicate a mixture of many products. Most frequently, the further cleavage of the Si-H, Si-CH_3 and Si-C_6H_5 bonds can be observed after a primary cleavage process. Frequent aspect observed in mass spectra is a loss of H_2. It is observed several times in the spectra MPS and DMPS. We compare two cases with different behavior. For example, the dissociation of the second H from $(MPS\text{-}H)^+$ after the first H cleavage gives the ion with *m/z* = 121, which finally

produces the *m/z* = 120 peak. Next example is the dissociation of CH_3 group from MPS^+ followed by the loss of two hydrogens. This dissociation leads to produce the *m/z* = 107 before cleavage of 2H and *m/z* = 105 after.

We would like to focus to these two data sets from mass spectra of MPS: (*m/z* = 122, 121, 120 and 107, 106 and 105). However, they have also different aspects. In the first case, the product after loss of one hydrogen atom (*m/z* = 121) is detected in relatively high intensity and then the second dissociation (*m/z* = 120) shows lower intensity. It corresponds to classic expectable mechanism. If we consider one hydrogen atom is dissociated in certain time, the dissociation of the next hydrogen needs extra time. If the reaction ends in finite time, it is sufficient for decomposition of one hydrogen atom, only. Some of the molecules dissociated two hydrogen atoms in such time, but it was minority of them. That is why intensity of peak 121 is higher than the peak 120. The peak 122 of MPS^+ is lower than 121, as the MPS^+ is subject to other competitive reactions in the same time, not only to dissociation of hydrogen.

In the second case, the product of cleavage of one Si-H bond with *m/z* = 106 is almost absent, and there is present directly the product $(MPS\text{-}CH_3\text{-}2H)^+$ (or $(C_6H_5Si)^+$) with *m/z* = 105. The classic mechanism from previous paragraph can be applicable only in the special case. In general it must be valid, that energy barrier of the second decomposition of hydrogen must be minimal in comparison of the energy of the first one. We would like to demonstrate some principles, which we believe are generally valid also in other cases.

In both cases we propose energy profile of the reaction. As we mentioned above, all data which we use in Figures 21 and 22 are from theoretical calculations. The numbers at lines in the figures are the energy barrier for certain reaction in electronvolts. One can calculate some values from experimental data as a difference between the experimental appearance energies from Table 18 for certain products.

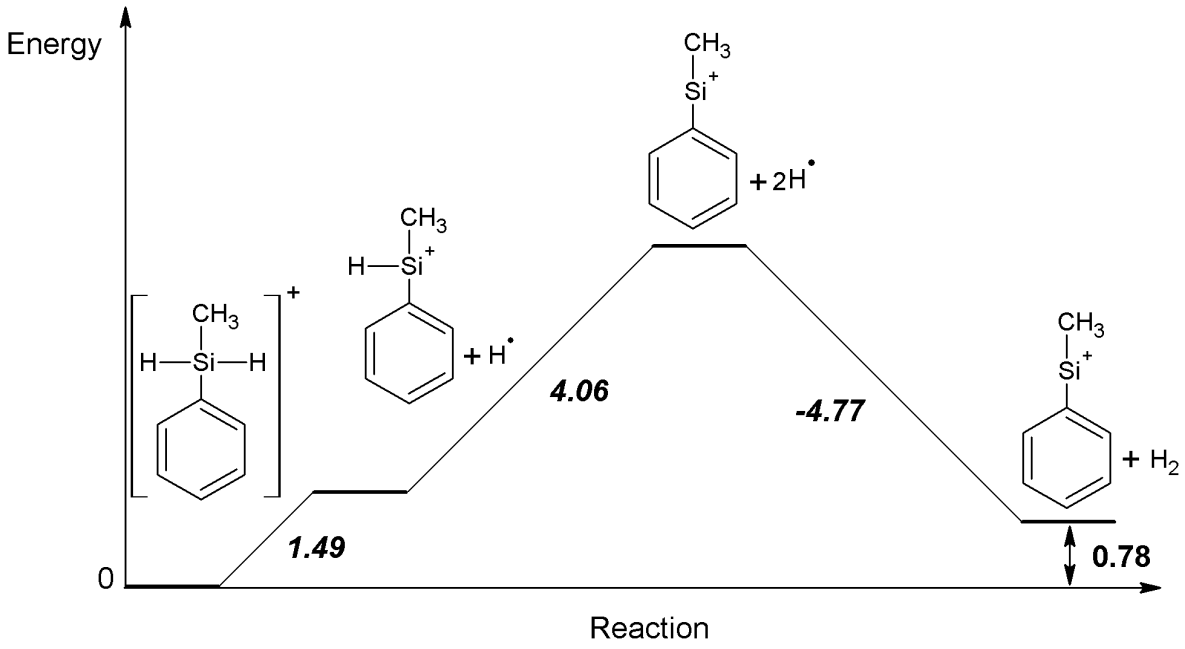

Figure 21. Energy profile for the H loss from methylphenylsilane cation derived from the B3LYP/6-311++G(d,p) calculations. The italic numbers are the bond dissociation energies (in eV).

It can be seen from Figure 21, that there is a relatively low energy barrier to decomposition of the first hydrogen, and relatively high energy barrier for decomposition of the second hydrogen. That would support the data from mass spectra, however only the relative intensities of the peaks at *m/z* = 121 and 120. The experimental bond dissociation energies are not in agreement and the dissociation of second H is only a 50 meV above the dissociation of the first H in MPS^+ (which is however below our electron energy beam resolution). The probable explanation can be found as a competitive process for $C_6H_6^+$ with low threshold at 9.46 eV can be more dominant than is the loss of 2H atoms. We included also the next step – recombination of two hydrogen radicals to the hydrogen molecule, which gives to the reaction some benefit of energy. However, in the case of such mechanism the step will probably not have influence. If some recombination of radical occurs, it returns the energy usually in form of heat. This heat cannot be used directly to the dissociation of bond. All the costs of dissociation of H_2 are seemingly 0.78 eV, but in reality the energy, which was consumed (1.49+4.06) eV was consumed directly in the molecule. On the other hand, the energy of recombination (-4.77 eV) was released far from the main molecule. There is no reason, why the second dissociation of hydrogen should be favorable due to next H_2 recombination. There is only low probability, how

the recombination can play a role. It is the transfer of radical after collision of H* with the segment of main molecule. However, such reaction would require exact collision of H* with some other hydrogen bonded on Si. The collision with any other atoms must be eliminated.

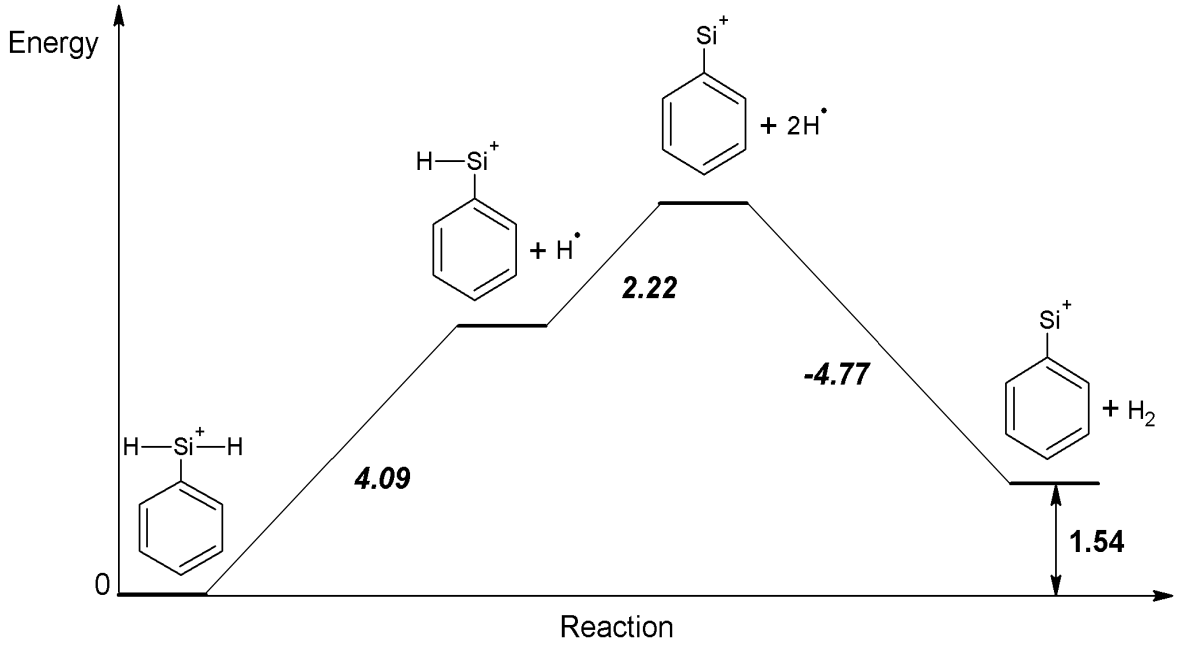

Figure 22. Energy profile for the CH_3 loss from methylphenylsilane cation derived from the B3LYP/6-311++G(d,p) calculations. The italic numbers are the bond dissociation energies (in eV).

The Figure 22 shows consecutive dissociation of two hydrogen atoms from $(MPS\text{-}CH_3)^+$, that is the case of peaks 107, 106 and 105. They have relatively specific picture in mass spectrum: intensive peaks 107 and 105 and small peak 106. In that case, the segment after dissociation of the first hydrogen $(MPS\text{-}CH_3\text{-}H)^+$ is immediately transformed to the $(MPS\text{-}CH_3\text{-}2H)^+$. The recombination of hydrogen does not play a role as well as in the previous case. In reality, we observe energy barrier of the second dissociation significantly lower than the first one. However, the energy barrier of 4.09 eV is relatively high as well as 4.06 eV from Figure 21. We can not support these results with experimental data as we were not able to measure the threshold of the very weak $(MPS\text{-}CH_3\text{-}H)^+$ ion at *m/z* = 106, however the dissociation of both hydrogens from $(MPS\text{-}CH_3)^+$ is experimentally evaluated only at 0.9 eV that is in contrast with the theoretical 6.31 eV barrier.

The consecutive reactions of the C_6H_5 loss from $MPS^{+\bullet}$ molecular ion are shown in Scheme 6. Here, we investigate two fragmentation possibilities. Firstly, when the phenyl radical is

produced, three different products can be observed: the benzene molecule (reaction channel 1), the C_6H_6+H products (reaction channel 2), and C_6H_5+H_2 (reaction channel 3). The energy profiles for these three individual reactions are shown in Figures 23, 24, and 25.

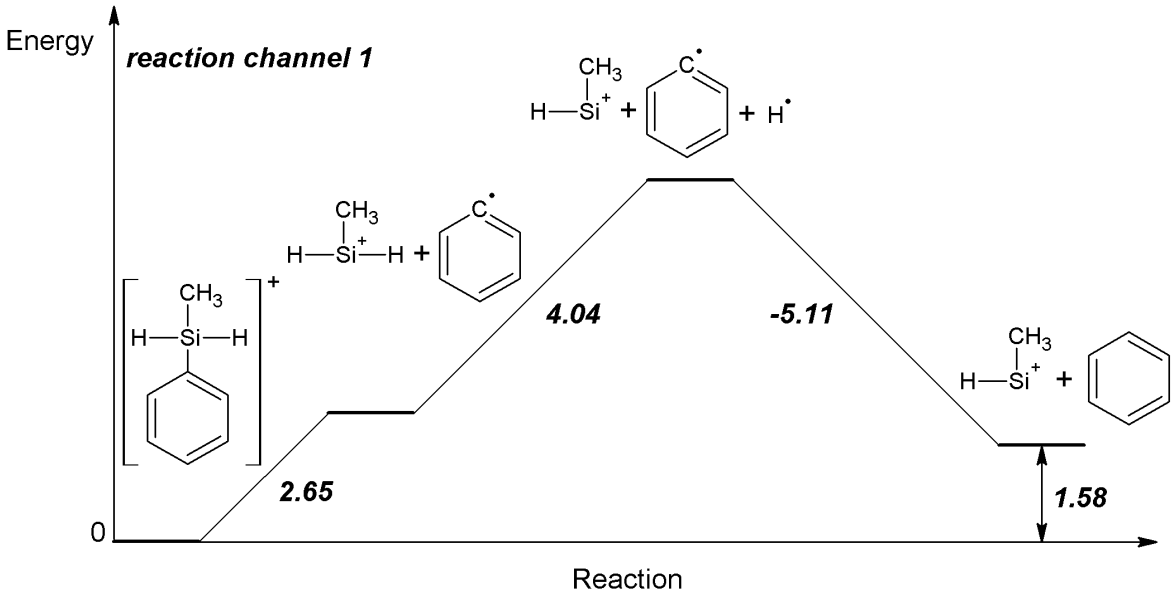

Figure 23. Energy profile for the C_6H_6 loss (*m/z* = 44) from methylphenylsilane cation derived from the B3LYP/6-311++G(d,p) calculations. The italic numbers are the bond dissociation energies (in eV).

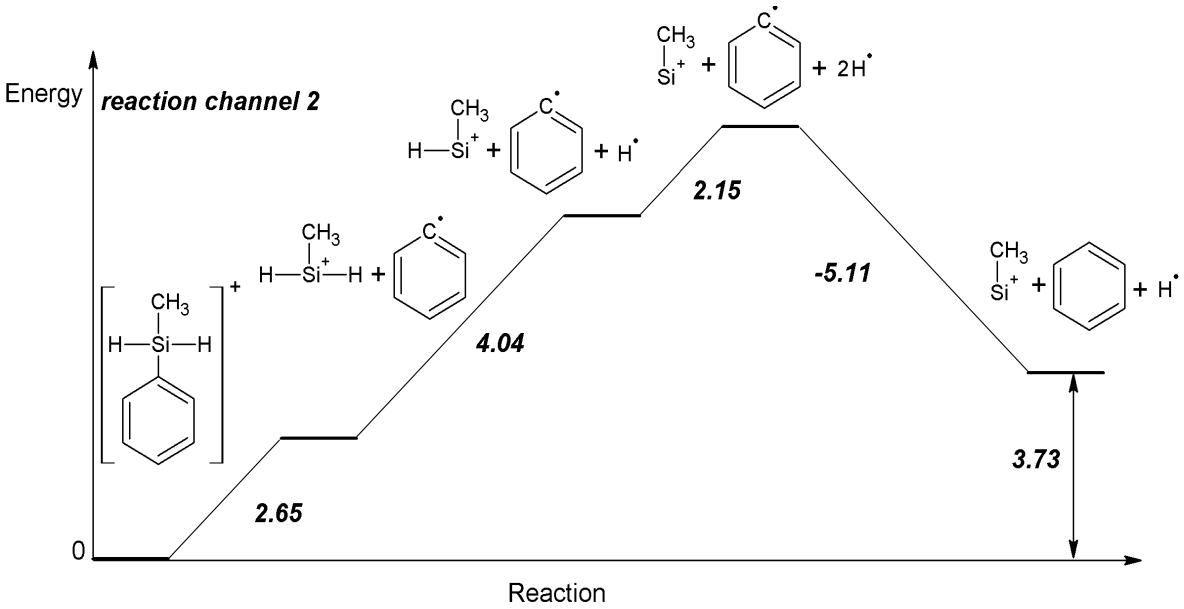

Figure 24. Energy profile for the C_6H_6+H loss (*m/z* = 43) from methylphenylsilane cation derived from the B3LYP/6-311G++(d,p) calculations. The italic numbers are the bond dissociation energies (in eV).

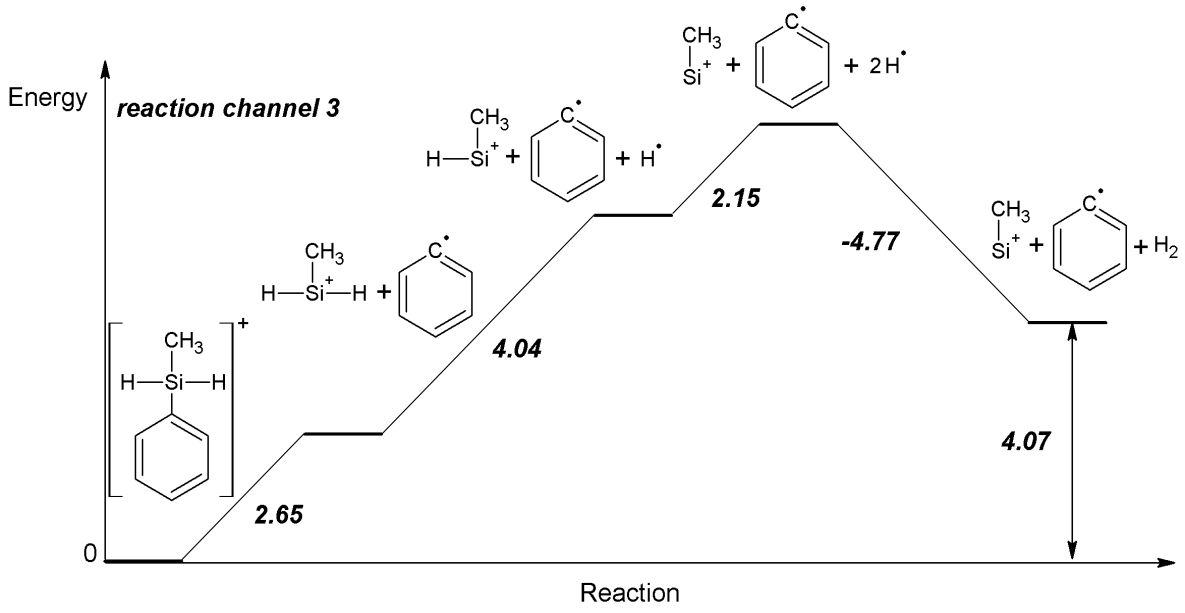

Figure 25. Energy profile for the C_6H_5+H_2 loss (*m/z* = 43) from methylphenylsilane cation derived from the B3LYP/6-311G++(d,p) calculations. The italic numbers are the bond dissociation energies (in eV).

Secondly, when the C_6H_5 is produced like cation, the *m/z* = 78 ion, corresponding to $C_6H_6^+$ fragment can be formed. The production of the $C_6H_6^+$ fragment is described in the Scheme 7.

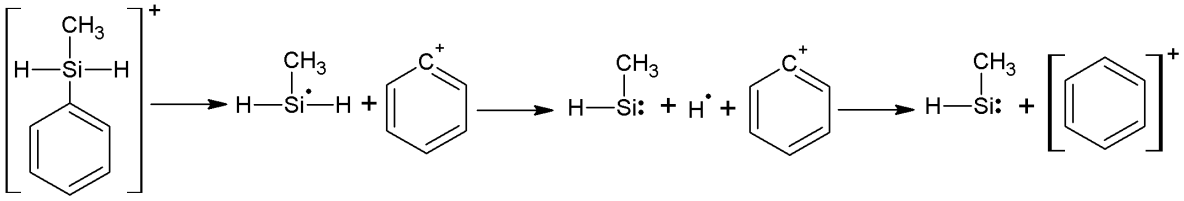

Scheme 7. The production of the $C_6H_6^+$ fragment.

The corresponding energy profile is given in the Figure 26.

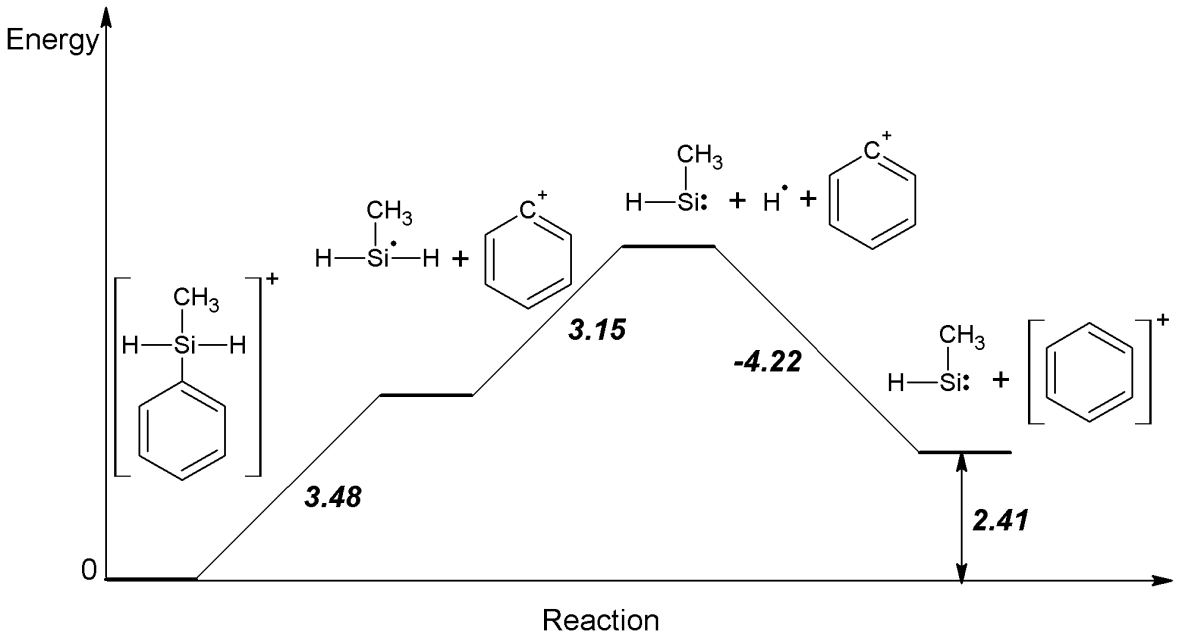

Figure 26. Energy profile for the $C_6H_6^+$ formation from methylphenylsilane cation derived from the B3LYP/6-311++G(d,p) calculations. The italic numbers are the bond dissociation energies (in eV).

5.3.3.2 Anionic fragmentation mechanism

Here, we have also investigated the fragmentation mechanism, which is an alternative mechanism to the EII technique. This process consists of electron attachment to the molecule and formation of the so called transient negative ion [132, 133] and consecutive dissociation of bonds. We believe that the model prediction can be applied to investigation of similar fragmentation products. We demonstrate this ability on the case of dissociative electron attachment mechanism instead of the EII mechanism. In that case, similar reactions can be observed as in EII, but the intensities of peaks in mass spectra will be probably different. We present the predictions based on calculated data only without any knowledge of experimental mass spectra.

We would like to discuss the two cases (Peaks 122/121/120 and 107/106/105) for the MPS compound. We have investigated the EII both theoretically and experimentally. We have reason to believe that the conclusions from simulations followed the experimental trends in previous case. In the case of dissociative electron attachment, the experimental analysis was not provided. We suppose that the experimental data qualitatively follow the tentative experimental data. Here, we have also calculated the appearance energies of anionic fragments in order to investigate the

anionic mechanism of fragmentation process. We have followed the same way to calculate the appearance energy as in the positive ions, but here negative ions are considered. The appearance energies of anionic fragments for the MPS, DMPS and TMPS compounds calculated by the DFT(B3LYP)/6-311++G(d,p) calculations (Table 24).

Table 24. The appearance energies of anionic fragments for the MPS, DMPS and TMPS compounds calculated by the DFT(B3LYP)/6-311++G(d,p) method.

MPS			DMPS			TMPS		
m/z	species	Appearance energy (eV)	*m/z*	Species	Appearance energy (eV)	*m/z*	Species	Appearance energy (eV)
122	$C_6H_5SiH_2CH_3^-$	1.04	136	$C_6H_5SiH(CH_3)_2^-$	1.08	150	$C_6H_5Si(CH_3)_3^-$	1.14
121	$C_6H_5SiHCH_3^-$	2.99	135	$C_6H_5Si(CH_3)_2^-$	3.19	135	$C_6H_5Si(CH_3)_2^-$	2.88
120	$C_6H_5SiCH_3^-$ (-2H)	6.38	121	$C_6H_5SiHCH_3^-$	2.70	107	$C_6H_7Si^-$	8.00
120	$C_6H_5SiCH_3^-$ ($-H_2$)	1.61	106	$C_6H_5SiH^-$ ($-2CH_3$)	5.54	105	$C_6H_5Si^-$	9.22
107	$C_6H_5SiH_2^-$	2.43	106	$C_6H_5SiH^-$ ($-C_2H_6$)	1.44	77	$C_6H_5^-$	3.51
106	$C_6H_5SiH^-$	5.83	105	$C_6H_5Si^-$ ($-2CH_3+H$)	9.53	74	$C_3H_{10}Si^-$	6.22
105	$C_6H_5Si^-$ ($-CH_3$-2H)	9.82	105	$C_6H_5Si^-$ ($-C_2H_6+H$)	5.43	73	$(CH_3)_3Si^-$	3.49
105	$C_6H_5Si^-$ ($-CH_3-H_2$)	5.05	78	$C_6H_6^-$	3.88	67.5	$(TMPS-CH_3)^{-2}$	8.07
78	$C_6H_6^-$	3.90	68	$DMPS^{-2}$	6.24	53	$C_6H_5SiH^{-2}$	6.30
69	$C_3H_5Si^-$	6.47	67.5	$(DMPS-H)^{-2}$	8.39	43	CH_3Si^-	5.77
59	$C_2H_7Si^-$	5.07	60.5	$(DMPS-CH_3)^{-2}$	7.96			
45	$CH_3SiH_2^-$	3.12	59	$(CH_3)_2SiH^-$	5.10			
44	CH_4Si^-	1.56	58	$C_2H_6Si^-$	1.82			
43	CH_3Si^- ($-C_6H_6$-H)	5.81	43	CH_3Si^-	5.52			
	CH_3Si^- ($-C_6H_5-H_2$)	6.15						
28	$C_2H_4^-$	8.55						

The fragmentation products can be numerous also in this case. We focus to the same reactions, which we analyzed in previous case. For the fragments of primary cleavage of the Si-H, Si-CH_3, Si-Ph bonds, the situation will be similar to the EII experiment. There will be present all the possible products of primary bond cleavage. They will be evenly represented than in the case of the EII. The bond dissociation energies are more similar than in the case of the EII. The situation of consecutive reactions by the specific mechanism will be different (Figure 27). For the classic mechanism, the dissociation of one hydrogen atom needs high energy (4 eV). The dissociation of two hydrogens needs even higher energy (7 eV). With our mechanism, the appearance of fragment with *m/z* = 120 could be possible but not sure. Even in our mechanism it requires relatively high energy. On the other hand, the peak 121 should be invisible.

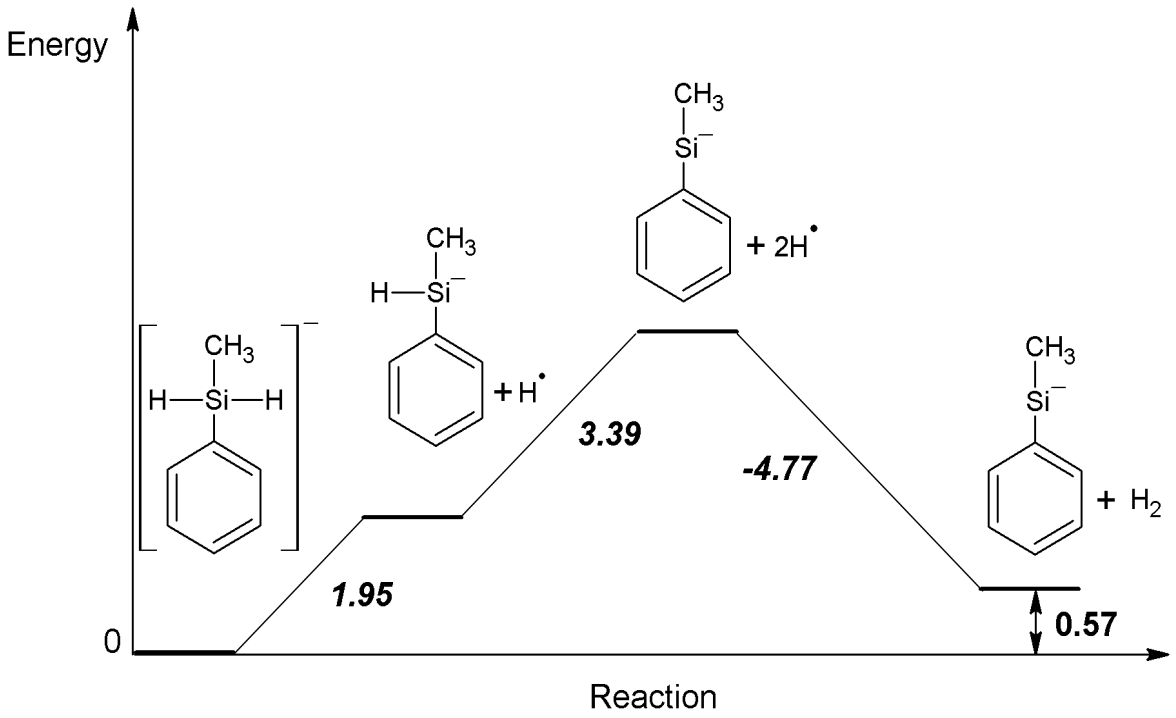

Figure 27. Energy profile for the H loss from methylphenylsilane anion derived from the B3LYP/6-311++G(d,p) calculations. The italic numbers are the bond dissociation energies (in eV).

The energy profile for the series of peaks from 105-107 is presented in Figure 28. We can compare them to the Figure 22 for the EII experiment. The barrier for single hydrogen dissociation is slightly lower in the case of anionic mechanism. Thus, the peak 106 in mass spectra for anionic mechanism will be probably slightly more intensive than the same peak in the EII mechanism. However, there is question how intensively will appear the fragment with *m/z* = 107 which is precursor for the peak 106. The peak 105 should appear, too.

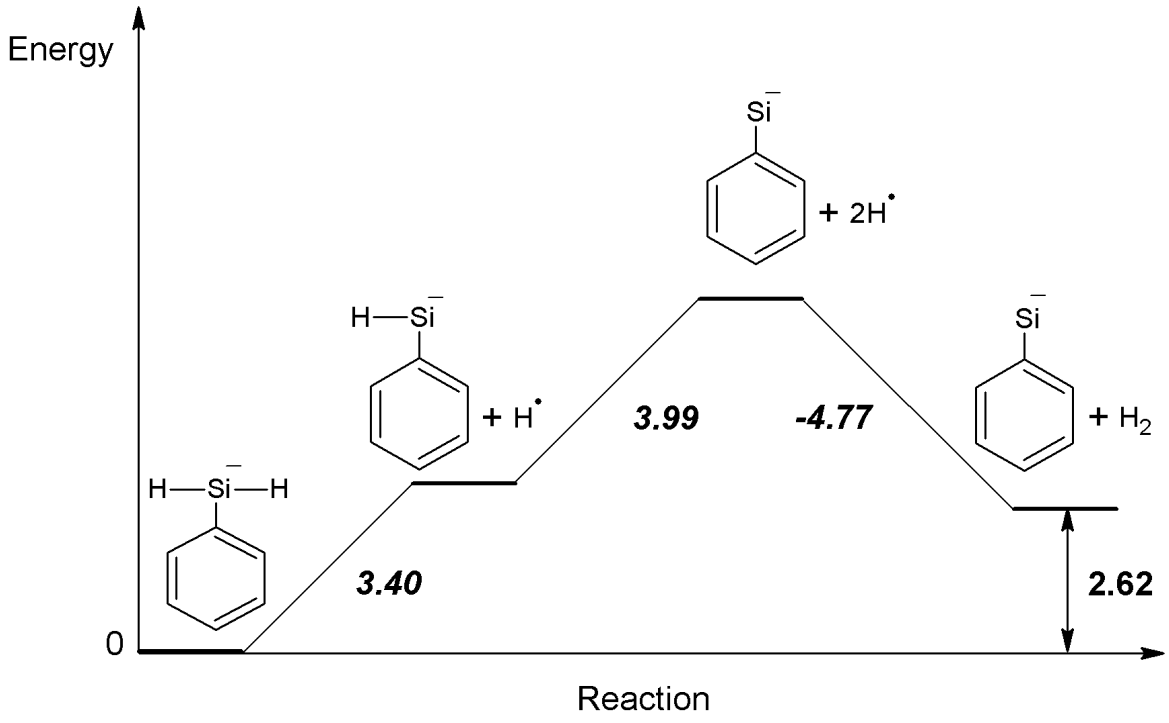

Figure 28. Energy profile for the CH_3 loss from methylphenylsilane anion derived from the B3LYP/6-311++G(d,p) calculations. The italic numbers are the bond dissociation energies (in eV).

5.3.3.3 New approach to the fragmentation

We would like to propose alternative fragmentation mechanism for interpretation of mass spectra of MPS. We had hypothesis that the decomposition of hydrogen molecule could run in one step. In contrast to the classic mechanism, the energy of H_2 recombination is not lost in the heat. All energies would be consumed and released in the main molecule. The mechanism avoids a step of the decomposition of one hydrogen atom. It could explain, why in the case of *m/z* = 107 and 105 fragment with *m/z* = 106 is missing.

The mechanism consists of scissoring of the bonds (H-Si-H). In one moment, two hydrogen atoms become very close and some complex can be formed. From that complex state, they can return to initial state or continue by subtraction of hydrogen molecule. The alternative fragmentation mechanism is presented in the Scheme 8.

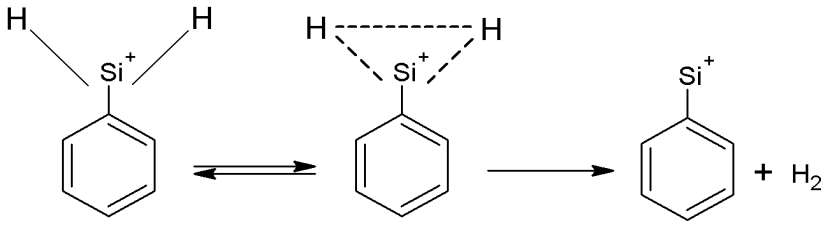

Scheme 8. Schematic form of the alternative fragmentation mechanism for MPS.

In reality, the reaction has still one limitation. It is because the scissoring of bonds also consumes some amount of energy. We optimized the geometry of molecule and then we compressed the shear angle. When the bond between hydrogens was undoubtedly created, the hydrogen molecule was pulled out from the fragment. The energy of such shear deformation is presented in Figure 29a. The maximum is approximately 4.25 eV. However, such value is a maximum limit value. The energy could be probably significantly lower. We reached the limit value, as we did first only bending of angle and then pulling out the hydrogen molecule from the main molecule. In reality both the partial steps run at the same time, which has a consequence in decrease of such energy barrier. We found that it could be 3.5 eV. Optimization of all the parameters procedure (bending angle, stretching, and mutual position of two hydrogens) could lead to even lower barrier.

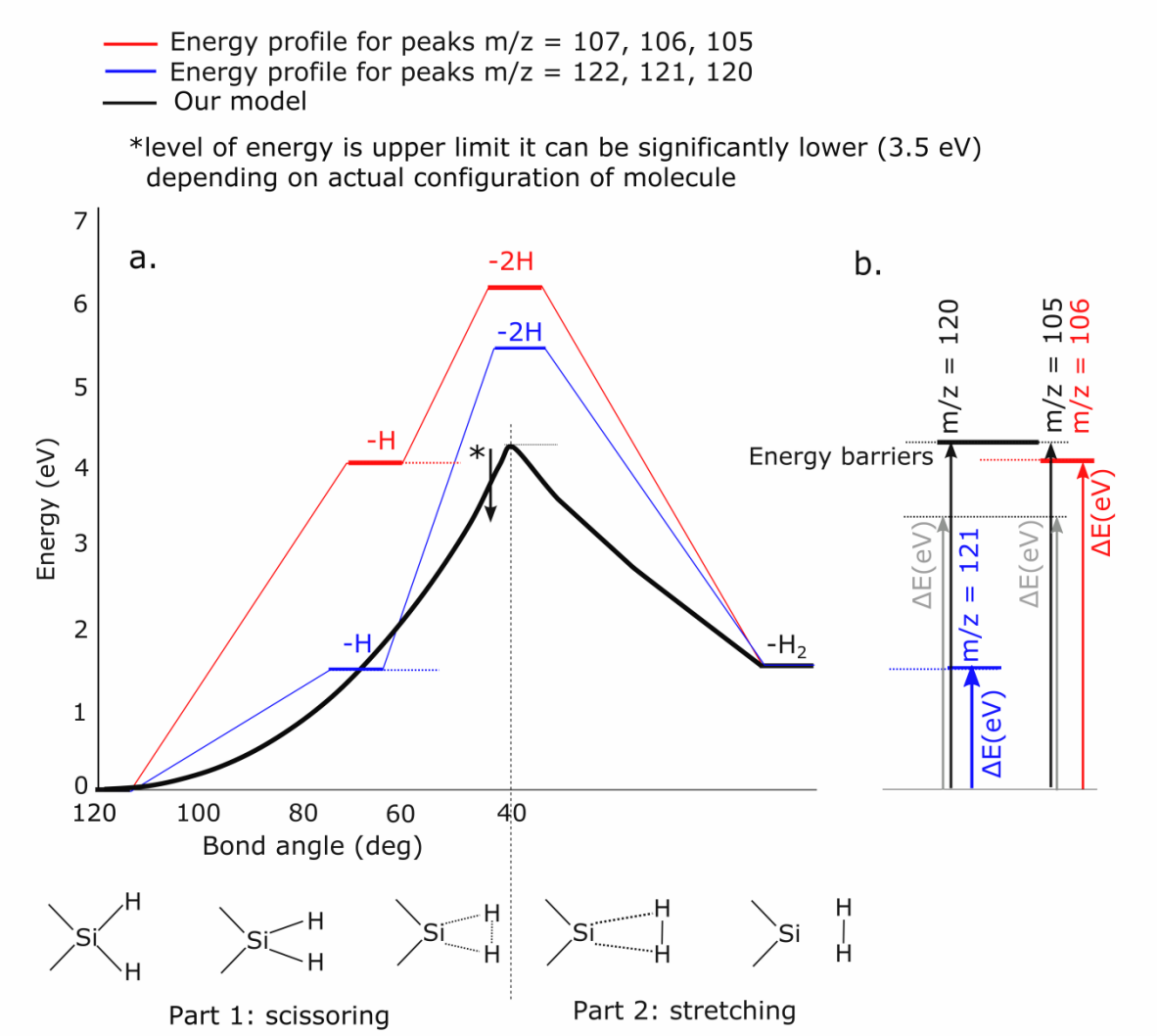

Figure 29. Energy scan for the dissociation of methylphenylsilane ion derived from the B3LYP/6-311++G(d,p) calculations.

In the case from Figure 22, the energy barrier for dissociation of two hydrogens is 4.09+2.22, i.e. 6.31 eV. In our mechanism the barrier is approximately 3.5 eV. It might be suspected that the shear deformation of bonds could be energetically preferred. The Figure 29b shows the comparison of energy barriers for dissociation of H (blue and red arrow) or H_2 by our mechanism (grey arrow). In the first case, the blue energy barrier is related to the appearance of $(MPS\text{-}H)^+$ (*m/z* = 121) and the grey energy barrier $(MPS\text{-}H_2)^+$ (*m/z* = 120). The blue barrier is lower than grey. On the other hand, the red barrier creation of $(MPS\text{-}CH_3\text{-}H)^+$ is higher (*m/z* = 106) than energy barrier of $(MPS\text{-}CH_3\text{-}H_2)^+$ (*m/z* = 105). The comparison shows us that dissociation of H is much more probable for the peak series 122, 121 than in 107, 106.

Qualitatively, it is in correlation with mass spectra, where peak 121 is relatively intensive and the peak 106 is very small.

The mechanism of hydrogen subtraction can be compared from aspect of momentum of inertia of molecule. It determines the behavior of molecule in thermal bath. The momentum of inertia was calculated as $J = \Sigma mr^2$, where m is the mass of atom and r is the distance from the center of mass for the molecule. The momentum of inertia for MPS^+ (Scheme 9a) is significantly higher than $(MPS\text{-}CH_3)^+$ (Scheme 9b, c). The kinetic energy of MPS^+ molecule leads rather to translation motion. After dissociation of CH_3 group, the rotation velocity of fragment is increased as: $\omega_2/\omega_1 = (J_1/J_2)^{1/2}$, where ω is angular velocity. Resultant of thermal motion of molecule is determined by motion of more heavy atoms (Si, C). The light hydrogens follow the motion of the other atoms. The preferred motion of hydrogens in the case of Scheme 9a is oscillation, whereas in the case of Scheme 9b and c, the motion of molecule supports rather the scissoring of H-Si-H angle. The scissoring motion leads to the mechanism from Scheme 8.

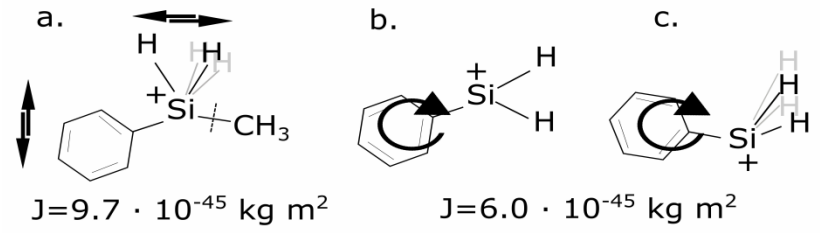

Scheme 9. momentum of inertia of the fragments; a) high momentum: translation; b. low momentum rotation; c: scissoring of hydrogens during rotation.

One aspect of the optimization is the development of energy density. The Figure 30 shows the scans of electron densities from Figure 29. The Figure 30a shows the original molecule. One can see that the maximum electron density is set between Si and H atoms. So the covalent bonds Si-H exist. The Figure 30b shows the transitive state, where the Si-H bonds still partially exist, but the new one is created. Then (Figure 30c), the hydrogen molecule leaves the molecule and electron density is between the two hydrogens, this indicates that there is a new covalent bond between the hydrogens (i.e. hydrogen molecule was formed). Among these three pictures, the case b has the highest energy. It is a transitive state, where the structure can return back to the original structure or continue to dissociation of hydrogen.

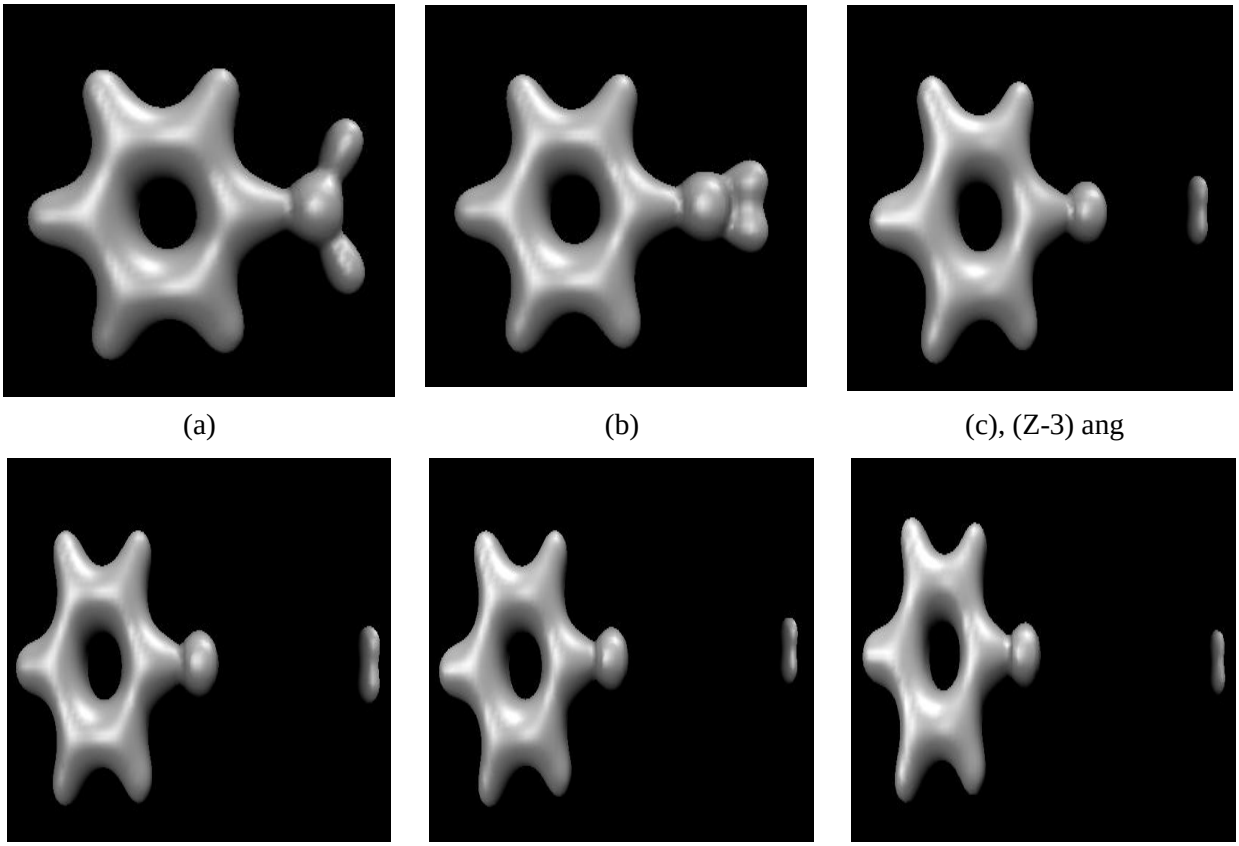

Figure 30. Electron densities plots of the $C_6H_5SiH_2^+$ fragment calculated by B3LYP/6-311++G(d,p) method.

Such mechanism can be also expected in the *m/z* = 45 – 43. The product of primary cleavage has *m/z* = 45 (dissociation of phenyl group). The next product of decomposition (*m/z* = 44) has low signal whereas the most intensive signal is *m/z* = 43. The products of the mechanism can be found in the mass spectra. It is relatively frequent pattern – double peak where the values of *m/z* (peak 1)-*m/z* (Peak 2) ≈ 2. Such structures (ions with peaks 107/105) are visible in all the diagrams. As well peaks 95/93/91 are in all three spectra and 121/119 in TMPS.

The DMPS molecule differs from MPS, that it has only one Si-H bond. So the mechanism is not possible in form of Scheme 8 (i.e. dissociation of H_2 molecule). However, some peaks *m/z* = 55/53/51 are observed, which reflect dissociation of H_2. However, the same mechanism can be considered also for dissociation of cationic benzene $(C_6H_6)^+$ in one step (peak *m/z* = 78) instead of phenyl group and hydrogen (*m/z* = 77). The same situation (peaks *m/z* 78>77) can be found as well in MPS. It is only not observed in mass spectra of TMPS. The mechanism, which we

proposed, requires at least one atom of hydrogen bonded on silicon. The specific property of hydrogen is that it has only one electron. If the electron is consumed to the covalent bond H-H or H-Ph, it automatically leads to dissociation of the bond H-Si. This is not the case of the CH_3 or Phenyl groups. That factor is visible in spectra TMPS. In the case, that the mechanism would be valid also for CH_3-CH_3 bond, we should see relatively intensive peak *m/z* = 120 (TMPS-C_2H_6) in the mass spectrum of TMPS. That peak is in reality rather small.

5.4 Potential energy surface of $C_6H_5SiH_2^+$ ionic fragment

We have previously investigated the PES for simple molecule (propane). We have found that this simulation for some simple molecule worked well. Here, we would like to continue with this property but for more complicated molecule. As we have seen from the cationic fragmentation mechanism of the MPS compound, the primary bond cleavage of the Si-CH_3 bond leads to produce the $C_6H_5SiH_2^+$ fragment. We would like to clarify the fragmentation mechanism concerning the shear deformation of the bond angle (H-Si-H) in this the $C_6H_5SiH_2^+$ fragment. In that fragmentation mechanism, we have found that the maximal energy barrier to have this mechanism was about 4 eV. The calculation of the PES can be useful for this clarification because it helps us to find the exact realistic energy barrier which is necessary for this model. The DFT calculations with B3LYP/6-311++G(d,p) was used to calculate the PES property. We suppose that two parameters have an important influence on the potential energy values. Therefore, we changed the Si-H bond lengths and the H-Si-H bond angle in the $C_6H_5SiH_2^+$ fragment to find the different potential energies. The PES of the $C_6H_5SiH_2^+$ fragment with some small stretching and angle shear deformation is shown in the Figure 31.

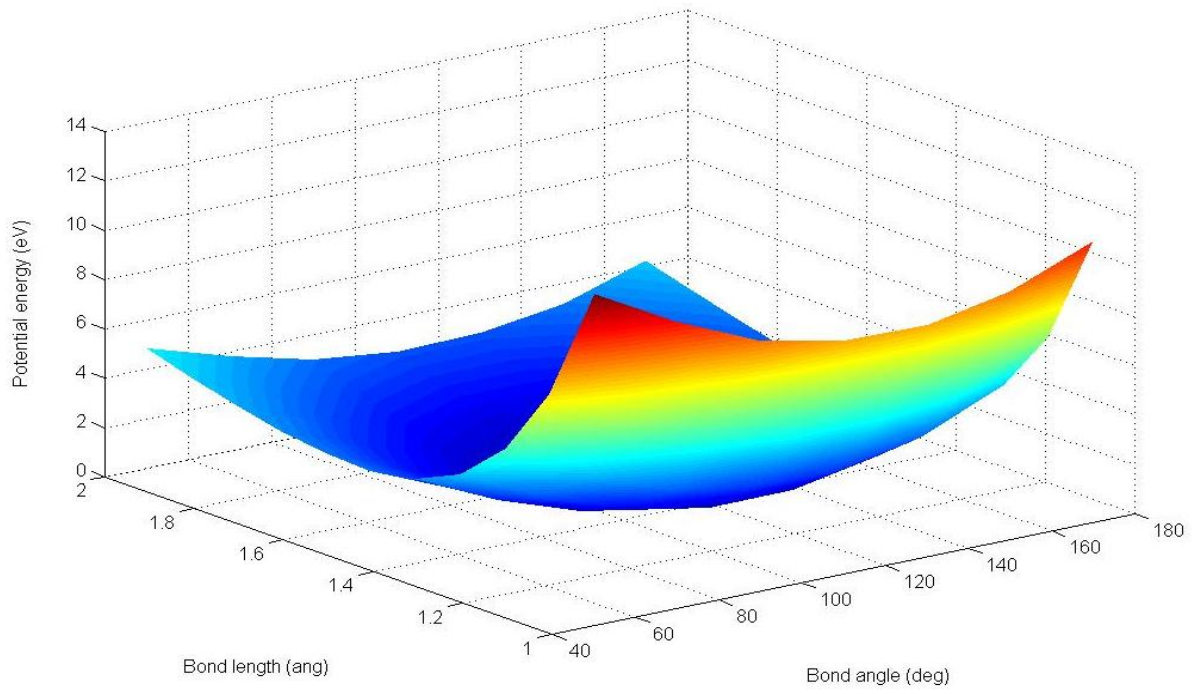

Figure 31. Potential energy surface of the $C_6H_5SiH_2^+$ fragment with some small stretching and angle shear deformation calculated using the DFT(B3LYP)/6-311++G(d,p) method.

The PES of the $C_6H_5SiH_2^+$ fragment with some large stretching and angle shear deformation is shown in the Figure 32. The color map of the PES of the $C_6H_5SiH_2^+$ fragment is given in the Figure 33. We know that the real energy barrier must be somehow lower than the calculated value (4 eV). From the Figure 33, it is evident that the Si-H bond length stretching gives large energy barrier, but the compression of the (H-Si-H) shear angle with the Si-H bond length stretching gives so large energy barrier. Therefore, there is visible that the shear deformation of the bond angle with the Si-H bond length stretching is less energetically demanding than only the Si-H bond length stretching. For definite evidence, we need at least the approaching to the real energy barrier value.

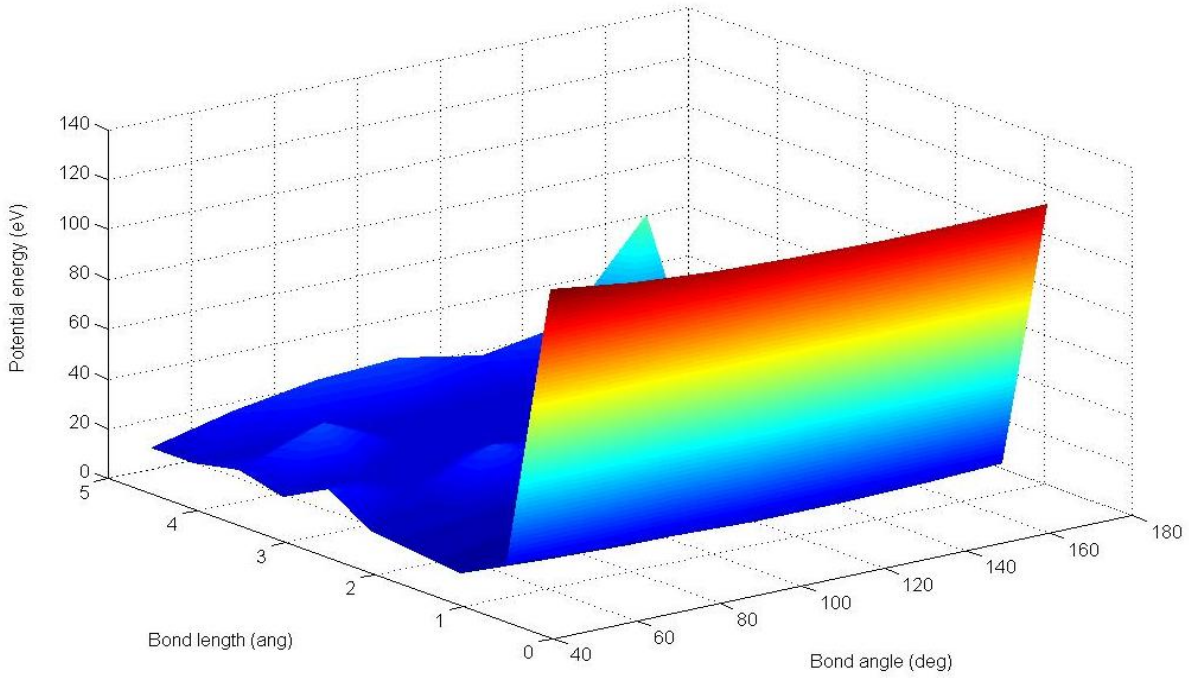

Figure 32. Potential energy surface of the $C_6H_5SiH_2^+$ fragment with some large stretching and angle shear deformation calculated using the DFT(B3LYP)/6-311++G(d,p) method.

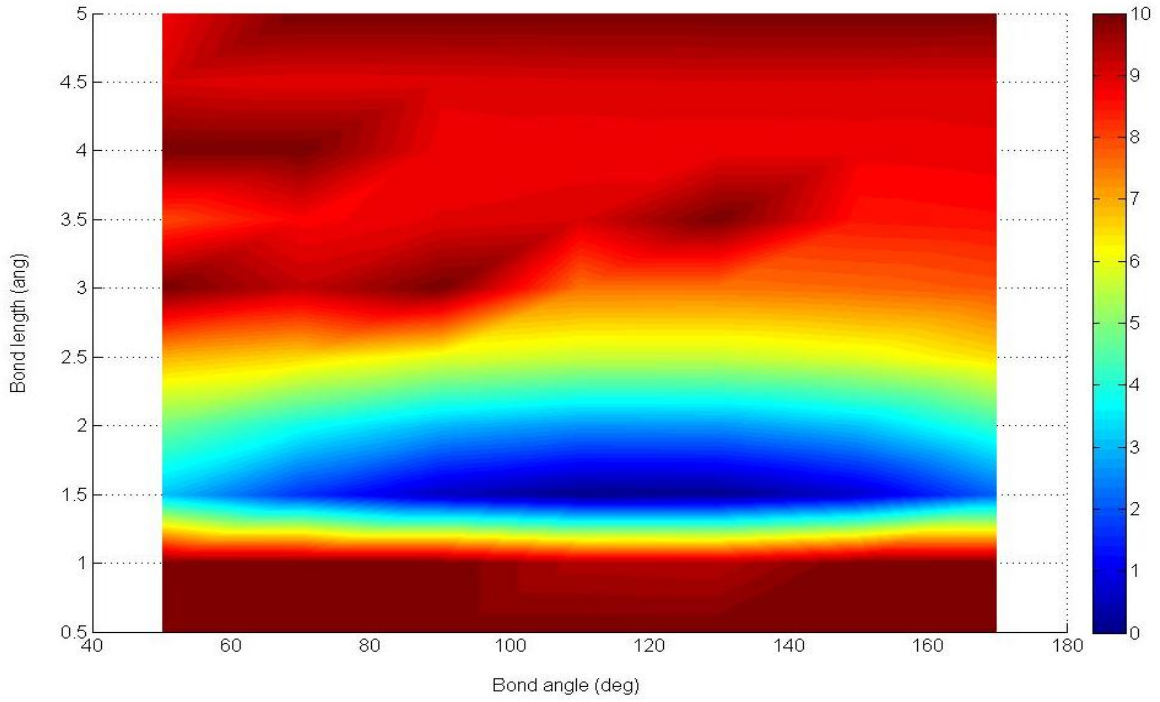

Figure 33. Color map of the potential energy surface of the $C_6H_5SiH_2^+$ fragment calculated using the DFT(B3LYP)/6-311++G(d,p) method.

6 Final conclusions

The fragmentation energy of various molecules was calculated by quantum chemical computations: *ab initio* methods (Hartree-Fock and post-Hartree-Fock) and the density functional theory (DFT) calculations. The fragmentation energy was tested on simple molecule (propane molecule) and consequently applied to more complex compounds (organosilicon compounds) such as methylphenylsilane, dimethylphenylsilane, and trimethylphenylsilane that have similar structure. The energy calculated by quantum chemical methods can be verified by experimental work using electron impact ionization experiment. Fragmentation energies of individual partial reactions can be calculated by quantum mechanical methods. Energies can be used as input properties for the calculation of fragmentation kinetics. Relative concentrations of fragmentation products can be calculated, too. The calculated concentrations of fragments can be compared to experimental intensities from mass spectrometry. It was found that the DFT calculations are better than *ab initio* methods to investigate fragmentation process of molecules. Quantum chemical calculations of the HOMO and LUMO frontier orbital gap give information about the chemical reactivity and kinetic stability of the molecule.

The oragnosilicon compounds were selected for this study because they play a key role for understanding and developing the plasma technologies such as plasma enhanced chemical vapor deposition (PECVD), as well as silicon atoms support binding to inorganic substrates including glass, or ceramics. The fragmentation mechanism is complex. It can be seen on the mass spectra, which give general information about fragmentation products. Therefore, we have presented a combined theoretical and experimental study on organosilicones fragmentation process. We found that the calculated data are in good correlation with experimental data for electron impact ionization. The ionization energies and the appearance energies of some products of the MPS and TMPS molecules were estimated. The dissociative ionization of the MPS molecule is mainly resulting in formation of $SiCH_3^+$ ion. The dissociative ionization of the TMPS molecule has intensive channels for $(TMPS\text{-}CH_3)^+$, $(TMPS\text{-}CH_3)^{+2}$, $HSi(CH_3)_3^+$ and $SiCH_3^+$ ions. We have shown that dissociation of single CH_3 ligand from all three target molecules is less favourable for the MPS molecule, probably due to a lower spatial repulsion between the ligands. The increase of CH_3 ligands number on the Si atom causes the decrease of the bond dissociation energy for the Si-CH_3 bond. Contrary to this, the loss of the hydrogen atom is visible only for the MPS and DMPS with comparable energetic demand.

Fragmentation mechanism is composed of three phases: ionization, primary bond cleavage, and consecutive reactions of bond cleavage. We found the differences in the primary bond cleavage (first cleavage after the ionization). We observed primary dissociation of phenyl group in MPS and DMPS whereas the dissociation of methyl group was primarily observed in TMPS. The organosilicon molecules release the hydrogen during the plasma induced fragmentation. We focused to mechanism of hydrogen subtraction from methylphenylsilane during plasma induced fragmentation process. The MPS in contrast to DMPS has two hydrogen atoms bounded on central silicon atom. It enables us to subtract the hydrogen molecule from the fragments. We believe that it is possible by two mechanisms. The first, classic mechanism consists of subtraction of two hydrogen atoms step-by-step. The second mechanism is the subtraction of two hydrogen atoms in one step. The second mechanism is associated with the scissoring and compression of the (H-Si-H) shear bond angle leading to consecutive subtraction of H_2 molecule. The second mechanism is observed only in special cases, when the energy barrier for the first subtraction of hydrogen is too large. Otherwise, the classic mechanism prevails. We verified by experiment particularly the relative cross-sections of cations that there is possibility to calculate also the cross-sections by theoretical calculation. The experimental data was in correlation with calculated results. We calculated the data for the subtraction of hydrogen molecule by dissociative electron attachment mechanism. In that case, the data were not measured experimentally. We would like to propose a prediction of future experimental works. It is concerning the peaks with *m/z* = 122/121/120 and 107/106/105 in mass spectra. The peaks *m/z* = 122/121/120 reflect classic subtraction of hydrogens one-by-one. It is the case of electron impact ionization and it would be probably observed also in the case of electron attachment mechanism. In the case of electron impact ionization, the peaks 107/106/105 reflect by a new mechanism and the intensity of peak 106 is nearly zero. In the case of electron attachment mechanism, the peak will have probably higher intensity. We can predict which mechanism is more probable according to the DFT calculated energy profile of reaction. The calculated predictions were in correlation with the composition of fragmentation products from mass spectra.

7 References

[1] G. Barroso, M. Morshedi, S. Oehninger, Hum. Reprod. 15 (2000) 1338-1344.

[2] L. Simon, G. Brunborg, M. Stevenson, D. Lutton, J. McManus, S. E. M. Lewis, Hum. Reprod. 25 (2010) 1594-1608.

[3] V. Čech, J. Studýnka, N. Conte, V. Peřina, Surf. Coat Technol. 201 (2007) 5512-5517.

[4] V. Čech, J. Studýnka, F. Janoš, V. Peřina, Plasma Process. Polym. 4 (2007) 776-780.

[5] V. Brites, G. Chambaud, M. Hochlaf, J. Kočišek, J. L. C. Diaz, S. Matejčík, F. Krčma, J. Phys. Chem. A 113 (2009) 6531-6536.

[6] J. Kočišek, O. Stružínský, H. Sahánková, F. Krčma, Š. Matejčík, Plasma Process. Polym. 9 (2012) 298-303.

[7] T. Arii, S. Otake, Y. Takata, S. Matsuura, J. Mass Spectrom. Soc. Jpn. 54 (2006) 243-249.

[8] R. L. Whetten, C. Yeretzian, Int. J. Mod. Phys. B 6 (1992) 3801-3814.

[9] R. Davis, M. Frearson, Mass Spectrometry. Analytical Chemistry by Open Learning, John Wiley & Sons, London, 1987.

[10] Central Connecticut State University, Department of Chemistry & Biochemistry, http://www.chemistry.ccsu.edu/glagovich/teaching/316/ms%20(old)/alkane-straight.html.

[11] L. Sleno, D. A. Volmer, J. Mass Spectrom. 39 (2004) 1091-1112.

[12] R. A. Zubarev, N. L. Kelleher, F. W. McLafferty, J. Am. Chem. Soc. 120 (1998) 3265-3266.

[13] L. M Mikesh, B. Ueberheide, A. Chi, J. J. Coon, J. E. P. Syka, J. Shabanowitz, and D. F. Hunt, Biochim. Biophys. Acta. 1764 (2006) 1811-1822.

[14] S. Denifl, Š. Matejčík, J. D. Skalný, M. Stano, P. Mach, J. Urban, P. Scheier, T. D. Märk, W. Barszczewska, Chem. Phys. Lett. 402 (2005) 80-87.

[15] L. A. Curtiss, K. Raghavachari, P.C Redfern, V. Rassolov, J. A. Pople, J. Chem. Phys. 109 (1998) 7764-7776.

[16] A. G Baboul, L. A. Curtiss, P.C Redfern, K. Raghavachari, J. Chem. Phys. 110 (1999) 7650-7657.

[17] J. A. Montgomery, M. J. Frisch, J.W. Ochterski, G.A. Petersson, J. Chem. Phys. 110 (1999) 2822-2827.

[18] D. L. Lichtenberger, A. S. Copenhaver, Bonding Energetics in Organometallic Compounds, ACS Symposium Series, Vol. 428, 1990.

[19] J. C. Choe, Int. J. Mass Spectrom. 242 (2005) 5-11.

[20] E. E. B. Campbell, F. Rohmund, Rep. Prog. Phys. 63 (2000) 1061-1109.

[21] C. Lifshitz, Int. J. Mass. Spectrom. 200 (2000) 423-442.

[22] S. Matt, O. Echt, T. Rauth, B. Dünser, M. Lezius, A. Stamatovic, P. Scheier, T. D. Märk, Z. Phys. D 40 (1997) 389-394.

[23] T. Wakabayashi, H. Shiromaru, S. Suzuki, K. Kikuchi, Y. Achiba, Surf. Rev. Lett. 3 (1996) 793-798.

[24] T. Kimura, T. Sugai, H. Shinohara, J. Chem. Phys. 110 (1999) 9681-9687.

[25] R. D. Beck, P. Weis, J. Rockenberger, R. Michel, D. Fuchs, M. Benz, M. M. Kappes, Surf. Rev. Lett. 3 (1996) 881-885.

[26] J. McMurry, Organic chemistry, Thomson Brooks/Cole, 2008, pp. 426.

[27] S. G. Lias, *"Mass Spectrum (electron ionization)" in NIST Chemistry WebBook, NIST Standard Reference Database Number 69*. Available from: http://webbook.nist.gov/chemistry/.

[28] E. Vašeková, M. Stano, Š. Matejčík, J. D. Skalný, P. Mach, J. Urban, T. D. Märk, Int. J. Mass Spectom. 235 (2004) 155-162.

[29] J. M. Gaidis, P. R. Briggs , T. W. Shannon, J. Phys. Chem. 75 (1971) 974-980.

[30] S. T. Nakagawa, I. Suzue, M. Itoh, M. Kageyama, Y. Mizuno, H. J. Whitlow, J. Nucl. Mater. 363-365 (2007) 1289-1293.

[31] L. Hanley, J. L. Whitten, S. L. Anderson, J. Phys. Chem. 92 (1988) 5803-5812.

[32] A. K. Ray, I. A. Howard, K. M. Kanal, Phys. Rev. B 45 (1992) 14247-14255.

[33] H. Kato, K. Yamashita, K. Morokuma, Chem. Phys. Lett. 190 (1992) 361-366.

[34] G. A. Dolgonos, G. H. Peslherbe, Chem. Phys. Lett. 398 (2004) 217-223.

[35] W. C. Eckhoff, G. E. Scuseria, Chem. Phys. Lett. 216 (1993) 399-404.

[36] A. D. Boese, G. E. Scuseria, Chem. Phys. Lett. 294 (1998) 233-236.

[37] R. E. Stanton, J. Chem. Phys. 96 (1992) 111-118.

[38] J. Y. Yi, J. Bernholc, J. Chem. Phys. 96 (1992) 8634-8636.

[39] C. H. Xu, G. E. Scuseria, Phys. Rev. Lett. 72 (1994) 669-672.

[40] B. L. Zhang, C. H. Xu, C. Z. Wang, C. T. Chan, K. M. Ho, Phys. Rev. B 46 (1992) 7333-7336.

[41] S. Matt, O. Echt, P. Scheier, T. D. Märk, Chem. Phys. Lett. 348 (2001) 194-202.

[42] S. Tomita, J. U. Andersen, C. Gottrup, P. Hvelplund, U. V. Pedersen, Phys. Rev. Lett. 8707 (2001) 073401-073404.

[43] M. Born, R. Oppenheimer, Ann. Phys. 389 (1927) 457-484.

[44] E. Schrodinger, Phys. Rev. 28 (1926) 1049-1070.

[45] M. Šob, M. Friák, D. Legut, J. Fiala, V. Vitek, Mat. Sci. Eng. A 387-389 (2004) 148-157.

[46] J. B. Foresman, Æ. Frisch, Exploring Chemistry with Electronic Structure Methods, Gaussian, Inc., U. S. A., 2000.

[47] D. R. Hartree, Proc. Comb. Phil. Soc. 24 (1928) 111-132.

[48] P. W. Atkins, R. S. Friedman, Molecular Quantum Mechanics, Oxford University Press, 1999.

[49] J. B. Foresman, M. H. Gordon, J. A. Pople, M.J. Frisch. J. Phys. Chem. 96 (1992) 135-149.

[50] E. G. Lewars, Computational Chemistry: Introduction to the Theory and Applications of Molecular and Quantum Mechanics, Kluwer Academic Publishers, 2003.

[51] A. R. Leach, Molecular Modelling: Principles and Applications, Addison Wesley Longman Limited, 1996.

[52] W. J. Hehre, L. Radom, Paul. V. R. Schleyer, John A. Pople, *Ab Initio* Molecular Orbital Theory, John Wiley & Sons, Inc., 1986.

[53] K. Raghavachari, J. B. Anderson, J. Phys. Chem. 100 (1996) 12960-12973.

[54] C. Møller, M.S. Plesset, Phys. Rev. 46 (1934) 618-622.

[55] R. J. Bartlett, Annu. Rev. Phys. Chem. 32 (1981) 359-401.

[56] M. Mueller, Fundamentals of Quantum Chemistry: Molecular Spectroscopy and Modern Electronic Structure Computations, Kluwer Academic/Plenum Publishers, New York, 2001.

[57] F. Jensen, Introduction to Computational Chemistry, John Wiley & Sons, Ltd., 2007.

[58] L. Szasz, The Electronic Structure of Atoms, John Wiley & Sons, Inc., 1992.

[59] C. D. Sherrill, H. F. Schaefer, Adv. Quant. Chem. 34 (1999) 143-269.

[60] I. Shavitt, The Method of Configuration Interaction, in: Methods of Electronic Structure Theory, Plenum Press, New York, 1977.

[61] J. A. Pople, M. H. Gordon, K. Raghavachari, J. Chem. Phys. 87 (1987) 5968-5975.

[62] D. Maurice, M. H. Gordon, Mol. Phys. 96 (1999) 1533-1541.

[63] M. H. Gordon, R. J. Rico, M. Oumi, T. J. Lee, Chem. Phys. Lett. 219 (1994) 21-29.

[64] K. Raghavachari, G. W. Trucks, J. A. Pople, M.H. Gordon, Chem. Phys. Lett. 157 (1989) 479-483.

[65] P. E. M. Siegbahn, The Configuration Interaction Method, in: Lecture Notes in Quantum Chemistry. Springer-Verlag, Berlin, 1992.

[66] D. C. Young, Computational Chemistry: A Practical Guide for Applying Techniques to Real World Problems, John Wiley & Sons, Inc., 2001.

[67] J. Čížek, J. Chem. Phys. 45 (1966) 4256-4267.

[68] J. Čížek, J. Paldus, Int. J. Quantum Chem. 5 (1971) 359-379.

[69] R. J. Bartlett, J. Phys. Chem. 93 (1989) 1697-1708.

[70] J. A. Pople, R. Krishnan, HB. Schlegel, JS. Binkley, Int. J. Quantum Chem. 14 (1978) 545-560.

[71] G. D. Purvis III, RJ. Bartlett, J. Chem. Phys. 76 (1982) 1910-1918.

[72] J. Noga, RJ. Bartlett, J. Chem. Phys. 86 (1987) 7041-7050.

[73] J. A. Pople, J. S. Binkley, R. Seeger, Int. J. Quantum Chem. Symp. 10 (1976) 1-19.

[74] Z. He, D. Cremer, Theor. Chim. Acta. 85 (1993) 305-323.

[75] M. W. Schmidt, M. S. Gordon, Annu. Rev. Phys. Chem. 49 (1998) 233-266.

[76] L. M. Cheung, K. R. Sundbergy, K. Ruedenberg, Int. J. Quantum Chem. 16 (1979) 1103-1137.

[77] B. O. Roos, Adv. Chem. Phys. 69 (1987) 399-445.

[78] P. Hohenberg, W. Kohn, Phys. Rev. 136 (1964) 864-871.

[79] W. Kohn, L. J. Sham, Phys. Rev. 140 (1965) 1133-1138.

[80] R. G. Parr, W. Yang, Density Functional Theory of Atoms and Molecules, International Series of Monographs on Chemistry, Oxford University Press, New York, 1989.

[81] A. D. Becke, J. Chem. Phys. 98 (1993) 5648-5652.

[82] J. P. Perdew, K. Burke, Y. Wang, Phys. Rev. B 54 (1996) 16533-16539.

[83] D. Joubert, Density Functionals: Theory and Applications, Springer-Verlag, Heidelberg, 1998.

[84] E. Tasal, M. Kumalar, Spectrochim. Acta, Part A 95 (2012) 282-299.

[85] R. J. Xavier, S. A. Raj, Spectrochim. Acta, Part A 101 (2013) 148-155.

[86] L. Padmaja, C. Ravikumar, D. Sajan, I. H. Joe, V. S. Jayakumar, G. Pettit, O. F. Neilsen, J. Raman Spectrosc. 40 (2009) 419-428.

[87] C. Ravikumar, I. H. Joe, V. S. Jayakumar, Chem. Phys. Lett. 460 (2008) 552-558.

[88] C. H. Lin, H. L. Chen, L. A. Wang, Microelectron. Eng. 57-58 (2001) 555-561.

[89] R. Morent, N. D. Geyter, S. V. Vlierberghe, P. Dubruel, C. Leys, L. Gengembre, E. Schacht, E. Payen, Prog. Org. Coat. 64 (2009) 304-310.

[90] V. Cech, A. Knob, H. Hosein, A. Babik, L. Drzal, Proc. Int. Conf. Composite Interfaces (Interface 21), (2012) 1-4.

[91] R. Barni, S. Zanini, C. Riccardi, Adv. Phys. Chem. 2012 (2012) 205380–205386.

[92] K. Igawa, J. Takada, T. Shimono, K. Tomooka, J. Am. Chem. Soc. 130 (2008) 16132-16133.

[93] S. E. Denmark, C. R. Butler, J. Am. Chem. Soc. 130 (2008) 3690-3704.

[94] J. C. Choe, Rapid Commun. Mass Spectrom. 17 (2003) 207-211.

[95] J. C. Choe, Int. J. Mass Spectrom. 237 (2004) 1-12.

[96] T. Veszprémi, Y. Harada, K. Ohno, H. J. Mutoh, J. Organomet. Chem. 266 (1984) 9-16.

[97] MOLPRO, version 2010.1, A package of *ab initio* programs, H. J. Werner, P. J. Knowles, G. Knizia, F. R. Manby, M. Schütz, P. Celani, T. Korona, R. Lindh, A. Mitrushenkov, G. Rauhut, K. R. Shamasundar, T. B. Adler, R. D. Amos, A. Bernhardsson, A. Berning, D. L. Cooper, M. J. O. Deegan, A. J. Dobbyn, F. Eckert, E. Goll, C. Hampel, A. Hesselmann, G. Hetzer, T. Hrenar, G. Jansen, C. Köppl, Y. Liu, A. W. Lloyd, R. A. Mata, A. J. May, S. J. McNicholas, W. Meyer, M. E. Mura, A. Nicklass, D. P. O'Neill, P. Palmieri, K. Pflüger, R. Pitzer, M. Reiher, T. Shiozaki, H. Stoll, A. J. Stone, R. Tarroni, T. Thorsteinsson, M. Wang, A. Wolf. Available from: http://www.molpro.net.

[98] D. L. Bunker, B. Garrett, T. Kleindienst, G. S. Long III, Combust. Flame 23 (1974) 373-379.

[99] D. T. Gillespie, J. Comput. Phys. 22 (1976) 403-434.

[100] I. Fleming, Frontier Orbitals and Organic Chemical Reactions, John Wiley & Sons, New York, 1976.

[101] I. B. Obot, A. S. Johnson. Comput. Chem. 43 (2012) 6658.

[102] A. Dwivedi, N. Misra, Der Pharma Chemica 2 (2) (2010) 58-62.

[103] S. Kalaichelvan, N. Sundaraganesan, O. Dereli, U. Sayin, Spectrochimica Acta Part A 85 (2012) 198-209.

[104] M. Koca, C. Arici, H. Muglu, C. D. Vurdu, F. Kandemirli, Y. Zalaoglu, G. Yildirim, Spectrochimica Acta Part A 137 (2015) 899-912.

[105] D. Chhabil, Fundamentals of Contemporary Mass Spectrometry, John Wiley & Sons, 2007.

[106] G. Dube, V. Chvalovský, Collect. Czech. Chem. Commun. 39 (1974) 2621-2629.

[107] I. Kuritka, P. Broza, J. Prycek, F. Schauer, Plasma Process. Polym. 4 (2007) 53-61.

[108] M. Stano, Š. Matejčík, J. D. Skalný, T. D. Märk, J. Phys. B: At. Mol. Opt. Phys. 36 (2003) 261-271.

[109] S. G. Lias, *"Ion Energetic Data" in NIST Chemistry WebBook, NIST Standard Reference Database Number 69*. Available from: http://webbook.nist.gov/chemistry/.

[110] G. H. Wannier, Phys. Rev. 90 (1953) 817-825.

[111] Y. K. Kim, W. Hwang, N. M. Weinberger, M. A. Ali, M. E. Rudd, J. Chem. Phys. 106 (1997)1026-1033.

[112] K. N. Joshipura, C. G. Limbachiya, Int. J. Mass Spectrom. 216 (2002) 239-247.

[113] P. McCallion, M. B. Shah, H. B. Gilbody, J. Phys. B: At., Mol. Opt. Phys. 25 (1992) 1061-1071.

[114] K. Fujii, S. K. Srivastava, J. Phys. B: At., Mol. Opt. Phys. 28 (1995) L559-L563.

[115] D. P. Almeida, M. A. Scopel, R. R. Silva, A. C. Fontes, Chem. Phys. Lett. 341 (2001) 490-494.

[116] Y. K. Kim, M. E. Rudd, Phys. Rev. A: At. Mol. Opt. Phys. 50 (1994) 3954-3967.

[117] H. Deutsch, K. Becker, S. Matt, T.D. Märk, Int. J. Mass Spectrom. 197 (2000) 37-69.

[118] G. Schaftenaar, J. H. Noordik, J. Comput. Aided Mol. Des. 14 (2000) 123-134.

[119] B. K. Sharma, Spectroscopy, Krishna Prakashan Media Meerut, 2007, ISBN: 8182830184.

[120] C. D. Finney, A. G. Harrison, Int. J. Mass Spectrom. Ion Phys. 9 (1972) 221-233.

[121] G. Bieri, F. Burger, E. Heilbronner, J. P. Maier, Helv. Chim. Acta. 60 (1977) 2213-2233.

[122] T. Kolke, W. C. Gardlner, Jr., J. Phys. Chem. 84 (1980) 2005-2009.

[123] R. S. Zhu, Z. F. Xu, M. C. Lin, J. Chem. Phys. 120 (2004) 6566-6573.

[124] S. H. Mousavipour, Z. Homayoon, J. Phys. Chem. A 107 (2003) 8566-8574.

[125] J-Y. Jezequel, F. Baronnet, M. Niclause, J. Chim. Phys. 75 (1978) 991-993.

[126] W. Kao, C. Yeh, J. Chem. Phys. 81 (1977) 2304-2306.

[127] A. M. Dean, J. Phys. Chem. 89 (1985) 4600-4608.

[128] W. Tsang, Combust. Flame 78 (1989) 71-86.

[129] M. A. Oehlschlaeger, D. F. Davidson, R. K. Hanson, Proc. Combust. Inst. 30 (2005) 1119-1127.

[130] A. Yu. Gladky, V. K. Ermolaev, V. N. Parmon, React. Kinet. Catal. Lett. 67 (1999) 183-189.

[131] A. Belmeliani, D. Perrin, R. Martin, J. Chem. Phys. 91 (1994) 313-328.

[132] C. R. Arumainayagam, H. L. Lee, R. B. Nelson, D. R. Haines, R. P. Gunawardane, Surf. Sci. Rep. 65 (2010) 1-44.

[133] E. Illenberger, J. Momigny, Topics in Physical Chemistry, vol 2 Gaseous Molecular Ions, Springer 1992.

8 List of abbreviations

IR	Infra-red
UV	ultraviolet
NMR	Nuclear magnetic resonance
TEM	trochoidal electron monochromator
QMS	quadrupole mass spectrometer
MBS	molecular beam source
G3	Gaussian-3 theory
G3B3	Gaussian-3 theory using density functional theory B3LYP
CBS-QB3	complete basis set-quadratic Becke 3
DFT	density functional theory
HF	Hartree-Fock
SCF	self-consistent field
$\hat{\mathrm{H}}_{mol}$	molecular Hamiltonian
E	total energy of the system
Ψ	wavefunction of the system
$\vec{r}$	position vectors of the electrons
$\vec{\mathrm{R}}$	position vectors of the nuclei
T_{el}	kinetic energy for the electrons
T_{nuc}	kinetic energy for the nuclei
V_{el-el}	repulsive electron-electron potential energy
$\mathrm{V}_{nuc-nuc}$	repulsive nuclear-nuclear potential energy
V_{el-nuc}	attractive electron-nuclear potential energy
BO	Born–Oppenheimer
SE	Schrödinger's equation
MP0	zero-order Møller-Plesset perturbation theory
MP2	second-order Møller-Plesset perturbation theory
MP3	third-order Møller-Plesset perturbation theory
MP4	fourth-order Møller-Plesset perturbation theory
ψ_i	Molecular spatial orbital *i*

c_{si}	expansion coefficient of the atomic orbital *s* in the molecular orbital *i*
Φ_s	atomic orbital s
m	number of atomic orbitals
LCAO	linear combination of atomic orbitals
CI	configuration interaction
CIS	configuration interaction with single excited state
CID	configuration interaction with double excited state
CISD	configuration interaction with single and double excited states
CISDT	configuration interaction with single, double, and triple excited states
FCI	full configuration interaction
CC	coupled cluster
CCSD	coupled cluster with single and double excitations
CCSD(T)	coupled cluster with single, double, and triple excitations
MCSCF	multi-configuration self-consistent field
MRCI	multireference configuration interaction
QCI	quadratic configuration interaction
QCISD	quadratic configuration interaction with single and double excitations
QCISD (T)	quadratic configuration interaction with single, double, and triple excitations
CASSCF	complete active space self-consistent field
B3LYP	Becke style three parameters density functional method with the Lee-Yang-Parr correlation
B3PW91	Becke style three parameters density functional method with the Perdew-Wang correlation
5CMOT	5-chloro-3-(2-(4-methylpiperrazin-1-yl)-2-oxo-ethyl) benzo[d] thiazol-2(3H)
GTO	Gaussian type orbital
STO	Slater type orbital
G	Gaussian
CKS	chemical kinetics simulator
KS	standard Kohn-Sham density functional theory calculations using spin-restricted approximation
UKS	standard Kohn-Sham density functional theory calculations using spin-

	unrestricted approximation
DZ	double-zeta basis set
VDZ	valence double-zeta basis set
VTZ	valence triple-zeta basis set
VQZ	valence quadruple-zeta basis set
V5Z	valence quintuple-zeta basis set
cc-pVDZ	correlation consistent-polarized valence double-zeta basis set
aug-cc-pVDZ	augmented correlation consistent-polarized valence double-zeta basis set
aug-cc-pVTZ	augmented correlation consistent-polarized valence triple-zeta basis set
aug-cc-pVQZ	augmented correlation consistent-polarized valence quadruple-zeta basis set
KS, B, LYP	Kohn-Sham calculation using Becke's exchange functional and the Lee-Yang-Parr correlation functional
KS, B3LYP	hybrid (B3LYP) functional consisting of weighted combinations of various density functionals together with a fraction of exact (Hartree-Fock) exchange
HOMO	highest occupied molecular orbital
LUMO	lowest unoccupied molecular orbital
PES	potential energy surface
PECVD	plasma enhanced chemical vapor deposition
PACVD	plasma assisted chemical vapor deposition
EII	electron impact ionization
MPS	Methylphenylsilane
DMPS	Dimethylphenylsilane
TMPS	Trimethylphenylsilane
HMDSO	Hexamethyldisiloxane
TEOS	Tetraethyl orthosilicate
BED	binary encounter dipole
ZPVE	zero-point vivrational energy
IE	ionization energy
BDE	bond dissociation energy
AE	appearance energy

9 Acknowledgements

I would like to thank my supervisor of doctoral thesis Mgr. Jan Žídek Ph.D. of Brno University of Technology, Faculty of Chemistry at the Institute of Materials Science for proper leading and supervision, patience and helpful advices during consultations without who this thesis will not come to exist. The experience and knowledge that I took during study had an enormous value for me.

I gratefully appreciate the help of doc. RNDr. František Krčma, Ph.D. of Brno University of Technology, Faculty of Chemistry at the Institute of Physical and Applied Chemistry (IPAC), motivation and continuous support to this work.

I would also like to thank to all my colleagues, at the Brno University of Technology, Faculty of Chemistry at the department of Physical and Applied Chemistry for making my stay at Faculty of Chemistry a pleasant one and for their technical and moral support.